A THEORY OF THE SUPERSONIC TURBULENT AXISYMMETRIC NEAR WAKE BEHIND BLUFF-BASE BODIES

A THESIS

Presented to

The Faculty of the Division of Graduate Studies and Research

By

Gopal Krishna Mehta

In Partial Fulfillment

of the Requirements for the Degree

Doctor of Philosophy

in the School of Aerospace Engineering

Georgia Institute of Technology

May, 1977

A THEORY OF THE SUPERSONIC TURBULENT AXISYMMETRIC NEAR WAKE BEHIND BLUFF-BASE BODIES

Approved:

Chairman

Date Approved by Chairman: 5/12/77

ACKNOWLEDGMENTS

It gives me great pleasure to record my deepest gratitude to Dr. Warren C. Strahle for his suggestion of the thesis topic, his guidance throughout the course of investigation, and for his constant willingness to discuss various aspects of this problem.

I owe special thanks to Professor James E. Hubbartt for many hours of useful discussions during the course of investigation. I also thank Dr. Strahle and Professor Hubbartt for the careful review of my manuscript and for their many useful suggestions. I wish to thank the other members of the committee, Drs. James C. Wu, Paul G. Mayer and Louis H. Bangert for their patient examination of the thesis.

I am grateful for the financial assistance provided by the Army Research Office under Contract Number DAHCOA-73-C-0038.

I wish to acknowledge the moral support given by my brother and sister-in-law. I also thank my fellow graduate students and many acquaintances outside the school for providing stimulating discussions, mostly non-academic, during the long course of this investigation.

My appreciation goes to Mrs. Peggy Weldon for an excellent job done in typing the thesis.

Finally, I wish to thank my parents for their great patience, love and encouragement throughout my life. Their years of selfless sacrifice are greatly appreciated.

TABLE OF CONTENTS

TABLE OF CONTENTS (Continued)

LIST OF TABLES

LIST OF ILLUSTRATIONS

LIST OF ILLUSTRATIONS (Continued)

LIST OF ILLUSTRATIONS (Continued)

NOMENCLATURE

a	speed of sound
A	centerline velocity parameter in Green's Profiles; area
A_u	$\int_0^{\delta} \frac{U}{U_e}\, rdr$
A_1	$\int_0^{\delta} \frac{\rho U}{\rho_e U_e}\, rdr$
A_1'	$\int_0^{\delta} \frac{U_i}{U_{e,i}}\, \eta' d\eta'$
A_2	$\int_0^{\delta} \frac{\rho U^2}{\rho_e U_e^2}\, rdr$
A_2'	$\int_0^{1} \frac{U_i^2}{U_{e,i}^2}\, \eta' d\eta'$
A_3	$\int_0^{\delta} \frac{\rho U^3}{\rho_e U_e^3}\, rdr$
A_3'	$\int_0^{1} \frac{U_i^3}{U_{e,i}^3}\, \eta' d\eta'$
B	centerline enthalpy parameter in Green's Profiles
c_p	specific heat at constant pressure
$C_{p,B}$	base pressure coefficient, $\frac{p_B - p_1}{1/2\ \rho_{e1} U_{e1}^2}$
D	denominator
h	static enthalpy; constant magnitude core region in Green's profiles

NOMENCLATURE (Continued)

H stagnation enthalpy

H_1' shape parameter, $\dfrac{A_1' - A_2'}{0.5 - A_1'} = \dfrac{\int_0^1 \dfrac{U_i}{U_{e,i}} \left(1 - \dfrac{U_i}{U_{e,i}}\right) \eta' d\eta'}{\int_0^1 \left(1 - \dfrac{U_i}{U_{e,i}}\right) \eta' d\eta'}$

H_2' shape parameter, $\dfrac{A_1' - A_3'}{0.5 - A_1'} = \dfrac{\int_0^1 \dfrac{U_i}{U_{e,i}} \left(1 - \dfrac{U_i^2}{U_{e,i}^2}\right) \eta' d\eta'}{\int_0^1 \left(1 - \dfrac{U_i}{U_{e,i}}\right) \eta' d\eta'}$

I injection parameter $\dfrac{\text{mass injected}}{\rho_{e1} U_{e1} A_B}$

K constant in eddy viscosity model

ℓ shear layer thickness

ℓ_c characteristic length

$\dot{m}$ mass flow rate

M Mach number

n parameter in Kubota et al. profiles; natural normal coordinate

N numerator; Nash's reattachment factor

p, P pressure

P_v parameter in Green's profiles, h_i/δ_i

r radial coordinate

R gas constant; base radius; radius of curvature

R_1 $-\dfrac{1}{\rho_e U_e^3} \int_0^\delta U \dfrac{\partial}{\partial r} (r\tau_T) dr$

NOMENCLATURE (Continued)

R_1' $\int_0^1 \left(\frac{\partial U_i/U_{e,i}}{\partial \eta'} \right)^2 \eta' d\eta'$

s natural streamline coordinate

S entropy

T temperature

U axial velocity

U_c characteristic velocity

v radial velocity

V total velocity

x axial coordinate

y radial distance from stagnation streamline

Y radial distance from body, (r - R)

γ ratio of specific heats

Δ_1 thickness of inner portion of boundary layer

Δ_2 thickness of inner portion after expansion

δ boundary layer or wake thickness

δ_2 thickness of viscous layer after separation

ϵ_T turbulent eddy viscosity

η incompressible radial coordinate; characteristic direction

η' non-dimensional incompressible radial coordinate, $\frac{\eta}{\delta_i}$

θ momentum thickness; flow angle

μ Mach angle defined by Eq. (4-13)

μ_T turbulent viscosity

ν Prandtl-Meyer angle defined by Eq. (4-13)

NOMENCLATURE (Continued)

ξ	incompressible axial coordinate; characteristic direction
ρ	density
τ_T	turbulent shear stress
ψ	streamfunction for compressible flow
Ψ	streamfunction for incompressible flow

Subscripts

b,B	value at the base
e,E	value in external flow
i	incompressible quantities
o	value at centerline; stagnation quantity
r	reference quantity
s	streamline
w	wall
∞	value at large distance
1	upstream condition
2	after expansion

Superscripts

*	value on stagnation streamline
^	normalized quantities

SUMMARY

An integral method is presented for the solution of the near wake problem in supersonic flight for the case of fully turbulent, axially symmetric flow behind bluff-base bodies. The method is an extension of the developments in wake flow associated with the names of Crocco-Lees, Reeves-Lees and Alber-Lees. The present model is for the case of adiabatic flow and essentially involves the investigation of three regions -- the corner region, the inviscid outer region, and the inner viscous region.

The solution of the corner region provides the initial conditions for the solution of the wake downstream of the base. Exact modelling of this region, at present, is not possible. Here, a simple model is proposed and used. The outer inviscid region, which is partially rotational (due to the presence of entropy gradients near the shear layer) and partially irrotational, is treated by an approximate method of characteristics. The use of this method results in an appreciable saving of computer time, and is in harmony with the present approximate technique used for solving the inner region. The inner region is represented by the integrated boundary layer equations. The shear stress is represented by the Boussinesq turbulent viscosity. The turbulent viscosity, in turn, is related to the product of a length and a velocity scale. The unknowns are obtained by a comparison with the self-preserving shear layer solution and far wake solution. Finally, by comparing with base flow experiments, a small compressibility correction factor is added to

shear stress term. The solutions have been obtained using two sets of velocity profiles. A compressible-incompressible transformation and the condition of isoenergeticity are used to evaluate necessary integrals in closed form. Out of the many possible starting solutions, a unique solution is singled out due to the existence of the Crocco-Lees singularity in the analysis.

The variation of various parameters such as initial boundary layer thickness, Mach number and base bleed, on the near wake has been studied, and the solutions are compared with experiments. The major conclusions arrived at are as follows:

1) Mach number is the primary variable affecting the base pressure. Base pressure decreases with the increase of Mach number. There is good agreement between theory and experiment.

2) The upstream boundary layer thickness is a secondary parameter; the base pressure increases with the increase of boundary layer thickness. Again, good agreement with experimental data is obtained. This indicates that the present modelling of the corner region and shear stress is reasonable for this approximate analysis.

3) The detailed results, such as centerline pressure variation, centerline Mach number variation and shear layer thickness variation agree well with the experiments. Usually, at high Mach numbers, the theory gives smaller pressure gradients in the compression region than the experiments. This is apparently due to the radial variation of pressure in the shear layer in the experiments, which is neglected in the present analysis.

4) At low base bleed rates, the theory shows a much smaller base pressure rise when compared to experiments. The inaccuracy of the boundary layer equations, in representing the region close to the base, may be the major reason for this result.

In general, good agreement with the experimental data is obtained. Result (4) is not considered a serious handicap as the motivation of the present investigation is to provide a computationally fast, yet reasonably accurate, base flow theory for later use in external burning studies.

CHAPTER I

INTRODUCTION

The reduced pressure acting behind the base of a projectile results in a drag component called base drag. The base drag of a body in supersonic flight usually constitutes a substantial portion of the total drag and its calculation and reduction is of great practical importance.

The base flow pattern of a projectile in supersonic flight is shown in Figure 1. A uniform stream with a turbulent boundary layer approaches the base and separates near the corner. Experimentally, it has been observed that the expansion region is followed by a weak lip shock.[1] The viscous part of the separated boundary layer develops into a free shear layer in a region of approximately constant pressure. This constant pressure region is followed by a compression, compression waves coalesce to form a wake or trailing shock away from the axis. The final base pressure is the outcome of the equilibrium of the scavenging effect of the outer flow which tries to reduce the base pressure and the viscous transport effect, which forms a non-uniform velocity flow. The flow velocity of the shear layer which is unable to overcome the sharp pressure rise is reversed to form a recirculatory region, while higher velocity fluid escapes to the downstream wake.

A number of methods are presently under investigation for reducing the base drag. These methods can be categorized under base bleed, base

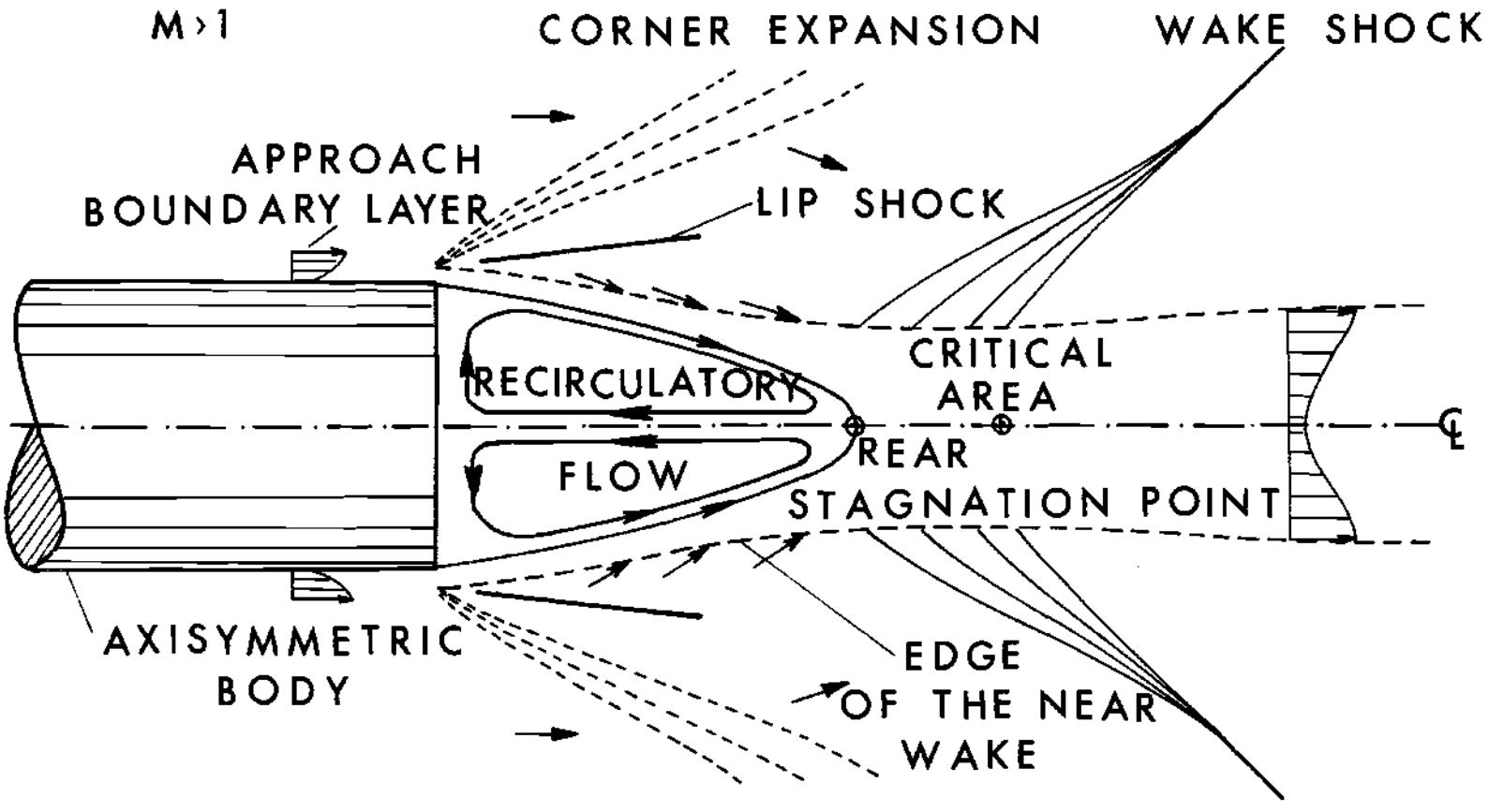

Figure 1. Schematic Representation of Axisymmetric Base Flow Field.

burning, external burning, or a combination of these, and are schematically shown in Figure 2. Inclusion of these methods may bring a slight change in the conventional base flow picture described above. For example, it is possible to blow off the complete recirculatory region by large mass injection through the base[2] or have a compression in the initial region instead of a corner expansion fan with external burning.[3,4]

The external burning method, as shown in Figure 2, usually involves combustion in the inviscid portion of the near wake. This method, as first applied by Strahle[3] to the simple two dimensional case, showed that significant base drag reduction can be obtained using this concept. In order to apply this concept to a practical projectile, which is often axisymmetric, it is first necessary to construct a satisfactory axisymmetric base flow theory. The complete solution of the Navier-Stokes equations for the turbulent recirculatory flows are still in the early stages of development. Further, these solutions are tedious and very time consuming and, hence, are not very attractive for preliminary investigations and design. In this dissertation, an approximate axisymmetric base flow theory for the near supersonic turbulent wake, based on the Crocco-Lees[5] approach is described. The present model allows for base bleed, as base bleed may be a promising adjunct to external burning to improve the performance. Also, an entropy layer in the inviscid stream has been included, because several concepts of external burning would introduce the fuel by injection into the supersonic stream, causing injection shocks.

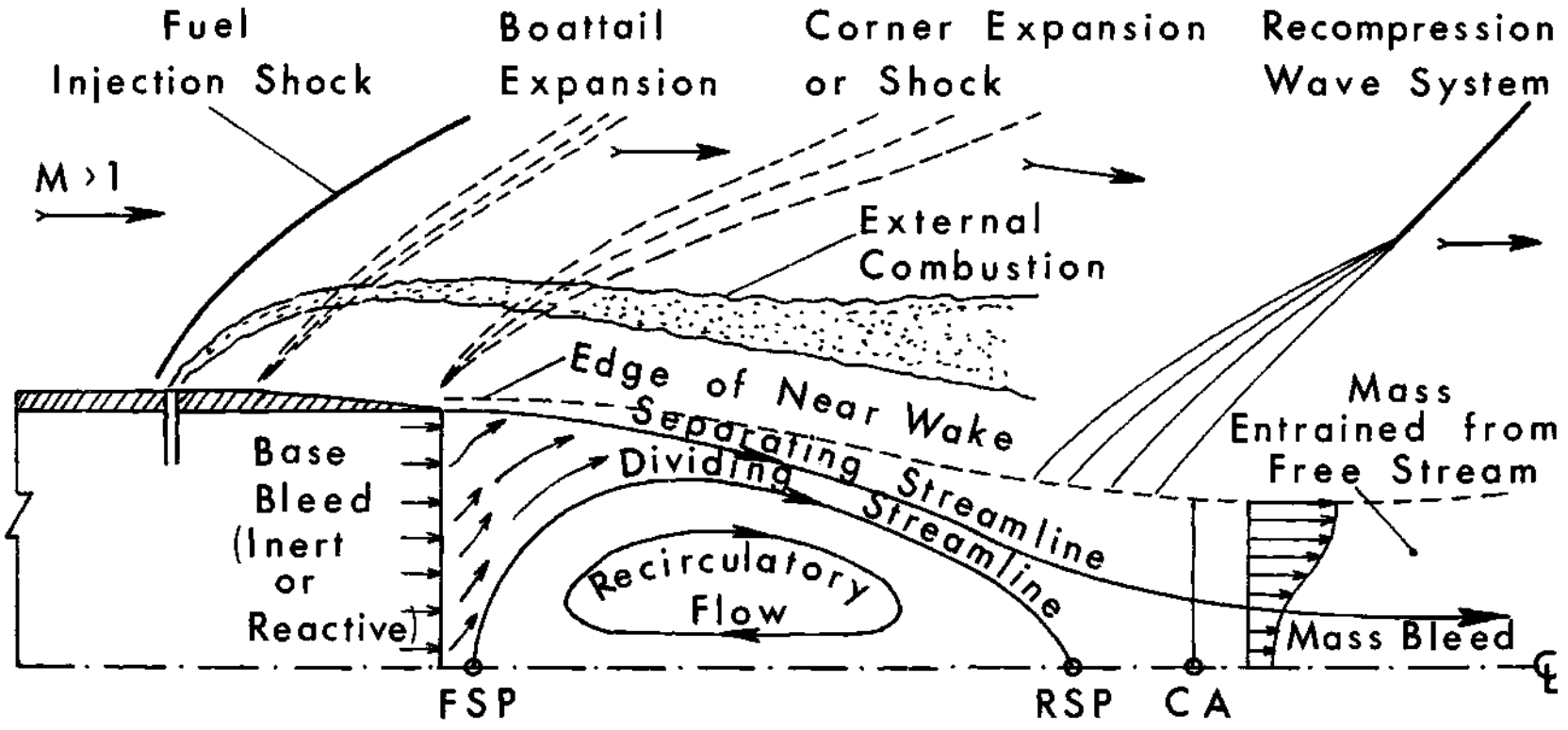

Figure 2. Base Flow with External Burning and Base Bleed. CA = Critical Area, FSP = Forward Stagnation Point, RSP = Rear Stagnation Point.

Background

Early studies of base flow problems concentrated upon obtaining a correlation between base pressure and Mach number.[6-14] Cope[12] and Chapman,[14] working independently, presented a model elucidating the essential features of the flow behind the base of a bluff-body. Chapman, in his correlation, also included the effect of the Reynolds number and the boundary layer thickness.

In the early 1950's, two approximate methods of solving the base flow problem appeared in the literature, and are known as the Crocco-Lees[5] method and the Chapman[10,15] and Korst[16] method. These two lines of approach are still attractive for current research in the field of base flows. The Chapman and Korst approach rests on the dissection of the complete near wake flow field into its constituent parts, each of which is solved separately. The complete solution is then obtained by merging these individual solutions together with appropriate matching conditions. Chapman[10,15] assumed a constant pressure behind the base. The dividing streamline, calculated using the boundary layer equations, is a straight line. The unique base pressure solution is then obtained by imposing the condition that the total pressure obtained by isentropic compression along the dividing streamline is equal to the terminal static pressure. Korst[16] and Kirk[17] independently tackled the corresponding turbulent base flow problem using an expression for the mixing coefficient. Korst assumed that compression in the inviscid flow takes place through the trailing shock. Nash[18] pointed out that if the boundary layer was properly accounted for, the Korst and Kirk results were at

variance with the experimental results. He further pointed out that it is erroneous to assume that the reattachment factor, N ($= \frac{\text{Reattachment pressure}}{\text{Total pressure rise}}$), is equal to 1.0 and suggested that N should be evaluated empirically. It was found that N varies from 1.6 to 0.35 from the incompressible to the high supersonic range. McDonald[19] regarded the use of the factor N too empirical, as it depended upon both Reynolds number and Mach number. He suggested that the shape parameter ($\frac{\delta^*}{\theta}$) of the boundary layer at reattachment should be used as the downstream boundary condition. McDonald,[20,21] Hill,[22] Przirembel and Page,[23] Mueller,[24] and Roache[25] extended the analysis to axisymmetric flow configurations. The strong point of this approach is its simplicity. However, certain basic uncertainties and restrictions, such as (a) matching conditions and their dependence on various parameters like boundary layer thickness, Mach number, and base bleed, (b) the effect of loss of detail in the recompression region because of sudden recompression in this model, and (c) an unsatisfactory explanation for the Crocco-Lees singular point, still mar this physically easily understandable model. Ref. (26) presents a survey of the literature related to this method.

The Crocco and Lees[5] method can be called an extension of Karman's momentum integral method, applied to separated flows. Surprisingly good results and trends were obtained even though the validity of the boundary layer approximation in the near wake still remains in question. The method essentially involves maintaining a balance between the external flow described by inviscid flow equations, and the inner viscous flow, represented by integral equations. Using a compressibility

transformation and a semi-empirical model for viscous mixing, with other simplifications, a relation between the integral properties of the flow was obtained for the two dimensional case. It was established that unlike the potential flow solutions of the problem, a unique solution is obtained because of the presence of a saddle point singularity (called the critical point in the solution), and no empirical downstream boundary condition is required. The saddle point singularity has a physical significance similar to that of the throat of a deLaval nozzle. Thus, in spite of the use of the boundary layer equations, the base flow problem is found to be of boundary value nature (unlike the usual boundary layer problem where all the conditions are applied on the starting boundary). Davis[27] and deKrasinski[28] extended this analysis to the axisymmetric case. Reeves and Lees[29] replaced the semi-empirical mixing rate of Crocco-Lees by a mechanical energy relation for the two dimensional laminar case. The velocity profiles chosen were Stewartson solutions[30] of the Falkner-Skan equation (or Cohen and Reshotko[31] solutions for the non-adiabatic case). Golik, Webb and Lees[32] tried to improve the solution using higher moment equations and more free parameters. They ran into a large recirculation region and matching difficulties. Alber and Lees,[33] using an eddy viscosity model, extended Reeves and Lees' analysis to the two dimensional turbulent case, with very good quantitative comparison with experiments (for a more complete list of references, see Ref. (34)).

Recently, some attempts have been made to employ the differential equations to either partially or completely solve the near wake.

Ohrenberger and Baum[35] used the integral laminar boundary layer equations for the recirculatory region. The flow was taken as non-isoenergetic and the shear stress contribution near the axis in the centerline energy equation was included. This resulted in another saddle point singularity which determined the initial condition for enthalpy near the base. The outer flow, governed by the parabolic type equations, was solved using an implicit-finite difference scheme and was matched with the inner region. Weiss[36] treated the recirculation region using the complete Navier-Stokes equations and coupled it with an adjacent shear layer (computed by using the boundary layer equations) and an outer rotational inviscid flow. The method required large computation time, particularly at higher Reynolds number. Some other studies made using the full Navier-Stokes equations are given in Refs. (37-39). However, the solutions of the complete Navier-Stokes equations applicable to the turbulent near wake are still in the early stages of development.

Objectives

The objective of the present work is to provide a comparatively fast, yet reasonably accurate, axisymmetric turbulent supersonic base flow theory for preliminary design purposes and for later use in external burning studies. Any attempt at employing the full Navier-Stokes equations is ruled out, as it would be both complex and time consuming on a computer. As pointed out earlier, the Chapman and Korst approach has certain basic deficiencies, and, without many experimental guidelines, it is not clear what changes in assumptions would be required to accommodate external burning. Hence, the Crocco-Lees approach is

selected, and it is decided to extend the work of Alber and Lees with necessary modifications. In this dissertation, the effect of the upstream boundary layer thickness, upstream Mach number and base bleed on the supersonic, turbulent near wake flow field of an axisymmetric body are studied, and the results are compared with the experiments.*

*An independent work,[40] closely related to the present one, recently appeared in the report literature and will be discussed in the last chapter.

CHAPTER II

FLOW MODEL AND OUTLINE OF PROBLEM APPROACH

Base flow is one problem where theory lags behind experiment. Experimental studies made on the flow behind the bluff bodies have helped to delineate the various features of the near wake flow field and also have shed light on their relative importance. This, in turn, has helped in making justifiable approximations in order to simplify analytical modelling. In this chapter, these experimental observations and the flow model adopted for analytic investigation are described. Also, an outline of the present approach is given.

Flow Model

The conventional base flow pattern of a projectile in supersonic flight is shown in Fig. 1 and has been described in the Introduction. However, some of the features described are found to be of secondary importance and can be neglected, under certain situations, in a simplified theory, such as the present one. It has been shown by previous studies[1,41,42] that at moderate Mach numbers, the lip shock and the lip shock-wake shock interactions have secondary effects on the base flow and hence will be neglected in the present analysis of the near wake. Also the work of Hastings[42] showed that after such extreme expansions, as occurring in most cases, the viscous forces remain predominant only in a small portion of the initial boundary layer. The outer portion of the boundary layer transforms into an almost inviscid

but rotational layer. Also, a rotational layer can be caused in the inviscid stream due to the presence of injection shocks and external burning.

Hence, with the inclusion of these modifications, the near wake flow field (without base bleed or combustion) considered here for the analytical modelling can be schematically represented by Figure 3. A uniform supersonic flow at constant pressure and Mach number, with a finite boundary layer thickness, approaches the base of an axisymmetric body. It undergoes a corner expansion near the corner. The viscous part beyond the base consists of (1) the recirculatory region and (2) the shear layer, while the inviscid part consists of (3) the rotational layer, which merges into the shear layer, and (4) the irrotational region.

Outline of the Problem Approach

Figure 4 is the flow diagram for the present approach. The input variables are M_{e1}, δ_1/R and I. The unknown of the problem is base pressure, p_b. The complete flow field is assumed to be adiabatic with turbulent Prandtl number equal to 1 and to obey the perfect gas laws. For analysis' sake, the flow field is divided into two parts, viz., the corner flow region and the flow downstream of the base. The flow downstream of the base is further divided into an outer inviscid part and an inner viscous part. To start with, p_b is assumed. The solution of the corner region provides the initial conditions for the flow downstream of the base and is solved by an approximate model described in Chapter III. The outer inviscid part is solved using an approximate method of characteristics (Chapter IV), while the inner viscous part is

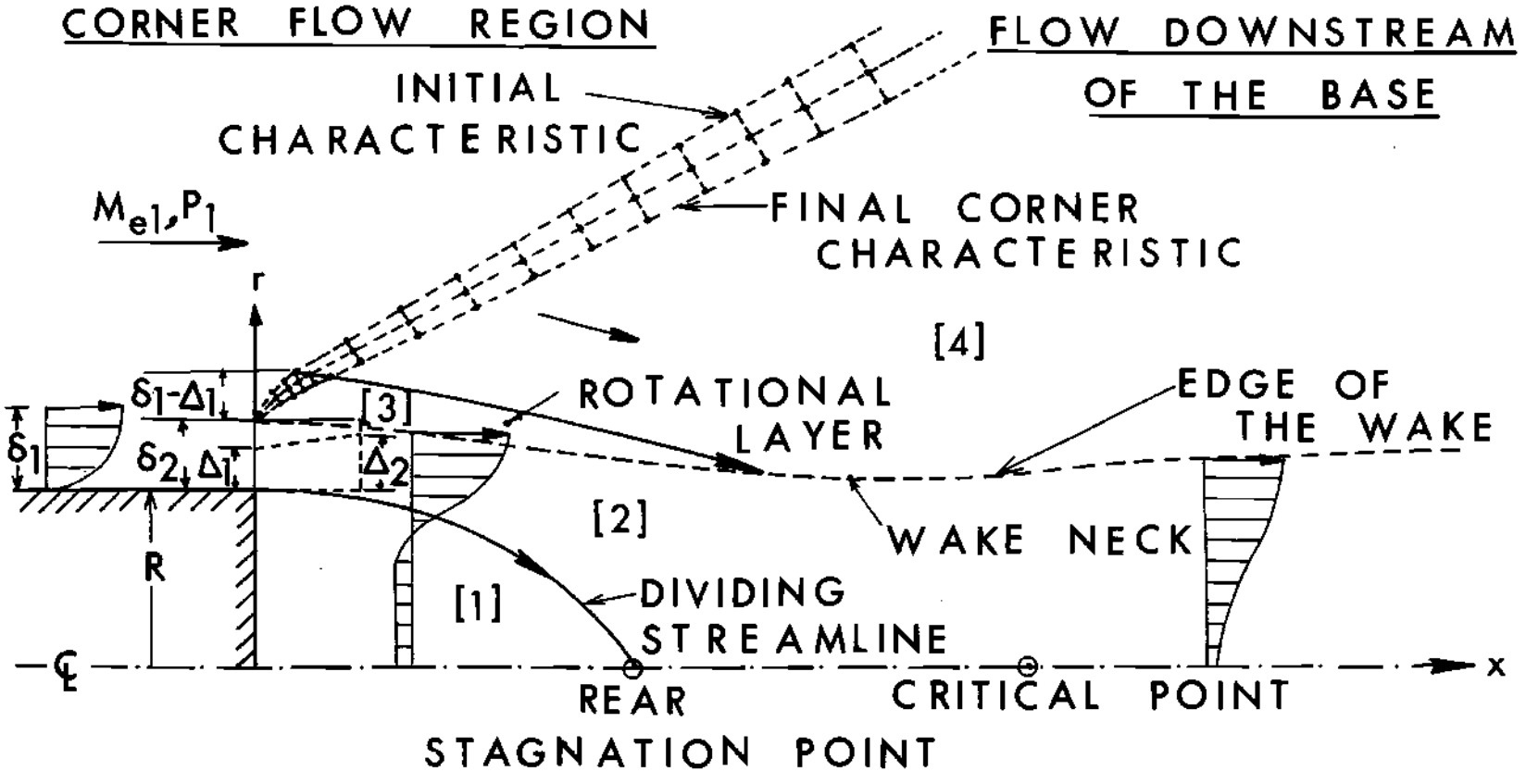

Figure 3. Axisymmetric Supersonic Near Wake Model.

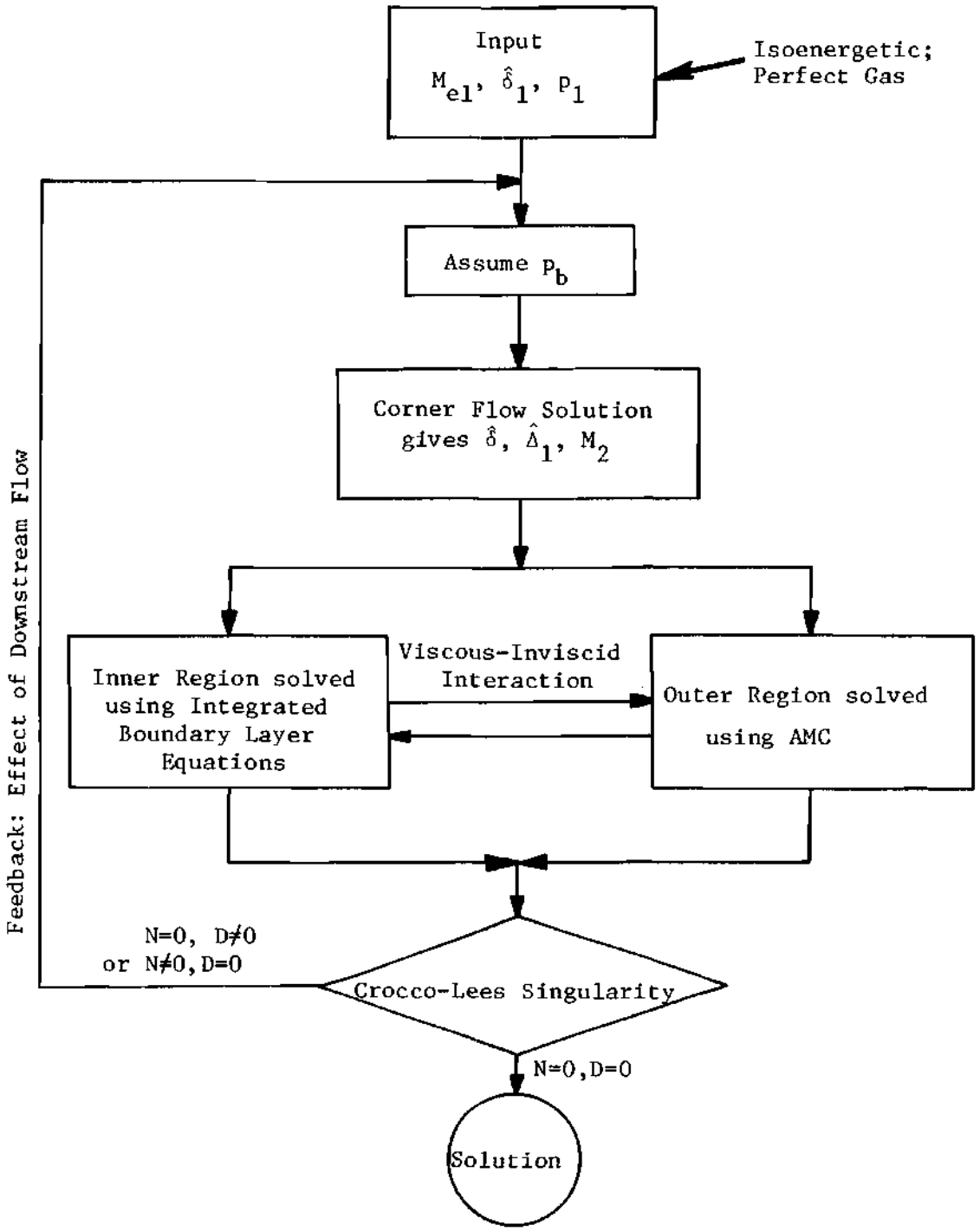

Figure 4. Flow Diagram of the Approach.

assumed to be governed by the boundary layer equations. Since the flow is turbulent, some modelling of shear stress is required. Here the turbulent viscosity concept is used to evaluate the shear stress. The boundary layer equations are integrated in the radial direction using an appropriate set of velocity profiles. The details of handling of shear stress, the governing equations and their solution are discussed in Chapter V. Thus, the simultaneous solution of the inviscid and viscous parts is started as an initial value problem, with a guessed value of base pressure. Downstream of the base, the solution encounters a saddle point singularity (known as the Crocco-Lees critical point). The physical significance of this singularity is the same as that of the throat in the deLaval nozzle, i.e., the flow which is subsonic in the mean to begin with in the shear layer turns supersonic in the mean. This saddle point singularity, in the computer program, arises because the denominator of the solution matrix changes sign before or after the numerator goes through zero, depending on the initial condition. It allows only one of the many solutions that can be started from the base to pass through it smoothly (for which both the numerators and denominator become zero simultaneously), i.e., it provides an extra constraint in the problem. Thus, in spite of the use of the parabolic boundary layer equations in the viscous part, the problem turns out to be a boundary value problem, with base pressure as the eigenvalue, and a unique solution is obtained to the base flow problem.

CHAPTER III

CORNER FLOW REGION

It is necessary to solve the corner flow region in order to obtain the initial conditions for the wake analysis. This region presents one of the most difficult problems in fluid mechanics because of the presence of both axial and transverse pressure gradients. Pressure signals can travel upstream through the subsonic portion of the boundary layer. Some of the work done in this field is given in Refs. (43-47). Experimental evidence shows[46] that the subsonic portion of the boundary layer turns through 90° at the corner and separation occurs below the corner. The major interest in solving the corner region for the present integral approach is to find the thickness of that portion of the boundary layer in which the viscous forces remain predominant. Alber and Lees used an approximate method of finding the thickness of this layer based on a streamtube analysis. The integrated continuity and momentum equations were applied to the control volume (shown in Figure 3 by dotted lines) at the corner. These are

$$\int_0^{\Delta_2} \rho U r dY = \int_0^{\Delta_1} \rho U r dY$$

$$\int_0^{\Delta_2} \rho U^2 dY - \int_0^{\Delta_1} \rho U^2 dY + \Delta_2 p_2 - \Delta_1 p_1 - \int_{\Delta_1}^{\Delta_2} p dY \simeq (\bar{\tau}_w - \bar{\tau}_s)\Delta x$$

(Alber et al. ignored the $\int p dY$ term in their analysis.) To obtain the integrals, the velocity profiles chosen were one seventh power profiles before the expansion and a quadratic profile after the expansion. Δx

is the shear stress interaction length. The shear stress was obtained using the Mellor and Gibson[48] result for a turbulent boundary layer undergoing maximum acceleration. Edge Mach numbers at stations (1) and (2) were related assuming isentropic flow along the boundary streamline. Δ_1 and Δ_2 were obtained by iteration. Two shortcomings were noticed when this analysis, including the $\int pdY$ term in the momentum equation, was tried. First, the magnitude of the shear stress term at the corner is unknown. Second, the results were sensitive to the magnitude of the shear stress term and the shape of the profile after expansion. Some of the profiles tried were quadratic, cubic, one-ninth power and constant velocity profiles. Because of this sensitivity, the above procedure was abandoned, and a simplified model was used.

Corner Expansion Model

The boundary layer is divided into an outer and an inner portion because the shear stresses become negligibly small in the outer portion after expansion. Hence, only the inner portion will contribute to the shear flow after separation. The present approach is to locate the dividing line such that the velocity gradient is smaller than a predefined quantity after expansion.

As the dissipation term is small in the outer portion of the boundary layer, this portion is assumed to undergo an isentropic expansion in the corner region. Thus, the velocity profile of the outer portion after expansion is obtained using the continuity equation and the isentropic relation. Then the ad hoc assumption is made that $\left(\frac{\partial U}{\partial Y}\right)_{\Delta_2} = K_1 \left(\frac{\partial U}{\partial Y}\right)_{\delta_1}$. K_1 is an arbitrary constant; it is of the order of

one as the gradients at the edge of the viscous boundaries are related, and is here taken equal to 1. The implication of this assumption is that the edge of the boundary layer after expansion is defined where the shear stress is of the same order as that on the edge of the boundary layer before expansion. Referring to Figure 5, the procedure followed for obtaining Δ_1 and M_2 for given δ_1,R,M_{e1}, p_b/p_1 (assumed) and using a 1/7th power velocity profile at station 1 is given below.

1) $\Delta_{1,i}$ for i=1 is initially defined as the thickness where $M_{1,i} = 1$ using a 1/7th power law. (From experience, it is found that the final value of Δ_1 is greater than $\Delta)_{M_1=1}$), that is

$$\Delta_{1,1} = \delta_1 \left\{ \frac{1 + \frac{\gamma-1}{2} M_{e1}^2}{(1+\frac{\gamma-1}{2})M_{e1}^2} \right\}^{3.5} \tag{3-1}$$

Other variables at this point are obtained using the following equations

$$M_{1,i} = \sqrt{\frac{(\Delta_{1,i}/\delta_1)^{2/7}}{\frac{1 + \frac{\gamma-1}{2} M_{e1}^2}{M_{e1}^2} - \frac{\gamma-1}{2} (\frac{\Delta_{1,i}}{\delta_1})^{2/7}}} \tag{3-2}$$

$$U_{1,i} = \sqrt{\gamma RT_o} \sqrt{\frac{M_{1,i}^2}{1 + \frac{\gamma-1}{2} M_{1,i}^2}} \tag{3-3}$$

$$\rho_{1,i} = \frac{P_1}{RT_o} (1 + \frac{\gamma-1}{2} M_{1,i}^2) \tag{3-4}$$

2) $M_{2,i}$ etc., the corresponding quantities after expansion, are then solved for using the isentropic relations along the streamline. $r_{2,1}$ is taken equal to $r_{1,1}$.

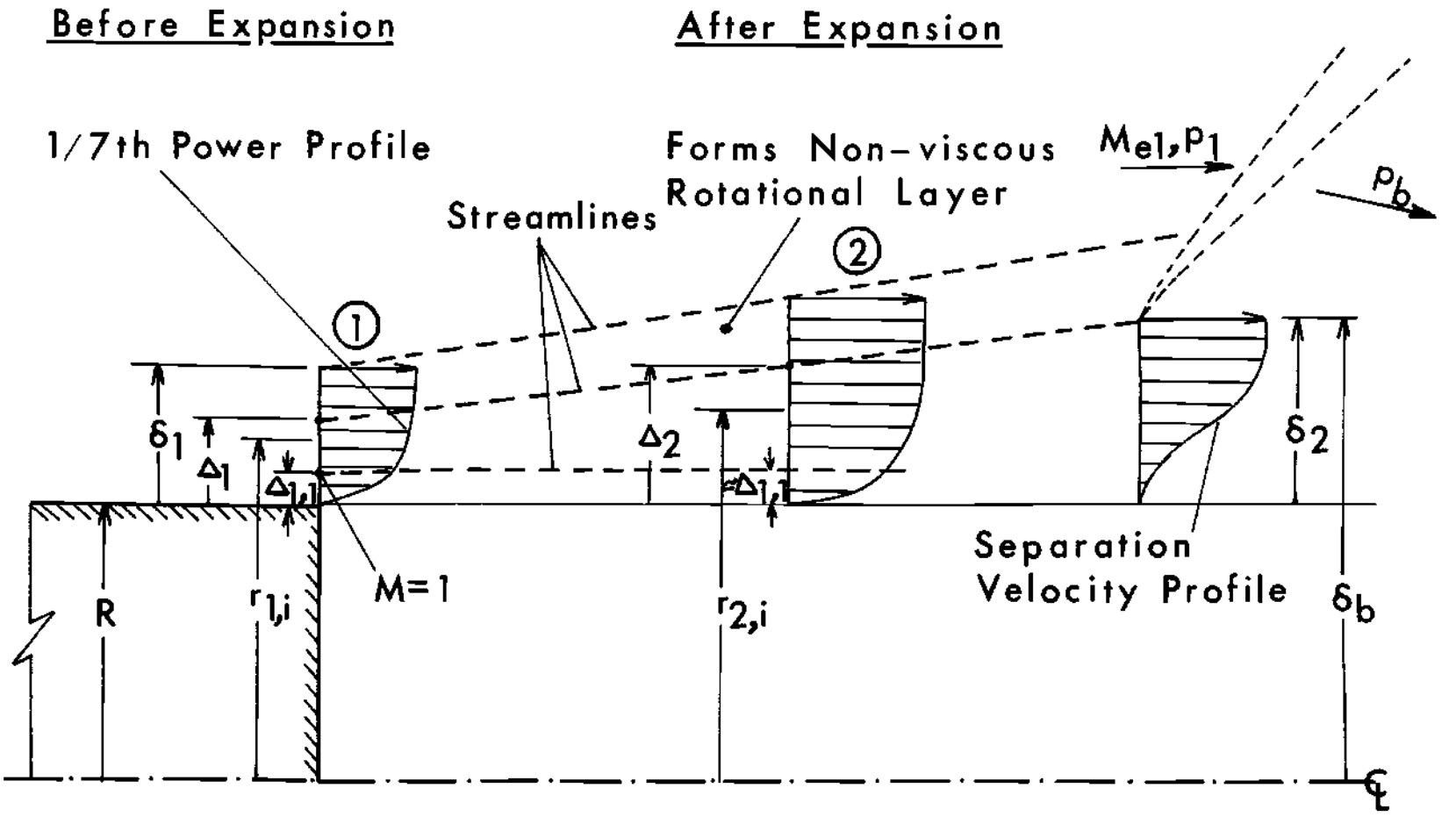

Figure 5. Corner Region Model.

$$M_{2,i} = \sqrt{\frac{\left\{1 + \frac{\gamma-1}{2} M_{1,i}^2\right\}\left(\frac{P_1}{P_b}\right)^{\frac{\gamma-1}{\gamma}} - 1}{\frac{\gamma-1}{2}}} \tag{3-5}$$

$$U_{2,i} = \sqrt{\gamma R T_o}\sqrt{\frac{M_{2,i}^2}{1 + \frac{\gamma-1}{2} M_{2,i}^2}} \tag{3-6}$$

$$\rho_{2,i} = \frac{P_1}{RT_o}\frac{P_b}{P_1}\left(1 + \frac{\gamma-1}{2} M_{2,i}^2\right) \tag{3-7}$$

3) An increment of ε_1 (to start with $0.1\delta_1$) is given to $\Delta_{1,i}$ to obtain $\Delta_{1,i+1}$. $M_{1,i+1}$, $U_{1,i+1}$ etc. using Eqs. (3-2) to (3-7). ε_2, the corresponding incremental thickness at station 2 is then obtained using the continuity equation.

$$A_{1,i+1} = \pi(r_{1,i+1}^2 - r_{1,i}^2) \tag{3-8}$$

$$A_{2,i+1} = \frac{(\rho U)_{1,i} + (\rho U)_{1,i+1}}{(\rho U)_{2,i} + (\rho U)_{2,i+1}} A_{1,i+1} \tag{3-9}$$

$$\varepsilon_2 = \sqrt{\frac{A_{2,i+1}}{\pi} + r_{2,i}^2} - r_{2,i} \tag{3-10}$$

$$r_{2,i+1} = r_{2,i} + \varepsilon_2 \tag{3-11}$$

4) The slope at station 2 is then equal to $(U_{2,i+1} - U_{2,i})/\varepsilon_2$. If it is larger than $\left(\frac{\partial U}{\partial Y}\right)_{\delta_1}$, which is here $U_e/7\delta_1$, steps 3 and 4 are repeated.

Convergence is then obtained by reducing the increment by half. The error in Δ_1 allowed in the present calculations is 0.01 δ_1. Table 1 gives some sample results.

Table 1. Sample Results for the Corner Flow Region

M_{e1}	p_b/p_1	δ_1/R	Δ_1/δ_1	Δ_2/δ_1
1.5	1	0.2	1	1
1.5	0.6	0.2	0.56	1.33
3.0	0.6	0.2	0.57	1.78
3.0	0.4	0.2	0.36	1.41
3.0	0.4	0.6	0.37	1.26

As intuitively expected, this formulation says that with no expansion (as with mass bleed or external burning), the whole of the boundary layer should be considered. The above results show that as the expansion ratio becomes larger, a smaller amount of the initial boundary layer will form the initial shear layer after expansion (which agrees with Hastings' observation). Admittedly, this analysis is simplified, but it will be later shown to pick up proper experimental trends.

Next, the Mach number, entropy, etc., on the initial characteristic are determined by assuming a one seventh power law again in the boundary layer, isoenergetic flow and constant pressure along the characteristic. The relations used in the outer portion of the boundary layer are

$$M = \sqrt{\left(\frac{y}{\delta_1}\right)^{2/7} * \frac{1}{\frac{1 + \frac{\gamma-1}{2} M_{e1}^2}{M_{e1}^2} - \frac{\gamma-1}{2} \left(\frac{y}{\delta_1}\right)^{2/7}}} \qquad (3\text{-}12)$$

$$S = c_p * \log\left(\frac{1 + \frac{\gamma-1}{2} M_{e1}^2}{1 + \frac{\gamma-1}{2} M^2}\right) \qquad (3\text{-}13)$$

assuming that the entropy of freestream is zero.

In reality, the expansion at the base, even for a body with sharp corner, is distributed over a finite distance because of the presence of the boundary layer. However, this distance is small for sharp edged bodies, and here, the expansion at the base is assumed to be corner expansion. The origin for this corner expansion is taken at a distance equal to the thickness of the viscous layer after separation, δ_2, as shown in Figure 3. δ_2 and Δ_2 are related through mass conservation equation.

CHAPTER IV

OUTER INVISCID REGION

In a strong interaction problem, as the present one, the solution of the outer inviscid portion is not known *a priori* and has to be obtained by solving both the viscous and inviscid regions simultaneously. Specifically, the unknowns obtained by solving the outer region are entropy and the flow angle at the edge of the shear layer. The outer flow after the base in the present formulation, as described in Chapter II and shown in Figure 3, in general consists of two parts, *viz.*, the rotational inviscid region adjacent to the shear layer, and the irrotational inviscid region. As these regions are both supersonic and inviscid, the governing equations are hyperbolic in nature, and the method of characteristics can be used to solve these regions. However in contrast with the irrotational planar case, the external flow in the present axisymmetric case is more complicated. In the former case, the geometry of the flow field is not involved in the relations of flow variables (that is, the characteristics are reducible) and for an initially uniform flow, the Prandtl-Meyer relation can be employed to relate M and θ. In the present case, the flow variables are functions of location, and the complete characteristic net has to be created. Thus, the accuracy of the solution in this region depends on the mesh size and on the allowable errors in the iterations. The present modelling of the inner viscous

flow region is approximate, and hence, there is no need to solve the outer flow with extreme accuracy, as this would result in a large computer time with no assurance of accuracy improvements. Webb[49] suggested the use of only right running characteristics, as the left running characteristics have only a weak effect. He showed that while the Prandtl-Meyer relation is a very poor approximation in the axisymmetric case, his approximate method compares favorably with the exact solution, except where the flow angles are small. A preliminary investigation showed additionally that at large distances downstream, Webb's method is inaccurate.

Here, an approximate method of characteristics (AMC), which is a combination of Webb's approach and the complete method of characteristics is used in solving the outer inviscid region. The AMC and its use is described below.

The Approximate Method of Characteristics

The governing equations for steady, inviscid, isoenergetic axisymmetric flow assuming a perfect gas in streamline coordinates are:[50]

continuity

$$\rho U r \, \Delta n = \text{constant} \tag{4-1}$$

s-momentum

$$\rho U \frac{\partial U}{\partial s} = -\frac{\partial p}{\partial s} \tag{4-2}$$

n-momentum

$$\rho \frac{U^2}{R} = -\frac{\partial p}{\partial n} = \rho U^2 \frac{\partial \theta}{\partial s} \tag{4-3}$$

Energy

$$h + \frac{U^2}{2} = H_o \tag{4-4}$$

Auxilliary thermodynamic relation

$$TdS = dh - \frac{1}{\rho} dp \tag{4-5}$$

These equations can be combined to give the following relations:

$$T \frac{\partial S}{\partial s} = 0 \tag{4-6}$$

$$\frac{\cot^2 \mu}{V} \frac{\partial V}{\partial s} - \frac{\partial \theta}{\partial n} = \frac{\sin \theta}{r} \tag{4-7}$$

$$\frac{1}{V} \frac{\partial V}{\partial n} - \frac{\partial \theta}{\partial s} = - \frac{T}{V^2} \frac{dS}{dn} \tag{4-8}$$

Eq. (4-6) states that entropy is constant along streamlines. Eqs. (4-7) and (4-8) can next be written in terms of characteristic coordinates. As shown in Figure 6, characteristic directions are inclined at the Mach angle to the streamline, i.e., inclined at $\theta \pm \mu$ to the horizontal direction. Eqs. (4-7) and (4-8) become

$$\frac{\partial}{\partial \eta} (\nu - \theta) = \sin \mu \frac{\sin \theta}{r} - \frac{\cos \mu}{V^2} T \frac{dS}{dn}$$

$$\frac{\partial}{\partial \xi} (\nu + \theta) = \sin \mu \frac{\sin \theta}{r} + \frac{\cos \mu}{V^2} T \frac{dS}{dn}$$

Using the geometrical relations

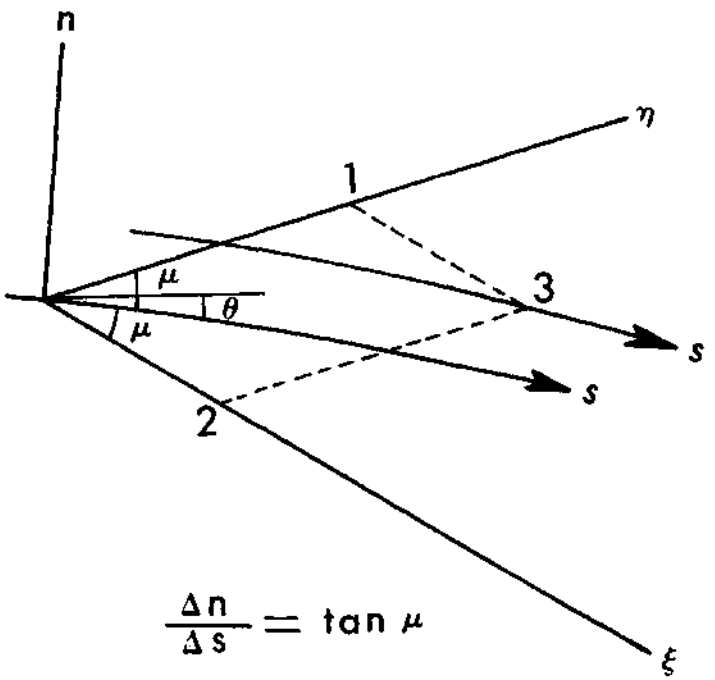

Figure 6. Relation of Characteristics to Natural Coordinates, and the Characteristic Net Work.

$$\frac{\partial \eta}{\partial n} = \text{cosec } \mu \text{ and } \frac{\partial \xi}{\partial n} = - \text{ cosec } \mu$$

one gets,

$$\frac{\partial}{\partial \eta} (\nu - \theta) = \sin \mu \frac{\sin \theta}{r} - \frac{\cot \mu}{\gamma RM^2} \frac{\partial S}{\partial \eta} \quad \text{along } \eta\text{-characteristic} \qquad (4\text{-}9)$$

and $$\frac{\partial}{\partial \xi} (\nu + \theta) = \sin \mu \frac{\sin \theta}{r} - \frac{\cot \mu}{\gamma RM^2} \frac{\partial S}{\partial \xi} \quad \text{along } \xi\text{-characteristic} \qquad (4\text{-}10)$$

Referring to Figure 6, if the properties at points 1 and 2 are known, the properties at point 3 can be written in finite difference form as follows:

$$\nu_3 + \theta_3 = \nu_1 + \theta_1 + \sin \mu_1 \frac{\sin \theta_1}{r_1} \Delta \xi_{13} - \frac{\cot \mu_1}{\gamma RM_1^2} (S_3 - S_1) \qquad (4\text{-}11)$$

$$\nu_3 - \theta_3 = \nu_2 - \theta_2 + \sin \mu_2 \frac{\sin \theta_2}{r_2} \Delta \eta_{23} - \frac{\cot \mu_2}{\gamma RM_2^2} (S_3 - S_2) \qquad (4\text{-}12)$$

Eqs. (4-6), (4-11) and (4-12) with the geometrical relations are sufficient to locate and to find the properties of point 3. Here, however, two points should be noted. First, to solve for ν_3 and θ_3 using Eqs. (4-11) and (4-12), a priori knowledge of the entropy at point 3 is required. Hence, S_3 has to be assumed, and then fixed by iteration using the continuity relation to find the streamline passing through point 3. Usually two iterations are sufficient. Second, the Prandtl-Meyer function is difficult to invert to find the Mach number or the Mach angle. It is found very advantageous from a computer time point of view to

curve fit M as a function of ν using a rational function technique (given in the Appendix), and the error in M is found to be less than 10^{-4} in the Mach number range of 1·5 and 4·0.

Knowing the properties on the initial characteristic (Chapter III), the pressure ratio, p_b/p_1, using Prandtl-Meyer expansion at the corner, and N number of corner characteristics (usually 5), properties on the final characteristic are found. Also, the streamline separating the rotational and irrotational inviscid regions is traced resulting in N-1 more points on the final corner characteristic than on the initial corner characteristic in the rotational region. Next the location and pressure of the point Δx downstream at the edge of the shear layer are found by solving the inner viscous flow (Chapter V). The entropy is found by tracing the streamline passing through this point. M, ν and μ are calculated using the relations

$$M = \sqrt{\frac{1}{\frac{\gamma-1}{2}} \left\{ \frac{1 + \frac{\gamma-1}{2} Me_1^2}{\exp\left(\frac{S}{c_p} - \frac{R}{c_p}\right)} \right\}}$$

$$\nu = \sqrt{(\gamma-1)} * \tan^{-1}\sqrt{\frac{M^2-1}{\gamma-1}} - \tan^{-1}\sqrt{M^2-1}$$

$$\mu = \sin^{-1}\left(\frac{1}{M}\right) \qquad (4\text{-}13)$$

Now θ at this point can be found using Eq. (4-11) if the origin of the right running characteristic passing through this point on the left running characteristic at the previous point can be located. This is done by iteration. Because of the discontinuity of the properties

at the lattice points, sometimes convergence is not obtained. To overcome this difficulty, r, θ and ν are curve fitted as functions of x using second degree polynomials.

As shown in Figure 7, if the net is drawn after each streamwise step, Δx, an extra point can be added on the left running characteristic in the rotational region. Also, as previously stated, such a construction will absorb a lot of computer time. Here, the idea of Webb that the reflected left running characteristics have only a weak effect is employed. The conditions at various points at the edge of the shear layer are found using the right running characteristics only, and the complete characteristic net is constructed only after one of the initial points is absorbed. In the irrotational region, the effect of the left running characteristics is much weaker due to the absence of entropy gradients, and the complete net is constructed only after about fifty steps, with intermediate points again being calculated by Webb's approximate technique. Near the wake region, where the flow angles are small, the error is reduced by taking a smaller step size in the streamwise direction. The present method is found to give a large reduction in computer time without appreciable loss in accuracy.

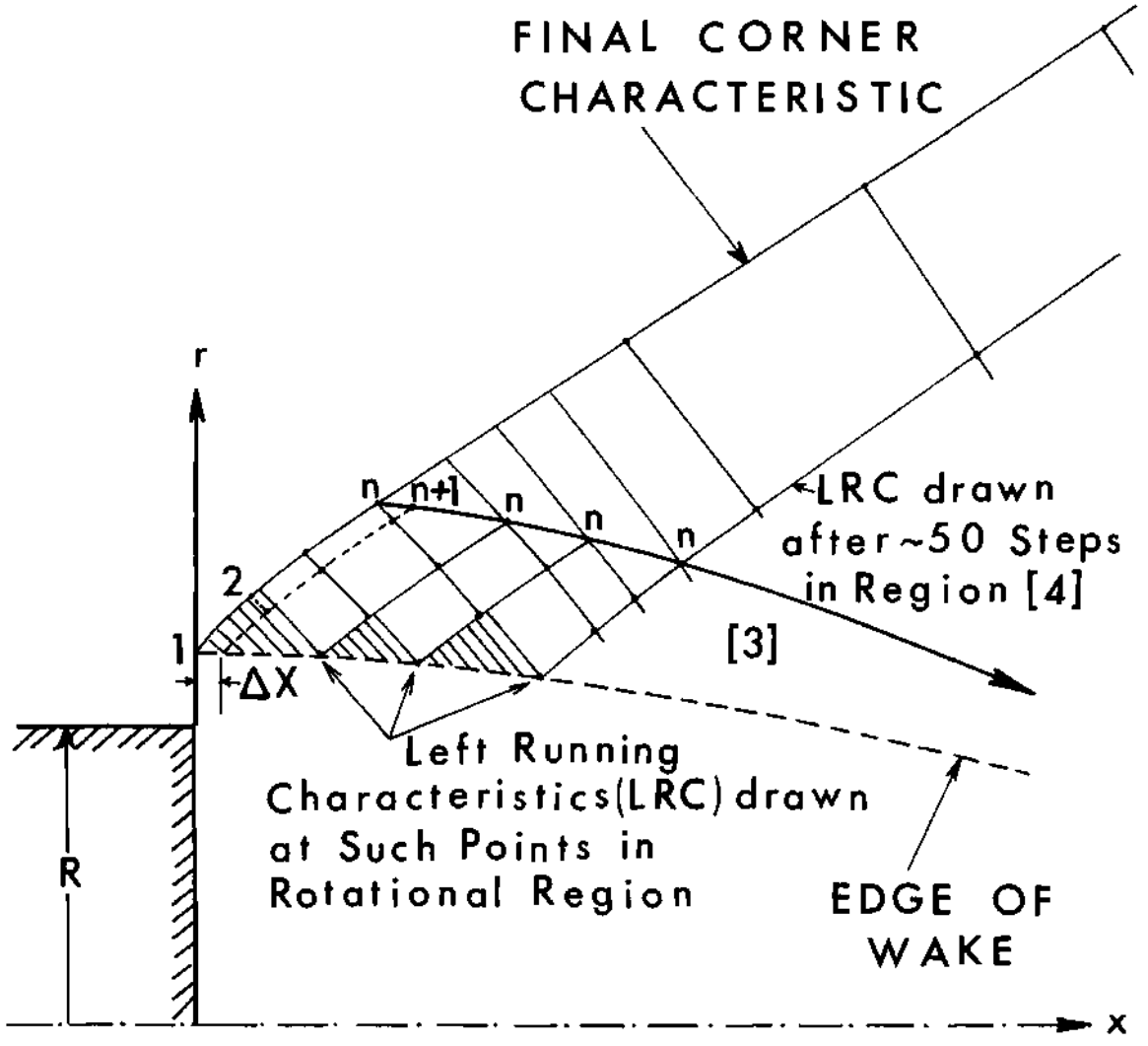

Figure 7. Approximate Method of Characteristics.

CHAPTER V

INNER REGION AND SOLUTION METHOD

The inner region consists of (1) a recirculatory region which is almost inviscid but rotational, and (2) a shear flow region. Even though experiments have shown that radial velocities and radial pressure variations are not negligible in the near wake, the application of the integral boundary layer equations to this region, initially by Crocco and Lees, and later by many others, has yielded quite satisfactory results and experimentally proven trends. Because of the use of the boundary layer equations, the solution is started as an initial value problem. This would have resulted in a non-unique value of the base pressure and hence a non-physical type of solution for the near wake, just like in the inviscid case, were it not for the presence of a saddle point singularity downstream of the base. This singularity imposes an extra constraint on the problem, resulting in a unique solution. Alber and Lees' extension to the two-dimensional turbulent case, employing an eddy viscosity model, has shown very encouraging results. Proper length scales such as the position of rear-stagnation point, the centerline pressure variation, etc., were obtained. The approach followed for the present axisymmetric case is similar to that of Alber and Lees.

Governing Equations

The flow is assumed adiabatic with turbulent Prandtl number equal to unity. The field equations used in the inner regime, neglecting

normal Reynolds stresses, density correlations etc., are the boundary layer equations for axisymmetric flow, viz.

continuity equation

$$\frac{\partial}{\partial x}(\rho U) + \frac{1}{r}\frac{\partial}{\partial r}(\rho v r) = 0 \tag{5-1}$$

momentum equation

$$\rho U \frac{\partial U}{\partial x} + \rho v \frac{\partial U}{\partial r} = -\frac{dp}{dx} + \frac{1}{r}\frac{\partial}{\partial r}(r\tau_T) \tag{5-2}$$

energy equation

$$H = h + \frac{U^2}{2} = \text{constant} \tag{5-3}$$

The fluid is assumed to be a perfect gas and therefore obeys the following constitutive relations:

equation of state

$$p = \rho RT \tag{5-4}$$

caloric equation

$$h = c_p T \tag{5-5}$$

Next, independent integral equations (partial differential equations integrated in radial direction to obtain ordinary differential equations) are obtained using Eqs. (5-1) and (5-2). As many integral equations as required can be obtained by multiplying the basic equations by different functions of dependent variables before integrating in the radial direction. Although there is no clear-cut proof whether the

lower order momentum equations give better result than the higher order one, it is essential that the equations chosen should be able to cover all the essential physical characteristics of the flow. In the present analysis, three integral equations, namely the overall continuity equation, the overall momentum equation and the mechanical energy equation, are used and are next obtained.

Multiply the continuity equation, Eq. (5-1), by r and integrate from the axis to the edge of the boundary layer, δ.

$$\int_0^\delta \frac{\partial}{\partial x}(\rho U)\, r\,dr + \int_0^\delta \frac{\partial}{\partial r}(\rho v r)\,dr = 0$$

or

$$\int_0^\delta \frac{\partial}{\partial x}(\rho U) r\,dr + \rho_e v_e \delta = 0$$

Interchanging the order of integration and differentiation, one gets

$$\frac{d}{dx}(\rho_e U_e A_1) - \rho_e U_e \delta \frac{d\delta}{dx} = -\rho_e v_e \delta \qquad (5\text{-}6)$$

The first term physically represents the rate of change of mass in the shear layer, while the second and the third terms give the net mass inflow (or outflow) rate into the shear layer. It should be noted that this equation does not usually enter in the treatment of boundary layer flows as it is normally assumed that perturbations caused by the boundary layer on the external flow are negligible. Here v_e is obtained from the solution of the external flow.

Next multiply Eq. (5-2) by r and integrate from 0 to δ,

$$\int_0^{\delta} \rho U \frac{\partial U}{\partial x} r dr + \int_0^{\delta} \rho v \frac{\partial U}{\partial r} r dr = - \int_0^{\delta} \frac{dp}{dx} r dr + \int_0^{\delta} \frac{1}{r} \frac{\partial}{\partial r} (r\tau_T) r dr$$

From the continuity equation, $\int_0^r \frac{\partial}{\partial x} (\rho U)\, r dr = -\rho v r$. Therefore,

$$\int_0^{\delta} \rho U \frac{\partial U}{\partial x} r dr - \int_0^{\delta} \frac{\partial U}{\partial r} \{ \int_0^r \frac{\partial}{\partial x} (\rho U) r dr \} dr = - \frac{dp}{dx} \frac{\delta^2}{2} + \int_0^{\delta} \frac{\partial}{\partial r} (r\tau_T) dr$$

Integrating by parts and again interchanging the order of integration and differentiation operations, one gets

$$\frac{d}{dx} (\rho_e U_e^2 A_2) - U_e \frac{d}{dx} (\rho_e U_e A_1) = - \frac{dp}{dx} \frac{\delta^2}{2} + \tau_1 \qquad (5\text{-}7)$$

Finally, one obtains a mechanical energy equation by multiplying Eq. (5-2) by Ur and integrating from 0 to δ,

$$\int_0^{\delta} \rho U^2 \frac{\partial U}{\partial x} r dr + \int_0^{\delta} \rho U v \frac{\partial U}{\partial r} r dr = - \int_0^{\delta} \frac{dP}{dx} U r dr + \int_0^{\delta} U \frac{\partial}{\partial r} (r\tau_T)\, dr$$

or
$$\int_0^{\delta} \rho U^2 \frac{\partial U}{\partial x} r dr - \int_0^{\delta} U \frac{\partial U}{\partial r} \{ \int_0^r \frac{\partial (\rho U)}{\partial x} r dr \} dr = - \int_0^{\delta} \frac{dP}{dx} U r dr + \int_0^{\delta} U \frac{\partial}{\partial r} (r\tau_T) dr$$

Again interchanging the order of differentiation and integration, one gets

$$\frac{d}{dx} \left(\frac{\rho_e U_e^3 A_3}{2} \right) - \frac{U_e^2}{2} \frac{d}{dx} (\rho_e U_e A_1) = - \frac{dp}{dx} U_e A_u - \rho_e U_e^3 R_1 + \tau_2 \qquad (5\text{-}8)$$

Here τ_1 and τ_2 are calculated from the momentum equation, and are taken non-zero when there is a vorticity layer, as this causes a velocity gradient at the edge. Inclusion of these results in an imbalance of the shear force at the edge. However, the magnitude of these quantities is small, and the change of base pressure caused by including these terms is less than 2%. On the other hand, keeping of these terms overcomes a computational difficulty (caused by negative mass flow rate into the shear layer) in the initial region of compression.

The mechanical energy equation has gained a prestigious position in near wake analysis, as usually it is the only equation which contains the viscous dissipation term and hence the information about the physical features of the flow, i.e., whether the flow is turbulent or laminar.

An extra equation will be required near the base to make the problem solvable, as described later. For simplicity, it is taken as the centerline momentum equation

$$\frac{dp}{dx} = - \rho_o U_o \frac{dU_o}{dx} \qquad (5\text{-}9)$$

No shear stress term is included in Eq. (5-9) because uniform flow is assumed along the centerline near the base, although this is suspected as the cause of some difficulty.

Shear Stress

In addition to the above, an auxillary relation describing the shear stress in terms of the known or calculable flow variables is required. This is the basic difficulty in extending the laminar flow treatment to the turbulent flows. However, many turbulent flow problems

have been satisfactorily solved using a functional relationship similar to the one which exists in laminar flows, viz.,

$$\tau_T = -\rho \overline{u'v'} = \mu_T \frac{\partial U}{\partial Y} \tag{5-10}$$

and μ_T is defined as $\rho\varepsilon_T$. This turbulent viscosity concept was first proposed by Boussinesq,[51] and is used in the present analysis. The basic criterion for the eddy viscosity model to give reasonable results is that the Reynolds shear stress caused by the rate of strain on the mean flow reaches the equilibrium or final value before the interaction between the Reynolds stress and the rate of strain becomes important.[52] To employ the turbulent viscosity concept, it is further necessary to describe the unknown μ_T or ε_T in terms of some known or calculable quantities. Here, an algebraic model of the mixing length form is employed, viz.,

$$\varepsilon_T = K \ell_c U_c \tag{5-11}$$

where ℓ_c and U_c are the characteristic velocity and length of the turbulence scales which dominate in the Reynolds stress. They are conceptually similar to the molecular velocity and the mean free bath. However, they are not fluid properties but are flow dependent.

In general, ℓ_c and U_c vary from point to point in the flow field, both across and along the flow. But in similar flows, where there is only one characteristic length scale and one characteristic velocity scale, the variation of these quantities across the flow is small. Examples of these flows are shear layers, jets and wakes far downstream.

The near wake behind the body does not fall in such categories. However, as Alber and Lees' work with the two-dimensional near wake indicates, the assumption of local similarity in which ℓ_c and U_c are related to the velocity profile scales can lead to satisfactory results in integral formulations, where the global influence of turbulence is important. Such an assumption is made in the present analysis. The values of the quantities on the right hand side of Eq. (5-11) are first fixed by comparing with incompressible simple flows, for which more reliable data is available. Then a compressibility correction is applied to obtain the final form.

Incompressible Eddy Viscosity Model

In near wake problems, the initial flow development is similar to that of a free shear layer, and the coefficient K of Eq. (5-11) can be chosen by comparing it with self-preserving shear layer results. However, the form and coefficient should be consistent with the far wake flow, which in the axisymmetric case requires that ϵ_T varies as $x^{-1/3}$ (53).

After a comparison of various form, the following form is chosen for the characteristic length upstream of the rear stagnation point

$$\ell_{c,i} = \sqrt{\int_0^{\delta_i - \eta_i^*} \frac{U_i - U_{o,i}}{U_{e,i} - U_{o,i}} \left(1 - \frac{U_i - U_{o,i}}{U_{e,i} - U_{o,i}}\right) y_i \, dy_i} \qquad (5\text{-}12a)$$

Downstream of the rear stagnation point ($U_{o,i} = 0$), the characteristic length is taken as

$$\ell_{c,i} = \sqrt{\int_0^{\delta_i} \frac{U_i}{U_{e,i}} \left(1 - \frac{U_i}{U_{e,i}}\right) \eta \, d\eta} \qquad (5\text{-}13a)$$

which is proportional to the square root of the momentum area.

On the basis of Abramovich's[54] study of the mixing between two layers moving at different velocities, $U_{c,i}$ is selected as $(U_{e,i}-U_{o,i})$ in the initial region; that is, in the initial region

$$U_{c,i} = (U_{e,i} - U_{o,i}) \tag{5-12b}$$

For free shear layers, the velocity profile is accurately represented by an error function, viz.

$$\frac{U_i}{U_{e,i}} = \frac{1}{2}\left[1 + \text{erf}\left(\frac{\sigma_i y_i}{\xi}\right)\right]$$

where σ_i is the spreading parameter. The value of σ_i is approximately 11 for incompressible flow. Comparing the value of eddy viscosity obtained using Eqs. (5-12a) and (5-12b) with Schlichting's[55] value, one gets

$$K)_{\text{free shear layer}} \simeq 0.07 \tag{5-14a}$$

Townsend[52] suggested that the two dimensional wake profile,

$$\frac{U_{e,i} - U_i}{U_{e,i} - U_{o,i}} = \exp\left(-\frac{1}{2}\frac{\eta^2}{\ell_o^2}\right) = \exp\left(-\frac{1}{2}\bar{\eta}^2\right) \tag{5-15}$$

is an adequate representation of an axisymmetric wake also. ℓ_o is the width of the mean velocity distribution defined by the condition

$$\frac{U_{e,i} - U_i(\ell_o)}{U_{e,i} - U_{o,i}} = e^{-1/2}$$

Substituting the velocity profile given by Eq. (5-15) into Eq. (5-13a), one gets

$$\ell_{c,i} = \sqrt{\frac{U_i}{U_{e,i}}\left(1 - \frac{U_i}{U_{e,i}}\right)\eta \, d\eta}$$

$$= \sqrt{\frac{U_{e,i} - U_{o,i}}{U_{e,i}} \ell_o^2 \int_0^\infty \exp\left(-\frac{1}{2}\bar{\eta}^2\right)\bar{\eta} \, d\bar{\eta} \left(\frac{U_{e,i} - U_{o,i}}{U_{e,i}}\right)^2 \ell_o^2 \int_0^\infty \left\{\exp\left(-\frac{1}{2}\bar{\eta}^2\right)\right\}^2 \bar{\eta} d\bar{\eta}}$$

As the second term is much smaller than the first one in the far wake,

$$\ell_{c,i} \approx \sqrt{\frac{U_{e,i} - U_{o,i}}{U_{e,i}} \ell_o^2 \int_0^\infty \exp\left(-\frac{1}{2}\bar{\eta}^2\right)\bar{\eta} \, d\bar{\eta}}$$

$$= \sqrt{\frac{U_{e,i} - U_{o,i}}{U_{e,i}} \ell_o^2} = \sqrt{\frac{U_{e,i} - U_{o,i}}{U_{e,i}}} \ell_o \qquad (5\text{-}16)$$

For the axisymmetric wake, Townsend also gives

$$\varepsilon_{T,i} = \frac{1}{R_{T,i}} (U_{e,i} - U_{o,i})\ell_o = \frac{1}{14 \cdot 7} (U_{e,i} - U_{o,i})\ell_o$$

$$= K_{\text{far wake}} \ \ell_{c,i} \ U_{c,i}$$

Substituting Eq. (5-16), one gets

$$K)_{\text{far wake}} \approx 0.07 \qquad (5\text{-}14b)$$

if one defines

$$U_{c,i} = \sqrt{(U_{e,i} - U_{o,i})U_{e,i}} \qquad (5\text{-}13b)$$

Therefore, the above chosen $\ell_{c,i}$ and $U_{c,i}$ give the same value of the coefficient K in the regions where the flow development is similar to free shear layer and to the far wake. Hence, K is taken as 0.07 throughout.

Compressible-Incompressible Transformation and Compressible Eddy Viscosity Form

For a closed form integration to evaluate the integrals and the proper modelling of the eddy viscosity, the following transformation has been used:

$$\eta d\eta = \frac{\rho a_e}{\rho_\infty a_\infty} r dr$$

$$d\xi = \frac{\rho_e a_e}{\rho_\infty a_\infty} dx$$

$$\Psi = \psi \qquad (5\text{-}17)$$

Because

$$\psi_y = \frac{\rho U r}{\rho_\infty} \quad \text{and} \quad \psi_x = -\frac{\rho v r}{\rho_\infty},$$

$$U_i = \frac{\Psi_\eta}{\eta} = \frac{a_\infty}{a_e} U$$

$$v_i = -\frac{\Psi_\xi}{\eta}$$

and

$$\frac{U_i}{U_{e,i}} = \frac{U}{U_e}$$

The field equations are transformed into incompressible form; that is

$$\frac{\partial(U_i \eta)}{\partial \xi} + \frac{\partial(v_i \eta)}{\partial \eta} = 0$$

and

$$U_i \frac{\partial U_i}{\partial \xi} + v_i \frac{\partial U_i}{\partial \eta} = U_{e,i} \frac{dU_{e,i}}{d\xi} + \tilde{\varepsilon}_T \frac{1}{\eta} \frac{\partial}{\partial \eta} \left(\eta \frac{\partial U_i}{\partial \eta}\right)$$

if it is assumed

$$\tilde{\varepsilon}_T = \frac{\rho^2 \varepsilon_T r^2}{\rho_e \rho_\infty \eta^2} = \tilde{\varepsilon}_T(x) \tag{5-18}$$

$\tilde{\varepsilon}_T(x)$, if it has the proper Mach number dependence, is the counterpart of the incompressible eddy viscosity. Alber, in the two-dimensional turbulent case, assuming $\tilde{\varepsilon}_T = \rho^2 \varepsilon_T / \rho_e \rho_\infty = \rho_r^2 / \rho_e^2 \; \varepsilon_{T,i}$ (where $\varepsilon_{T,i} = K \, U_{e,i} \theta_i$), showed that for $\rho_r = \rho_o$, a proper Mach number dependence is obtained, at least for the asymptotic or similar shear layer case. Making a similar assumption, i.e., $\rho^2 \varepsilon_T / \rho_e \rho_\infty = \rho_o^2 / \rho_e^2 \; \varepsilon_{T,i}$, and further assuming that $r^2/\eta^2 = \sqrt{\delta^2/\delta_i^2 \; \rho_e/\rho_o}$ (because for $\eta \to \delta_i$, r^2/η^2 behaves as δ^2/δ_i^2 and for $\eta \to 0$, r^2/η^2 behaves as ρ_e/ρ_o), the following expression for $\tilde{\varepsilon}_T$ is obtained:

$$\tilde{\varepsilon}_T(x) = \frac{\rho^2 \varepsilon_T r^2}{\rho_e \rho_\infty \eta^2}$$

$$= K \left(\frac{\rho_o}{\rho_e}\right)^{3/2} \cdot \delta \cdot \left(\frac{\ell_{c,i}}{\delta_i}\right) U_{c,i} \tag{5-19}$$

Unfortunately, a detailed check on the eddy viscosity model cannot be made due to lack of experimental data in the axisymmetric case. An approximate calculation of the value of pressure gradient at the rear stagnation point, obtained by curve fitting the n = 0.648 Kubota-Reeves-Buss[56] velocity profile, gave the same order of magnitude on the centerline as obtained through experiment.[4] Although a comparison of an integral quantity like the dissipation integral with the experimental data, if available, would have been much better, the above check at least shows that the order of magnitude is correct at a point in between the two extreme matched regions -- that is, between the free shear layer and the asymptotic far wake. Further verification of this model will have to come from a comparison of theoretical and experimental values of base pressure at various Mach numbers.

Using Eqs. (5-17), one can obtain the following relations between the compressible and incompressible quantities:

$$\delta^2 = \frac{\rho_\infty a_\infty}{\rho_e a_e} \frac{H_e - U_e^2 A_2'}{h_e} \delta_i^2$$

$$A_1 = \frac{h_e}{H_e - U_e^2 A_2'} \delta^2 A_1'$$

$$A_2 = \frac{h_e}{H_e - U_e^2 A_2'} \delta^2 A_2'$$

$$A_3 = \frac{h_e}{H_e - U_e^2 A_2'} \delta^2 A_3'$$

$$A_u = \frac{h_e}{H_e - U_e^2 A_2'} \delta^2 \{ \frac{H_e}{h_e} A_1' - \frac{U_e^2}{2h_e} A_3' \}$$

$$R_1 = \frac{\tilde{\varepsilon}_T(x)}{U_e} \frac{a_e}{a_\infty} R_1' \qquad (5\text{-}20)$$

where A_1', A_2', A_3', R_1' are incompressible non-dimensional integral quantities defined in the Nomenclature.

Profile Selection

In order to evaluate the integrals, it is next necessary to select the velocity profile for the inner region. An inadequate representation of the actual velocity profile will result in improper magnitudes of the appropriate integrals. On the other hand, a profile with too many free parameter will require too many integral equations, and hence may involve more complexity.

Near the base, Green's profiles[57] (a uniform velocity central core with cosine profile in the shear layer) are employed as they seem to give a good representation with and without uniform base bleed. This profile is shown in Figure 8, and is given by

$$\frac{U_i}{U_{e,i}} = 1 - 2A \qquad 0 \le \eta \le h_i$$

$$= 1 - A - A \cos \pi \left(\frac{\eta - h_i}{\ell_i}\right) \qquad h_i \le \eta \le \delta_i \qquad (5\text{-}21)$$

where $\ell_i = \delta_i - h_i$ = shear layer thickness. Here two parameters, namely A, the centerline velocity parameter and $P_v = h_i/\delta_i$, the central core parameter define the velocity profile completely. From Eq. (5-21) and Figure 8, it can be seen that A is equal to 0.5 at the base with no base

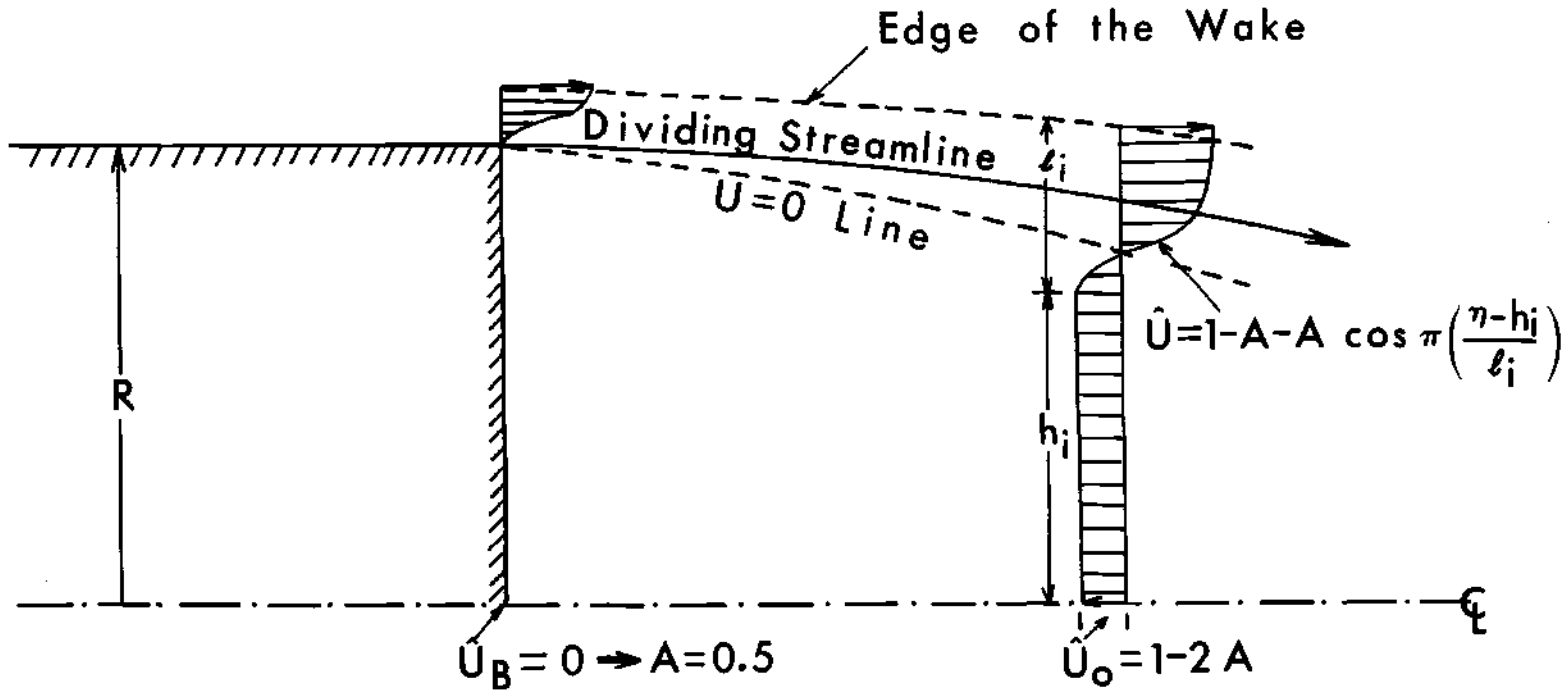

Figure 8. Incompressible Velocity Profiles Near the Base--Green's Two Parameter Profiles.

bleed ($U_{base} = 0$) and is less than 0.5 with base bleed. Using Eq. (5-21), the integrals can be readily written in terms of these parameters. These are

$$A_1' = \frac{1-A}{2} - A F_1$$

$$A_2' = \frac{(1-A)^2}{2} - 2A(1-A)F_1 + A^2 F_2$$

$$A_3' = \frac{(1-A)^3}{2} - 3A(1-A)^2 F_1 + 3A^2(1-A)F_2 - A^3 F_3$$

$$R_1' = \frac{\pi^2 A^2}{(1 - P_v)^2} \left(\frac{1-P_v^2}{4}\right)$$

where

$$F_1 = \frac{P_v^2}{2} - \frac{2(1-P_v)^2}{\pi^2}$$

$$F_2 = \frac{P_v^2}{2} + \frac{1-P_v^2}{4}$$

$$F_3 = \frac{P_v^2}{2} - \frac{14}{9}\frac{(1-P_v)^2}{\pi^2} \qquad (5\text{-}22)$$

The other quantities of interest are $U_{c,i}/U_{e,i}$ and ℓ_{c_i}/δ_i in Eq. (5-19). $U_{c,i}/U_{e,i}$ in the initial region is given by Eq. (5-12b) and is equal to 2A. η_i^*/δ_i is obtained from its definition, i.e.,

$$\int_0^{\eta_i^*} \frac{U_i}{U_{e,i}} \eta \, d\eta = 0$$

This gives the equation

$$\frac{A(1-h_i')^2}{\pi^2}\cos\pi X + \frac{(1-h_i')A}{\pi}\{(1-h_i')X + h_i'\}\sin\pi X - (1-A)(1-h_i')^2\frac{X^2}{2}$$

$$- (1-A)(1-h_i')h_i'X = (1-2A)\frac{h_i'^2}{2} + \frac{(1-h_i')^2A}{\pi^2} \qquad (5\text{-}23)$$

where $h_i' = \frac{h_i}{\delta_i}$, $\eta_i^{*'} = \frac{\eta_i^*}{\delta_i}$, $X = \frac{\eta_i^* - h_i}{\delta_i - h_i} = \frac{\eta_i^{*'} - h_i'}{1-h_i'}$.

Knowing h_i' and A, Eq. (5-23) is solved for η_i^*/δ_i by iteration using the Regula Falsi[58] method. $\ell_{c,i}/\delta_i$ is then obtained by substituting into Eq. (5-12a). This gives

$$\ell_{c,i}/\delta_i = 0.5\sqrt{\frac{(1-\eta_i^{*'})^2}{2} - (1-h_i')^2(S_3 - XS_4)} \qquad (5\text{-}24)$$

where $S_3 = \left[(1-X^2) - \frac{X\sin 2\pi X}{4\pi} + \frac{1-\cos 2\pi X}{8\pi^2}\right]$

$$S_4 = \frac{1}{2}\left[(1-X) - \frac{\sin 2\pi X}{2\pi}\right]$$

Away from the base, the Kubota-Reeves-Buss one parameter profiles[56] (similar solutions for axisymmetric wakes analogous to the Stewartson solution of the Falkner-Shan equation in the two-dimensional case), which describe the wake flow adequately away from the base, are selected to represent the velocity profile, and are shown in Figure 9. These profiles are integrated using Simpson's rule to determine the integral properties. These properties, U_o/U_e, U^*/U_e and $\ell_{c,i}/\delta_i$ (based on (Eqs. (5-12) and (5-13)) are shown in Figure 10, and are curve fitted as a function of n (pressure gradient parameter in the Kubota et al. analysis) using the method described in the Appendix. n varies from 0.5 to 0.75,

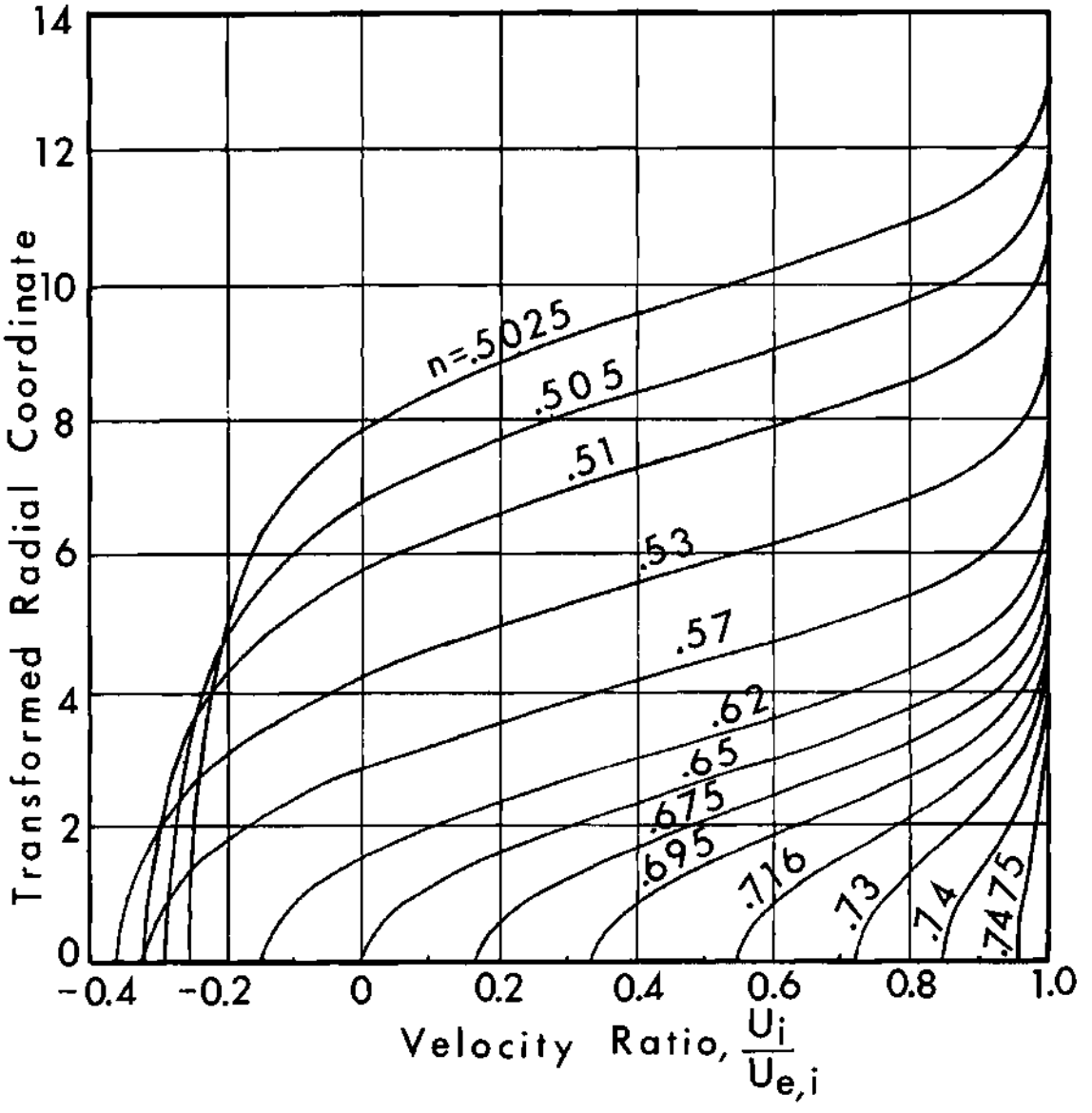

Figure 9. Kubota-Reeves-Buss' One Parameter Profiles.

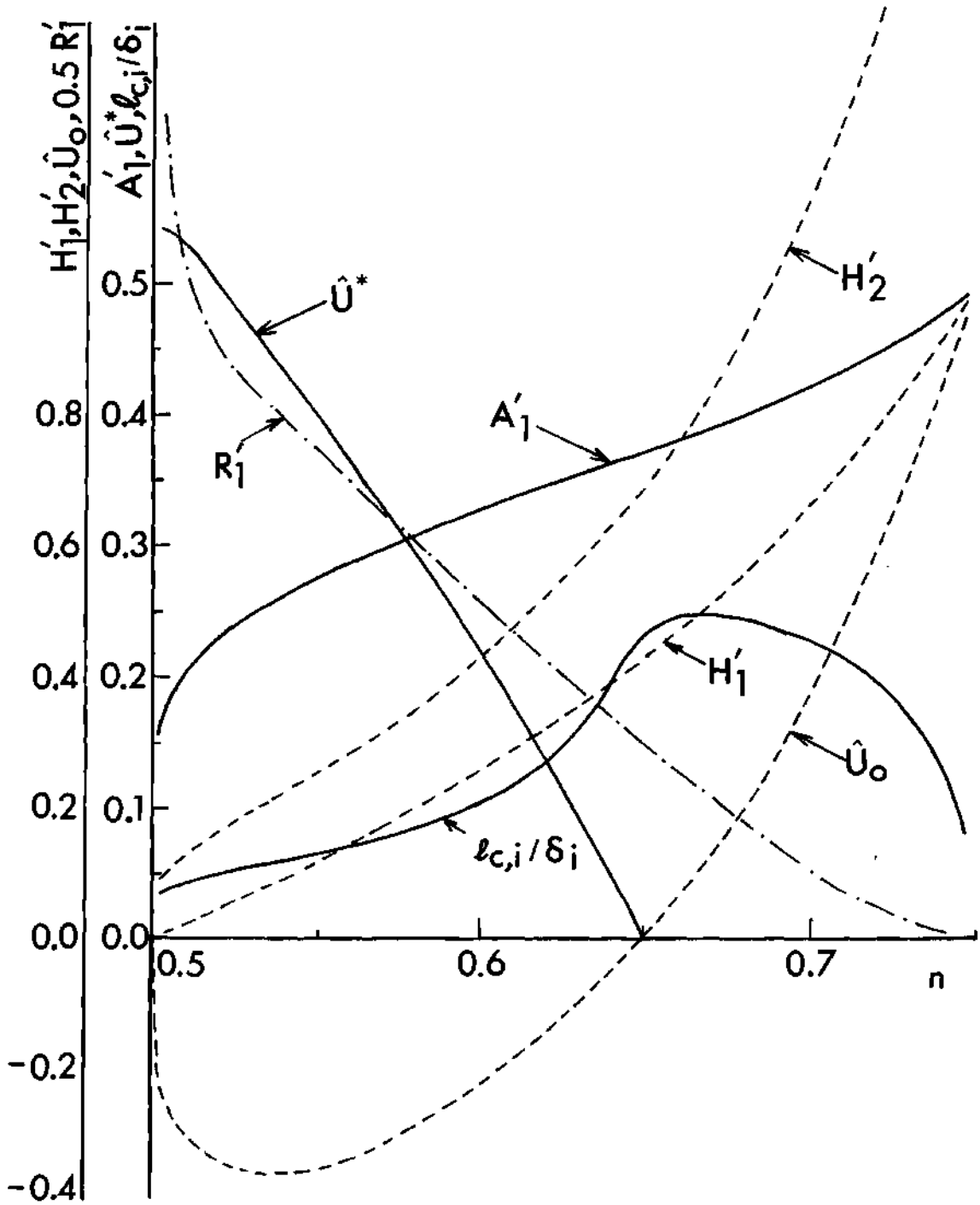

Figure 10. Behavior of Properties of the Kubota et al. Profiles with the Parameter, n.

with n = 0.75 corresponding to a solution for uniform flow ($U/U_e = 1$). For $0.5 < n < 0.648$, the centerline velocity is negative, while for $0.648 < n < 0.75$, it is positive. The expressions (up to the 5^{th} decimal place) obtained for the above quantities are:

For $0.5025 < n < 0.648$

$$A_1' = \frac{1.0 - 3.21497n + 0.54279n^2 + 3.77499n^3}{5.85466 - 28.02885n + 40.16253n^2 - 15.04077n^3}$$

$$H_1' = \frac{A_1' - A_2'}{0.5 - A_1'} = \frac{1.0 - 5.88952n + 11.56213n^2 - 7.56621n^3}{-1.91873 + 9.31737n - 14.4851n^2 - 7.04084n^3}$$

$$H_2' = \frac{A_1' - A_3'}{0.5 - A_1'} = \frac{1 - 6.48586n + 14.07363n^2 - 10.20602n^3}{-2.65934 + 14.62566n - 25.88102n^2 + 14.50306n}$$

$$R_1' = \frac{1 - 6.36621n + 12.87586n^2 - 8.26446n^3}{-0.19518 + 1.23131n - 2.92122n^2 + 2.48644n^3}$$

$$\frac{U_o}{U_e} = \frac{1 - 5.61534n + 10.42592n^2 - 6.39048n^2}{-0.85508 + 4.53164n - 7.74194n^2 + 4.19771n^3}$$

$$\frac{U^*}{U_e} = \frac{1 - 5.41081n + 9.75168n^2 - 5.78188n^3}{1.02865 - 5.13842n + 8.33606n^2 - 4.33627n^3}$$

$$\frac{\ell c_i}{\delta_i} = \frac{1 - 12.73157n + 35.47935n^2 - 27.96182n^3}{100(-2.50149 + 12.3204n - 19.93211n^2 + 10.61832n^3)}$$

For $0.648 < n < 0.675$

$$A_1' = \frac{1 - 3.2157n + 2.87905n^2 - 0.45486n^3}{6.54662 - 26.20812n + 34.39566n^2 - 14.71123n^3}$$

$$H_1' = \frac{1 - 4.88463n + 7.84174n^2 - 4.14984n^3}{-2.02297 + 7.8138n - 9.93104n^2 + 4.13772n^3}$$

$$H_2' = \frac{1 - 5.05386n + 8.37624n^2 - 4.5745n^3}{-2.06367 + 8.39312n - 11.32596n^2 + 5.06155n^3}$$

$$R_1' = \frac{1 + 3.36972n - 14.3410n^2 + 10.76048n^3}{0.64539 - 1.42794n + 1.90580n^2 - 1.38008n^3}$$

$$\frac{U_o}{U_e} = \frac{1 - 3.40084n + 3.59654n^2 - 1.12534n^3}{-1.41253 + 4.72459n - 5.25292n^2 + 1.94731n^3} \qquad (5.25)$$

Solution Method

As mentioned in the previous section, the Green profile described by Eq. (5-21) is employed to start the solution from the base. As these profiles introduce two parameters, A and P_v, and there are four basic unknown variables, p (or u_e), v_e, δ and S_e, the total number of unknowns to be solved for are six. Eqs. (5-6) to (5-8) are rewritten, after simplification, in the following forms:

$$\left(\frac{dA_1'}{dA} + \frac{U_e^2 A_1'}{H_e - U_e^2 A_2'} \frac{dA_2'}{dA}\right) \frac{dA}{dx} + \left(\frac{dA_1'}{dP_v} + \frac{U_e^2 A_1'}{H_e - U_e^2 A_2'} \frac{dA_2'}{dP_v}\right) \frac{dP_v}{dx}$$

$$+ \frac{2A_1' - \frac{H_e - U_e^2 A_2'}{h_e}}{\delta} \frac{d\delta}{dx} = R_{11} \qquad (5.26)$$

$$\left\{\frac{d(A_2'-A_1')}{dA}+\frac{U_e^2}{H_e-U_e^2A_2'}(A_2'-A_1')\frac{dA_2'}{dA}\right\}\frac{dA}{dx}+\left\{\frac{d(A_2'-A_1')}{dP_v}+\frac{U_e^2}{H_e-U_e^2A_2'}\right.$$

$$\left.\cdot(A_2'-A_1')\frac{dA_2'}{dP_v}\right\}\frac{dP_v}{dx}+2\frac{(A_2'-A_1')}{\delta}\frac{d\delta}{dx}=R_{22} \qquad (5\text{-}27)$$

$$\left\{\frac{d(A_3'-A_1')}{dA}+\frac{U_e^2}{H_e-U_e^2A_2'}(A_3'-A_1')\frac{dA_3'}{dA}\right\}\frac{dA}{dx}+\left\{\frac{d(A_3'-A_1')}{dP_v}\right.$$

$$\left.+\frac{U_e^2(A_3'-A_1')}{H_e-U_e^2A_2'}\frac{dA_3'}{dP_v}\right\}\frac{dP_v}{dx}+\frac{2(A_3'-A_1')}{\delta}\frac{d\delta}{dx}=R_{33} \qquad (5\text{-}28)$$

where

$$R_{11}=-\frac{V_e}{U_e}\frac{1}{\delta}\frac{H_e-U_e^2A_2'}{h_e}+A_1'(1+2A_2'\frac{U_e^2}{H_e-U_e^2A_2'})\frac{h_e}{U_e^2}\frac{1}{c_p}\frac{dS_e}{dx}$$

$$+A_1'\left\{(1+2A_2'\frac{U_e^2}{H_e-U_e^2A_2'})\frac{R}{c_p}\frac{h_e}{U_e^2}-1\right\}\frac{1}{p_e}\frac{dp_e}{dx}$$

$$R_{22}=\bar{\tau}+\left\{(2A_2'-A_1')+2A_2'(A_2'-A_1')\frac{U_e^2}{H_e-U_e^2A_2'}\right\}\frac{h_e}{U_e^2}\frac{1}{c_p}\frac{dS_e}{dx}$$

$$+\left\{(2A_2'-A_1'+2A_2'\overline{A_2'-A_1'}\frac{U_e^2}{H_e-U_e^2A_2'})\frac{R}{c_p}\frac{h_e}{U_e^2}-\right.$$

$$\left.(A_2'-A_1'+\frac{1}{2}\frac{R}{c_p}\frac{H_e-U_e^2A_2'}{U_e^2})\right\}\frac{1}{p_e}\frac{dp_e}{dx}$$

$$R_{33} = -2R_1' \bar{\chi} + 2\bar{\tau}$$

$$+ \left\{ (3A_3' - A_1') + 2A_2'(A_3' - A_1') \frac{U_e^2}{H_e - U_e^2 A_2'} \right\} \frac{h_e}{U_e^2} \frac{1}{c_p} \frac{dS_e}{dx}$$

$$+ \left\{ (3A_3' - A_1') + 2A_2' \overline{A_3' - A_1'} \frac{U_e^2}{H_e - U_e^2 A_2'} \right) \frac{R}{c_p} \frac{h_e}{U_e^2} -$$

$$\left. (A_3' - A_1' + \frac{R}{cp} \overline{\frac{2H_e}{U_e^2} A_1' - A_3'}) \right\} \frac{1}{p_e} \frac{dp_e}{dx}$$

$$\bar{\tau} = \frac{dS_e/dx}{c_p * \frac{U_e^2}{H_e - U_e^2 A_2'} \left\{ \frac{v_e \left(\frac{H_e - U_e^2 A_2'}{h_e} \right)^2}{\bar{\chi} \delta U_e} - 1 \right\}}$$

$$\bar{\chi} = \frac{H_e - U_e^2 A_2'}{h_e \delta^2} \left(\frac{\tilde{\varepsilon}_T}{U_{e,i}} \right)$$

$$= \frac{K}{\delta} \frac{H_e - U_e^2 A_2'}{h_e} \cdot \left(\frac{\rho_o}{\rho_e} \right)^{3/2} \cdot \frac{\ell_{c,i}}{\delta_i} \cdot \frac{U_c}{U_e} \qquad (5\text{-}29)$$

The values of A_1', A_2', A_3', R_1', dA_1'/dA, dA_2'/dA, dA_3'/dA, dA_1'/dP_v, dA_2'/dP_v and dA_3'/dP_v are obtained using Eqs. (5-22) to (5-24). Eqs. (5-26) to (5-28) are solved simultaneously for dA/dx, dP_v/dx and $d\delta/dx$ using the Gauss-Jordan complete elimination method with maximum pivot strategy,[59] and new values of δ, A and P_v are found at the next station using Euler's method with a variable step size (0.01 of the base radius in most portions of the flow). The pressure is evaluated from the centerline

momentum Eq. (5-9). v_e and S_e at the new station are found using the approximate method of characteristics described in Chapter IV.

Away from the base, the Kubota-Reeves-Buss profiles were used. The reason that these profiles are inadequate near the base is that as $n \to 0.5$ (or $U_o \to 0$ for no base bleed) at the base, $\hat{U}^* \to 0.546$ for these profiles; while at the separation point or base, $\hat{U}^* = 0$. Only one parameter is necessary to describe these profiles, and this parameter here is taken as the pressure gradient parameter in the Kubota et al. analysis. All the properties required for computation are curve fitted and given by Eq. (5-25) in terms of this parameter, n. As the Green's profiles and the Kubota et al. profiles are different with different shape factors, there will be a discontinuity in some quantities when transferring from the solution using the Green profiles to the solution using the Kubota et al. profiles. A sufficient number of conditions next should be provided to obtain a unique transfer point. It was decided to maintain the continuity of the mass flow rate through the shear layer, the thickness of the shear layer and the Mach number at the edge of the shear layer as the basic conditions so as to cause no discontinuity in the external flow solution. For the same thickness of the shear layer and edge Mach number, it is always possible to find the value of the parameter, n, for the given mass flow rate through the shear layer. In order to achieve a unique location, an extra constraint or condition is required, and an integral quantity, related to drag seems to be a reasonable choice. Hence the momentum shape parameter, H_1, was used as the final joining condition. However, later it was found that with the present set of profiles, the location of the joining point varied very

little when either the dividing streamline velocity (chosen by Alber et al.) or the momentum shape parameter was chosen as the last joining condition.

In almost all cases, before the profile changeover or matching occurred, the negative pressure gradient obtained through the use of Eq. (5-9) becomes very large resulting in an inflection point in the dividing streamline velocity distribution. This runaway tendency of pressure gradient is believed to be due to the absence of shear stress in the centerline momentum equation. To avoid this, the centerline momentum equation is replaced by

$$\frac{dp}{dx} = \frac{dp}{dx}\Big)_{x_o} + \frac{d^2p}{dx^2}\Big)_{x_o} (x - x_o)$$

downstream of the point $\frac{d^2U^*}{dx^2} = 0$ (i.e., $x = x_o$), until a match occurs with the Kubota et al. profiles. This ad hoc assumption is usually only required over a very short distance (about 0.5 R).

For large boundary layer thickness, high Mach numbers and large base bleed, the two profiles could not be matched in the near wake. An attempt to find another family of starting profiles that would match with the Kubota et al. profiles was not successful. Hence the Green profiles were used throughout for most of the calculations. However as one moves away from the base, the constant velocity core is eaten up by the shear layer. Once the value of the parameter, P_v, drops to 0.2, it is maintained constant as the magnitude of the centerline velocity becomes much larger than the experimentally measured reverse velocity

if P_v is allowed to go to zero. These profiles with $P_v = 0.2$ will be referred to as Green's one parameter profiles.

The unknowns, using one parameter profiles (Kubota et al. or Green), are U_e, δ, n or A, v_e and S_e; that is, the unknowns are reduced by one. Therefore, the three integrated equations, Eqs. (5-6) to (5-8), coupled with the solution of the external flow are sufficient to solve the problem. These integrated equations, after simplification, are

$$\left(\frac{dA_1'}{dn} + \frac{U_e^2}{H_e - U_e^2 A_2'} A_1' \frac{dA_2'}{dn}\right) \frac{dn}{dx} + \left(2A_1 - \frac{H_e - U_e^2 A_2'}{h_e}\right) \frac{1}{\delta} \frac{d\delta}{dx} +$$

$$A_1' \left\{\left(1 + 2 \frac{U_e^2}{H_e - U_e^2 A_2'} A_2'\right) - \frac{c_p}{R} \frac{U_e^2}{h_e}\right\} \frac{1}{U_e} \frac{dU_e}{dx} = RH_{11} \tag{5-30}$$

$$\left\{\frac{d(A_2' - A_1')}{dn} + \frac{U_e^2}{H_e - U_e^2 A_2'} (A_2' - A_1') \frac{dA_2'}{dn}\right\} \frac{dn}{dx} + 2(A_2' - A_1') \frac{1}{\delta} \frac{d\delta}{dx} +$$

$$\left\{(2A_2' - A_1') - (A_2' - A_1') \frac{U_e^2}{h_e} \frac{c_p}{R} + 2(A_2' - A_1')A_2' \frac{U_e^2}{H_e - U_e^2 A_2'}\right.$$

$$\left. - 0.5 \frac{H_e - U_e^2 A_2'}{h_e}\right\} \frac{1}{U_e} \frac{dU_e}{dx} = RH_{22} \tag{5-31}$$

$$\left\{\frac{d(A_3' - A_1')}{dn} + \frac{U_e^2}{H_e - U_e^2 A_2'} (A_3' - A_1') \frac{dA_2'}{dn}\right\} \frac{dn}{dx} + 2(A_3' - A_1') \frac{1}{\delta} \frac{d\delta}{dx} +$$

$$\left\{(3A_3' - A_1') - (A_3' - A_1') \frac{U_e^2}{h_e} \frac{c_p}{R} + 2(A_3' - A_1')A_2' \frac{U_e^2}{H_e - U_e^2 A_2'}\right.$$

$$\left. - 2A_u\right\} \frac{1}{U_e} \frac{dU_e}{dx} = RH_{33} \tag{5-32}$$

where $$RH_{11} = -\frac{v_e}{U_e}\frac{1}{\delta}\frac{H_e - U_e^2 A_2'}{h_e} + \frac{A_1'}{R}\frac{dS_e}{dx}$$

$$RH_{22} = \bar{\tau} + \left\{(A_2' - A_1')\frac{c_p}{R} + \frac{1}{2}\frac{U_e^2}{H_e - U_e^2 A_2'}\right\}\frac{1}{c_p}\frac{dS_e}{dx}$$

$$RH_{33} = -2R_1'\bar{\chi} + 2\bar{\tau} + \left\{(A_3' - A_1')\frac{c_p}{R} + \left(\frac{2H_e}{U_e^2}A_1' - A_3'\right)\right\}\frac{1}{c_p}\frac{dS_e}{dx} \qquad (5\text{-}33)$$

When the Kubota et al. profiles are used, A_1', A_2' etc. are given by Eq. (5-25), while for the Green one parameter profiles, these are given by Eqs. (5-22) to (5-24). $\bar{\chi}$ and $\bar{\tau}$ are defined by Eq. (5-29).

The simultaneous solution of Eqs. (5-30) to (5-32) for the three variables can be written in the form

$$\frac{dU_e}{dx} = \frac{N_{U_e}}{D}$$

$$\frac{d\delta}{dx} = \frac{N_\delta}{D}$$

$$\frac{dn(\text{or } A)}{dx} = \frac{N_{n\,(\text{or } A)}}{D} \qquad (5\text{-}34)$$

The complete solution is continued until the Crocco-Lees singularity is encountered. Near the singularity, for an incorrect value of p_b, either D goes to zero first or one of N's go to zero first, i.e., either the solution diverges or there is an extremum in one of the variables. On the other hand, if the value of p_b is correct, both N's and D go to zero simultaneously and the transition from subcritical to supercritical

flow is possible. It is only necessary to assure that $\frac{dn \text{ (or } A)}{dx} > 0$ (or <0), as n (or A) must increase (or decrease) monotonically through the critical point. In the present formulation, if the initial value of base pressure is too low, the determinant of the solution matrix goes through zero before the numerator, N_n and vice versa. For given initial conditions and a trial value of p_b, the present program is designed to give an increment in the proper direction to obtain the next trial value of p_b. Convergence is obtained by halving successive increments. It requires from about three to ten seconds (depending upon the initial boundary layer thickness and Mach number) on a CDC CYBER 70-74 using the central processing unit, CPU '0', to complete one iteration and about three iterations to enclose the base pressure by one significant figure. For making a proper jump (so that there is no change in sign of the derivatives) over the singularity to get to the far wake, it is usually found that the base pressure should be iterated at least to the sixth significant figure. The flow diagram for the inner region is given by Figure 11.

Comments

The present solution has been the result of a lot of trial and error attempts because of certain unforeseen difficulties. It seems advisable to mention various other alternatives pursued and their shortcomings as an aid to other investigators. The present investigation was initially started using Green's type profiles for both momentum and enthalpy, viz.,

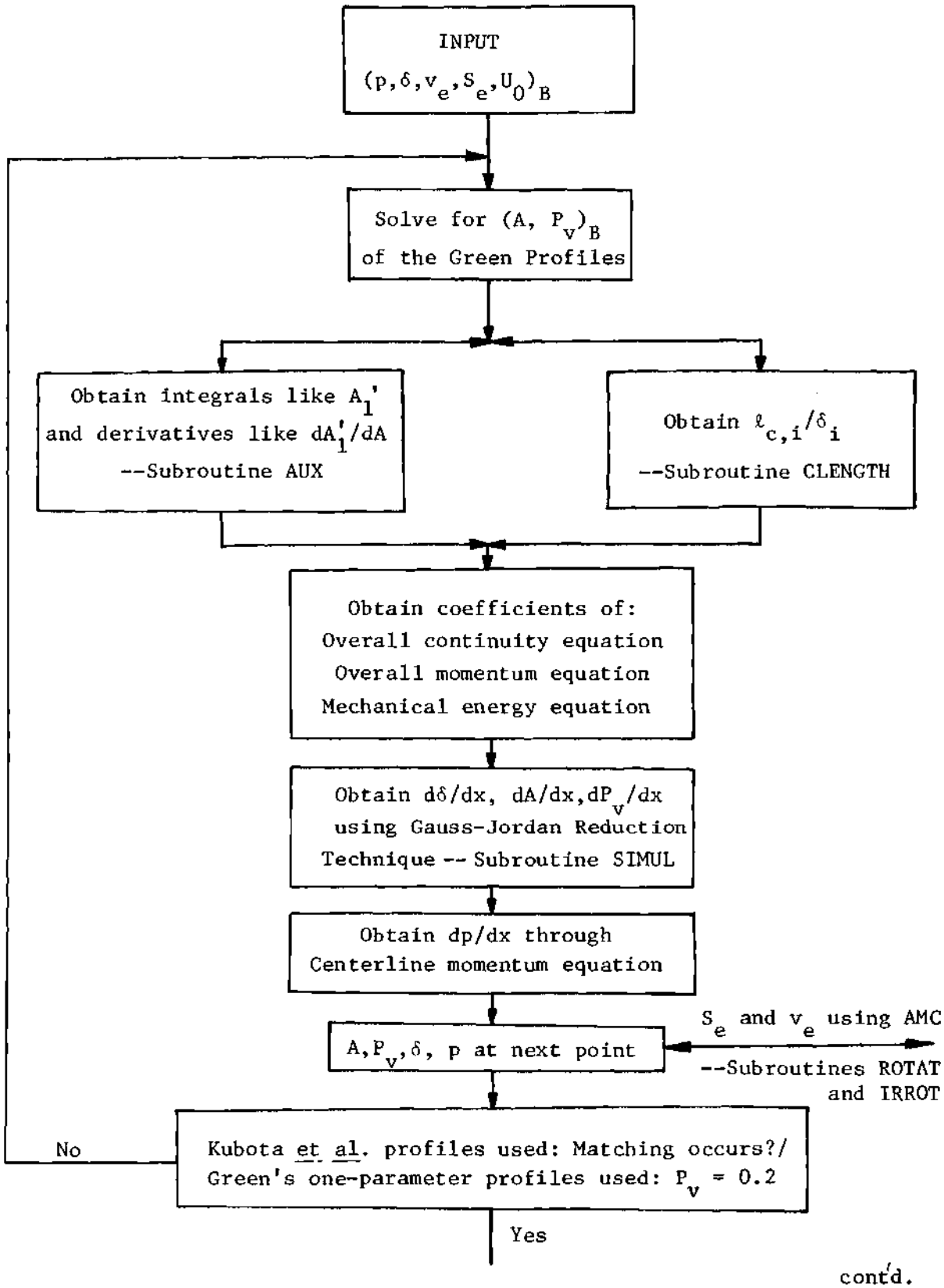

Figure 11. Flow Diagram for the Inner Region.

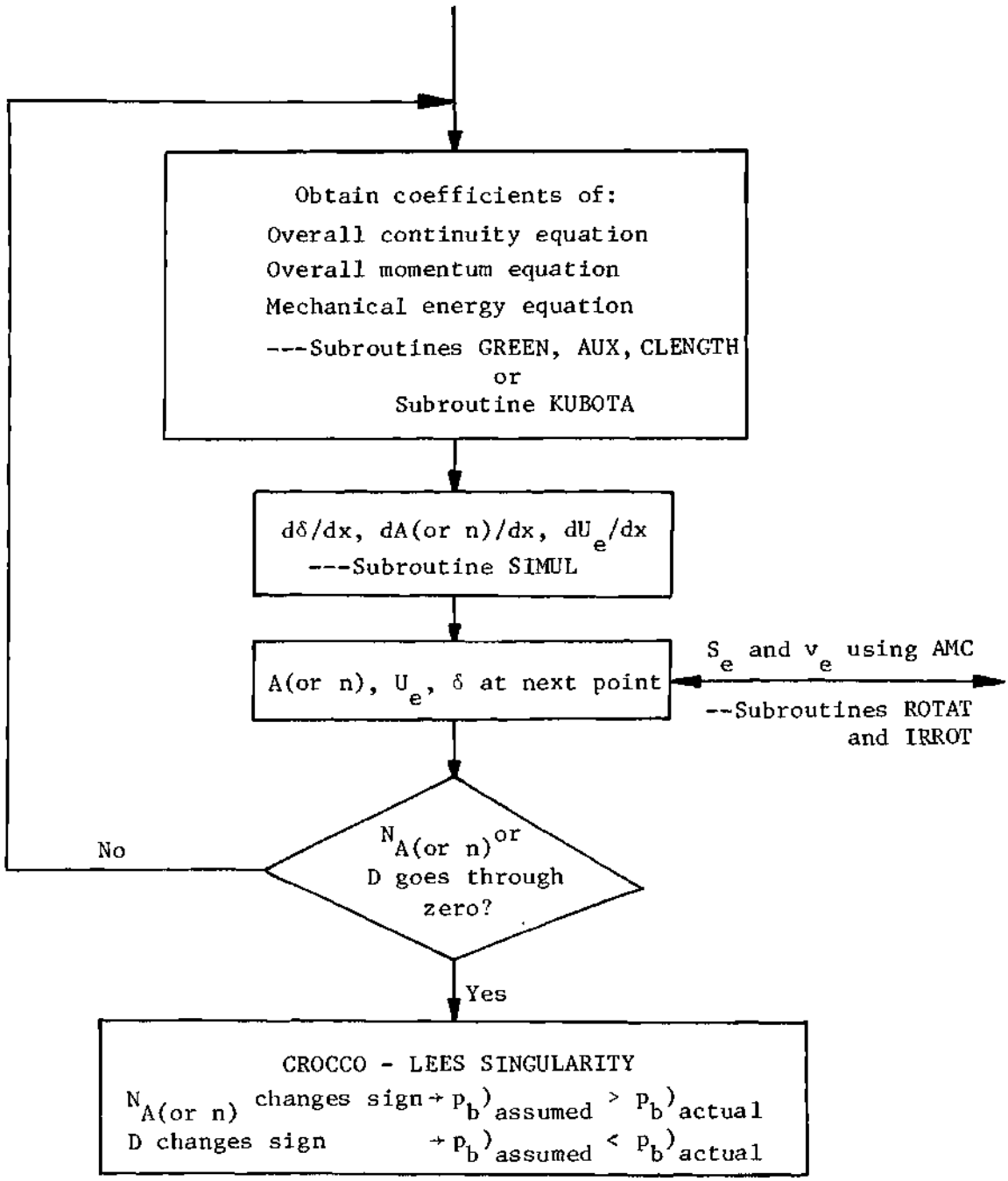

Figure 11. Flow Diagram for the Inner Region.

$$\frac{\rho U}{\rho_e U_e} = 1 - A - A \cos \pi \left(\frac{r-h_c}{\delta-h_c}\right)$$

$$\frac{h}{h_e} = 1 - B - B \cos \pi \left(\frac{r-h_c}{\delta-h_c}\right)$$

where h_c is the thickness of the constant velocity and enthalpy core. The parameter h_c/δ was to be dropped once it becomes zero. The use of above profiles resulted in seven unknowns, p (or U_e), v_e, δ, h_c/δ, S_e, A and B. As mentioned in the previous section, v_e and S_e are determined from the solution of external flow. Four equations, overall continuity, overall momentum, mechanical energy and overall energy, were taken as the governing equations. The solution was started with a constant pressure assumption, and this assumption was to be dropped once h_c/δ reached zero. However, it was found that before this parameter approached zero, the centerline Mach number attained a very high value. Also the initial drop in pressure observed in experiments (the drop in the axisymmetric case is much larger than in the two dimensional case) can not be achieved using the constant pressure assumption. So, alternatively, the half momentum equation (momentum equation integrated up to the U = 0 line) was used. This resulted in a singular point in the solution very close to the base. Use of other equations like the centerline momentum equation and second moment of momentum equation did not alleviate the problem, and no physical explanation of this singularity could be reached. Also, various other profiles like

$$\frac{\rho U}{\rho_e U_e} = 1 - A_1(1 - \bar{r}^z)^2$$

$$\frac{h}{h_e} = 1 - B_1(1 - \bar{r}^z)^2$$

where $\bar{r} = \frac{r}{\delta}$, and A_1, B_1 and z are profile parameters, and straight line profiles were tried, but with no success. The reason for choosing the above profiles was the simplicity in evaluating the integrals in closed form. However, these profiles do not satisfy the isoenergetic condition at every point in the shear layer; this was believed to be responsible for some of the troubles.

The next step in the investigation was to assume only the velocity profile and to use the isoenergetic condition. In order to again avoid the numerical integration, a compressible-incompressible transformation was used. Although this transformation requires certain additional approximations or assumptions on the behavior of the shear stress term, the accuracy of the assumptions seems to be compatible with the present approach. Qualitatively again, the same results were obtained.

Next, to circumvent the problems, it was decided to join the initial two parameter profiles with a single parameter profile. The Kubota-Reeves-Buss profiles were chosen. At moderate boundary layer thicknesses, the joining point occurred before the above mentioned singularity, and the complete solution was obtained with no trouble. But, as pointed out in the previous section of this chapter for high boundary layer thicknesses and Mach numbers, it was found that matching between these two profiles was not possible, while for very small boundary layer thickness, the singularity occurred before the matching could take place. Again the

use of other kinds of conservation equations did not succeed.

The next attempt was based on the result that no singularity was observed in the solution if an arbitrary dp/dx was imposed externally (whether zero or non-zero). That is, the simultaneous solution of the three equations (here continuity, momentum and mechanical energy), did not result in any singularity near the base as one marched away from the base. Consequently, dp/dx was then obtained using the centerline momentum equation, applied one step later than the solution for the other variables. This eliminated the singularity near the base.

Initially, it was thought that the above singularity should be of nodal type[59]; that is, N's and D should go to zero simultaneously regardless of the initial value of p_b. Thus, no extra constraint on the problem would be imposed. Golik-Webb-Lees[60] and Ai[61], in their analytical solutions of the two-dimensional laminar case, starting from the rear stagnation point and using simple profiles, found many singular points. These singularities, other than that at the Crocco-Lees critical point, turned out to be of the nodal type, and they occurred at high centerline velocities. The velocity in the present axisymmetric analysis is about twice as high as in Alber's two dimensional analysis. However, it was not possible to jump through the present singularity properly even with the use of a more accurate numerical scheme (Runga-Kutta method). Presently, it is conjectured that the present system of equations becomes unstable as one marches towards the rear stagnation point, and the solution of dp/dx one step later lends stability to the solution.

Thus the complete solutions was possible with the above line of approach, for a wide range of Mach number and boundary layer thickness,

without any computational difficulty. However, there was still an unwanted feature of a higher magnitude of centerline Mach number than experimentally observed. The way in which this has been dealt with in the present analysis has already been discussed in the previous section of this chapter.

CHAPTER VI

RESULTS AND COMPARISON WITH EXPERIMENTS

Figure 12 shows a typical centerline pressure distribution obtained using the present analysis and illustrates the convergence of the solution as the correct base pressure is approached. As shown, if the base pressure is smaller than the correct value, there is sudden drop of pressure and the solution blows up (denominator of the solution matrix going through zero first); while if the base pressure is larger than the correct value, the pressure keeps increasing and the centerline velocity drops (numerators of the solution matrix going through zero first). If the solution is allowed to continue in the latter case, another stagnation point is obtained (a very large value of assumed base pressure results in open wake, i.e., no stagnation point). Usually, if the solution is carried up to sixth decimal accuracy, it is possible to make a proper jump through the Crocco-Lees singularity; that is, numerators and denominator go through zero almost simultaneously. The numerical accuracy of the solution is checked by reducing the step size by one-half, both in the characteristics net as well as in the streamwise direction; the deviation of the pressure from the original step size solution is of the order of 0.5% (Figure 12).

Also shown in the figure is the solution obtained using the Prandtl-Meyer relation for the outer regime. Interestingly, the overshoot feature in the centerline pressure curve, peculiar to the axisymmetric

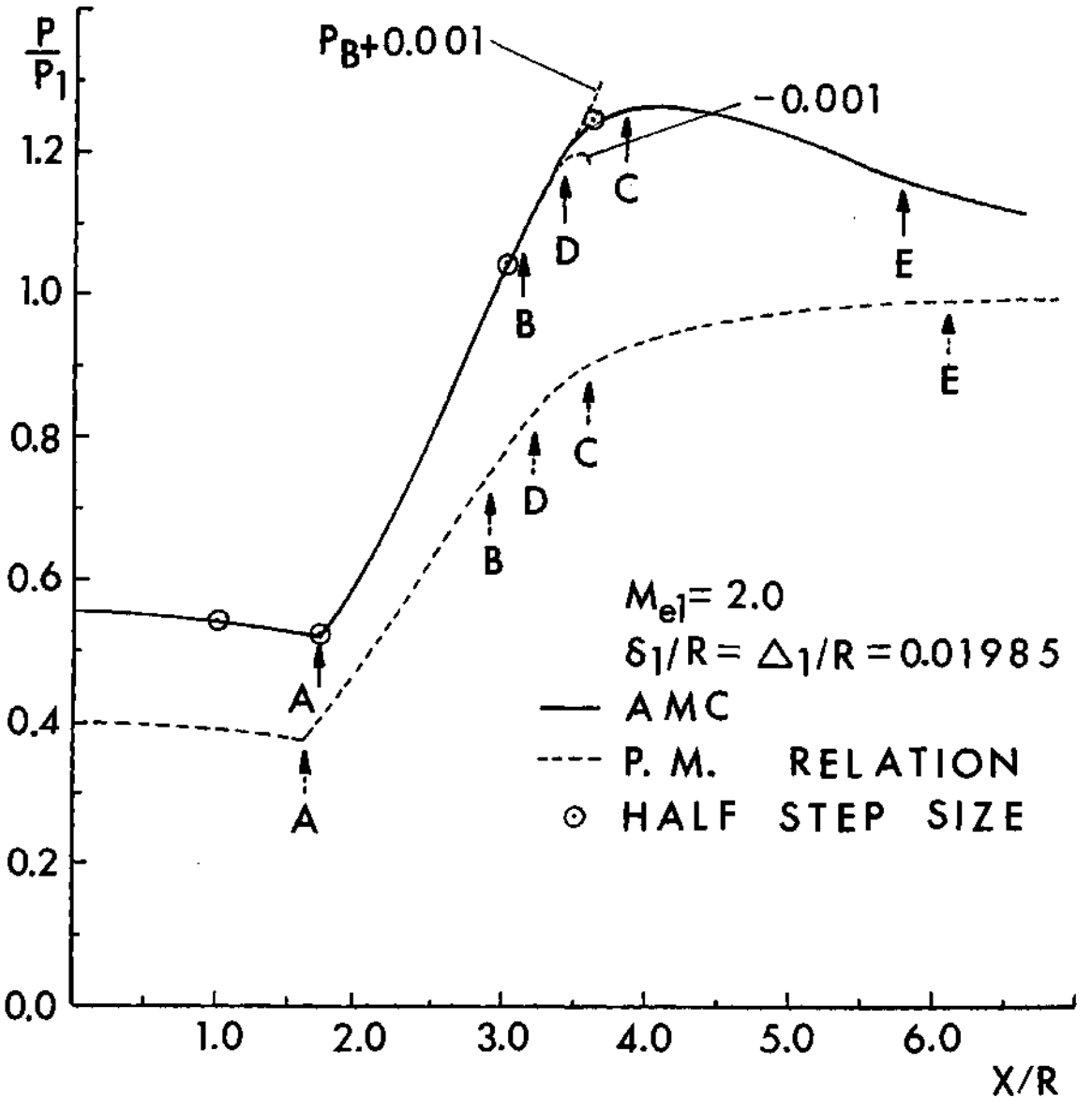

Figure 12. Typical Centerline Pressure Distribution (without Rotational Layer), Convergence Behavior of the Near Wake Solution and Solution using Prandtl-Meyer Relation for the External Flow. A = Parameter Drop Point, B = Rear Stagnation Point, C = Crocco-Lees Critical Point, D = Wake Neck, E = Centerline Mach 1 Point.

base flow disappears with the Prandtl-Meyer law, and, also as expected, the base pressure obtained is much smaller than that obtained with the axisymmetric method of characteristics. This demonstrates that the solution of the external flow plays a very important role in the present problem and must be adequately solved to get good results.

Another preliminary investigation made, was to study the effect of value of eddy viscosity coefficient, K. As explained in Chapter V, this was empirically selected as 0.07 by comparing with incompressible self-preserving flows. As shown in Figure 13, base pressure has quite strong dependence on the magnitude of K. However, it will be shown later that K= 0.07 is quite satisfactory from the standpoint of comparison between analytical and experimental results.

Figures 14 and 15 show the effect of the velocity profile on the near wake solution. The solution is started using the Green two parameter profiles. In one case, this solution is matched with the solution using the Green one parameter profiles, while in the other case, it is matched with the solution using the Kubota et al. one parameter profiles. The variation of shape parameters with the non-dimensional mass flow rate in shear layer is shown in Figure 16 for these two profiles. From Figures 14 and 15, it is seen that pressure and wake thickness are affected in a minor way due to change in profile, while detailed features like location of the rear stagnation point and the centerline Mach number distribution are found to be more profile dependent. This profile dependency of the detailed quantities is one of the major drawbacks of the integral methods. For accurate prediction of the flow field details, a good velocity profile is essential.

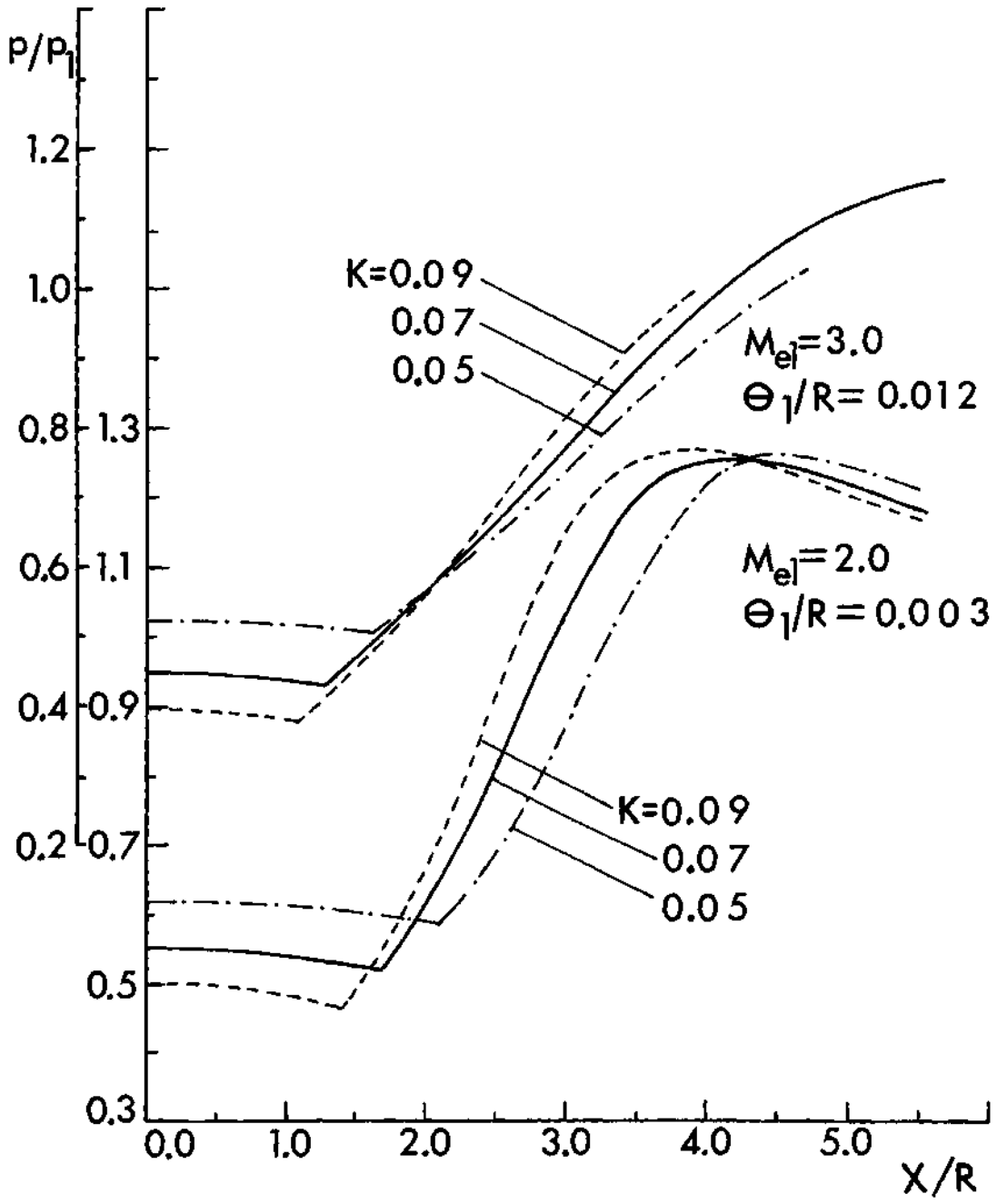

Figure 13. Effect of Coefficient of Eddy Viscosity on Centerline Pressure Distribution.

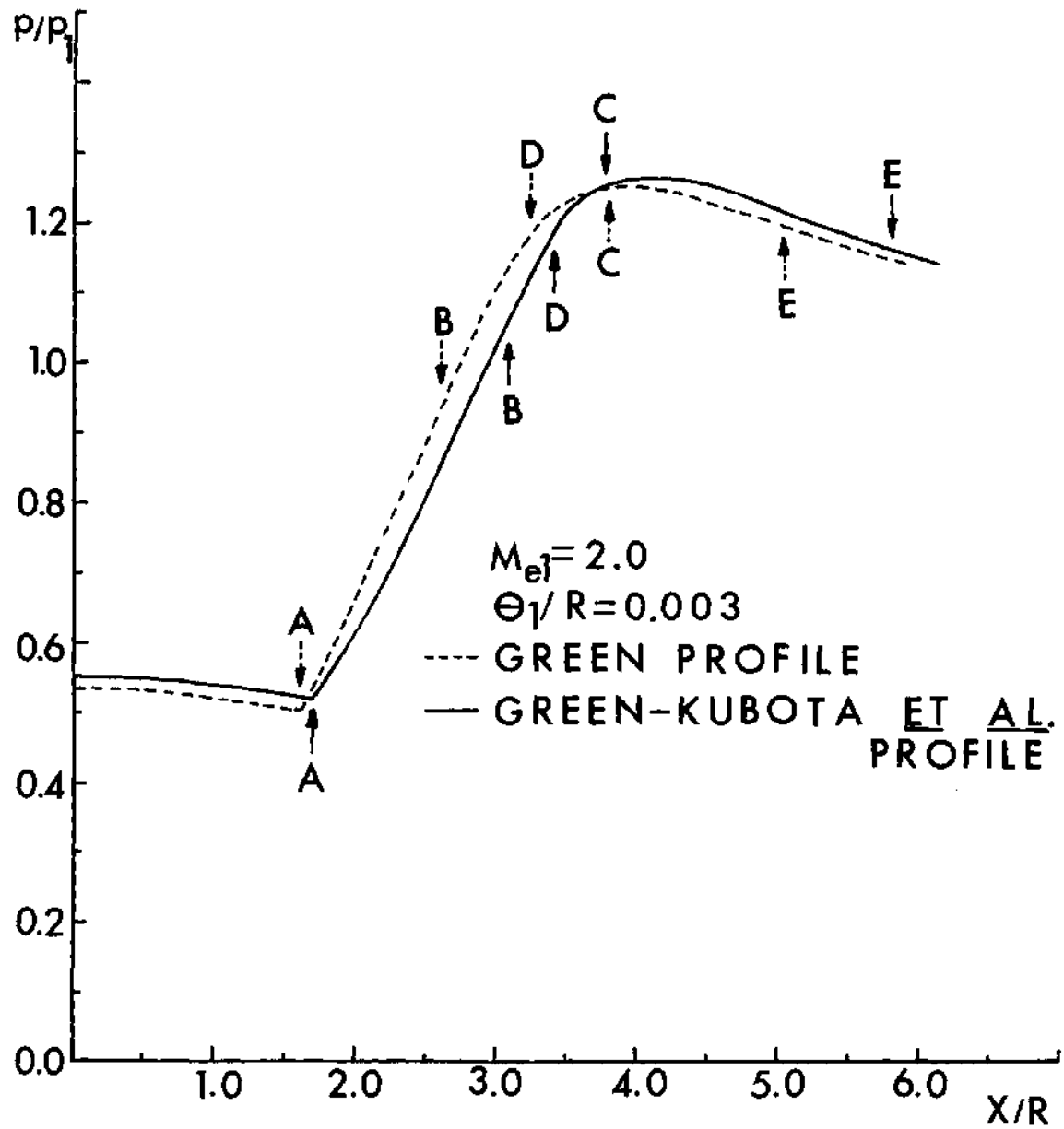

Figure 14. Effect of Velocity Profiles on Centerline Pressure Variation with Axial Distance.

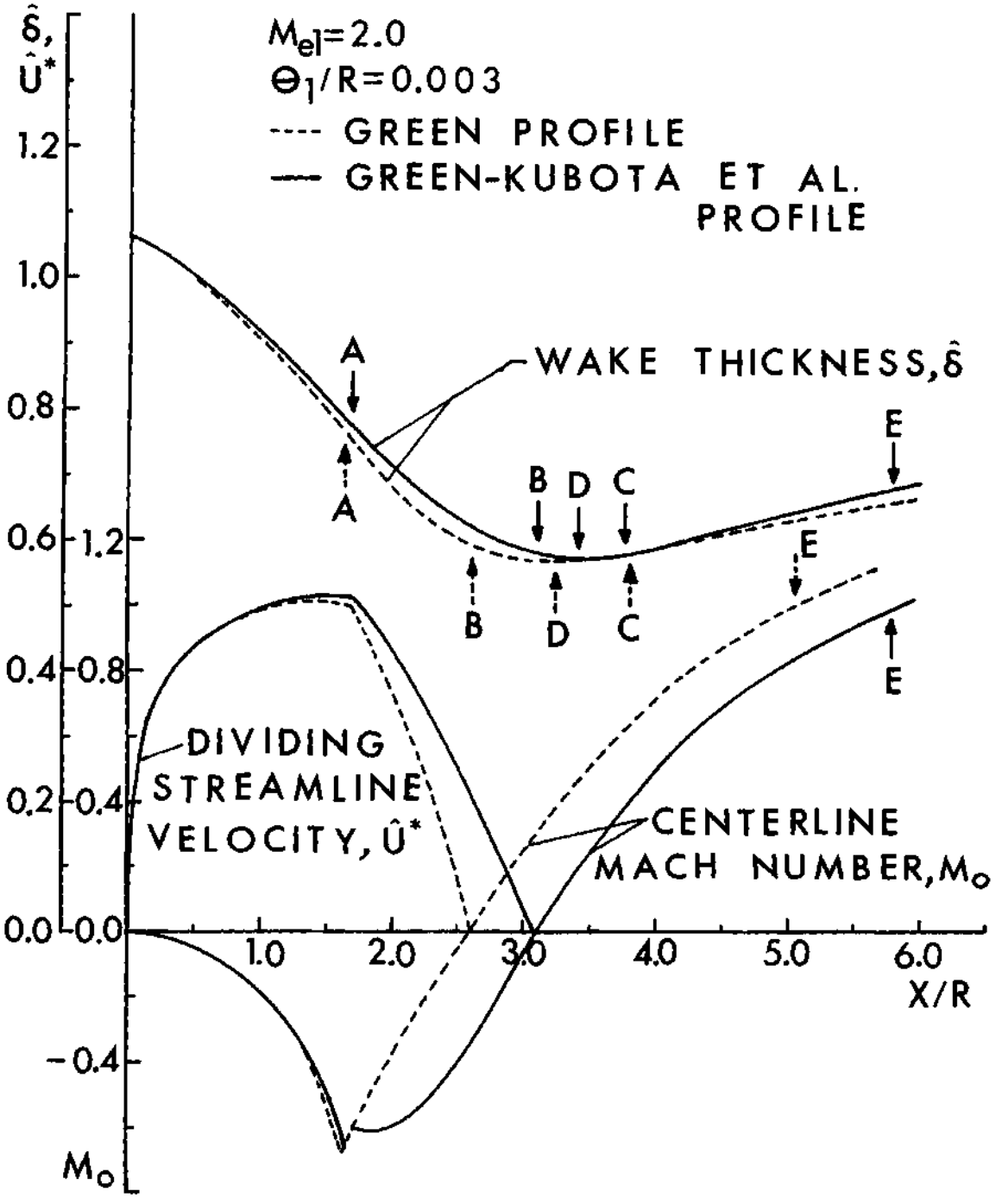

Figure 15. Effect of Velocity Profiles on M_o, $\hat{U}^*$ and $\hat{\delta}$ Variation with Axial Distance.

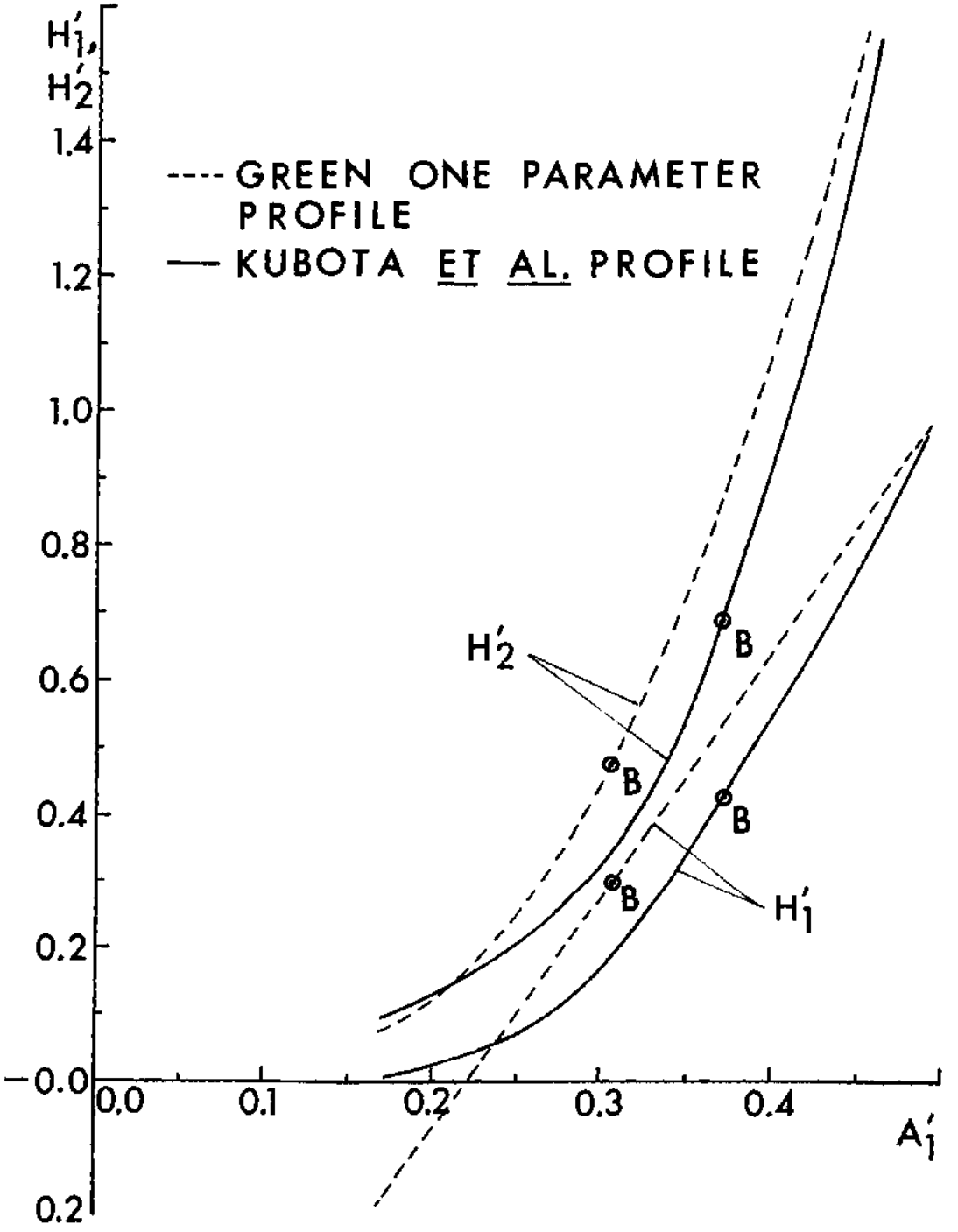

Figure 16. Variation of Shape Parameters of the Green One Parameter Profiles and Kubota et al. Profiles with A_1'.

Figures 17 and 18 show comparison of the centerline pressure and centerline Mach number distributions with experimental data of three different investigators[62-64] for Mach number near 2.0. The boundary layer thickness, for these test cases, varies over a wide range, from thin ($\theta_1/R = 0.0061$, $\delta_1/R = 0.0771$) to quite thick ($\theta_1/R = 0.05575$, $\delta_1/R = 0.59$). In all three cases, very good comparison between theory and experiment occurs, lending credibility to the present analysis. Experimental data of Ref. (64) seems to suffer from some tunnel wall interference because of a large wake thickness to test section height ratio ($\simeq 0.6$). It should be pointed out that the present analysis does not take into account the presence of the tunnel walls, model supports and probe, which are essential in an experimental set up. The experiments[62] have shown that if the probe diameter is less than 10% of the base diameter, the effect of probe on the base pressure is negligible (3 to 5%). But there are no data concerning its effect on the centerline pressure variation and location of rear stagnation point etc.

Figure 19 shows the effect of Mach number on the base pressure. Mach number is the primary variable affecting the base pressure. In spite of the large scatter in data available in the literature, Refs. (62-68), the present theory shows a respectable matching with the experiments, particularly at moderate Mach numbers. It seems, however, to slightly overpredict the base pressure at large Mach numbers (~ above 2.5) and slightly underpredict the base pressure at low Mach numbers (~ below 1.8) consistently. It is found that if instead of assuming the equivalent compressible eddy viscosity, $\tilde{\varepsilon}_T$, behavior as described by Eq. (5-19), one

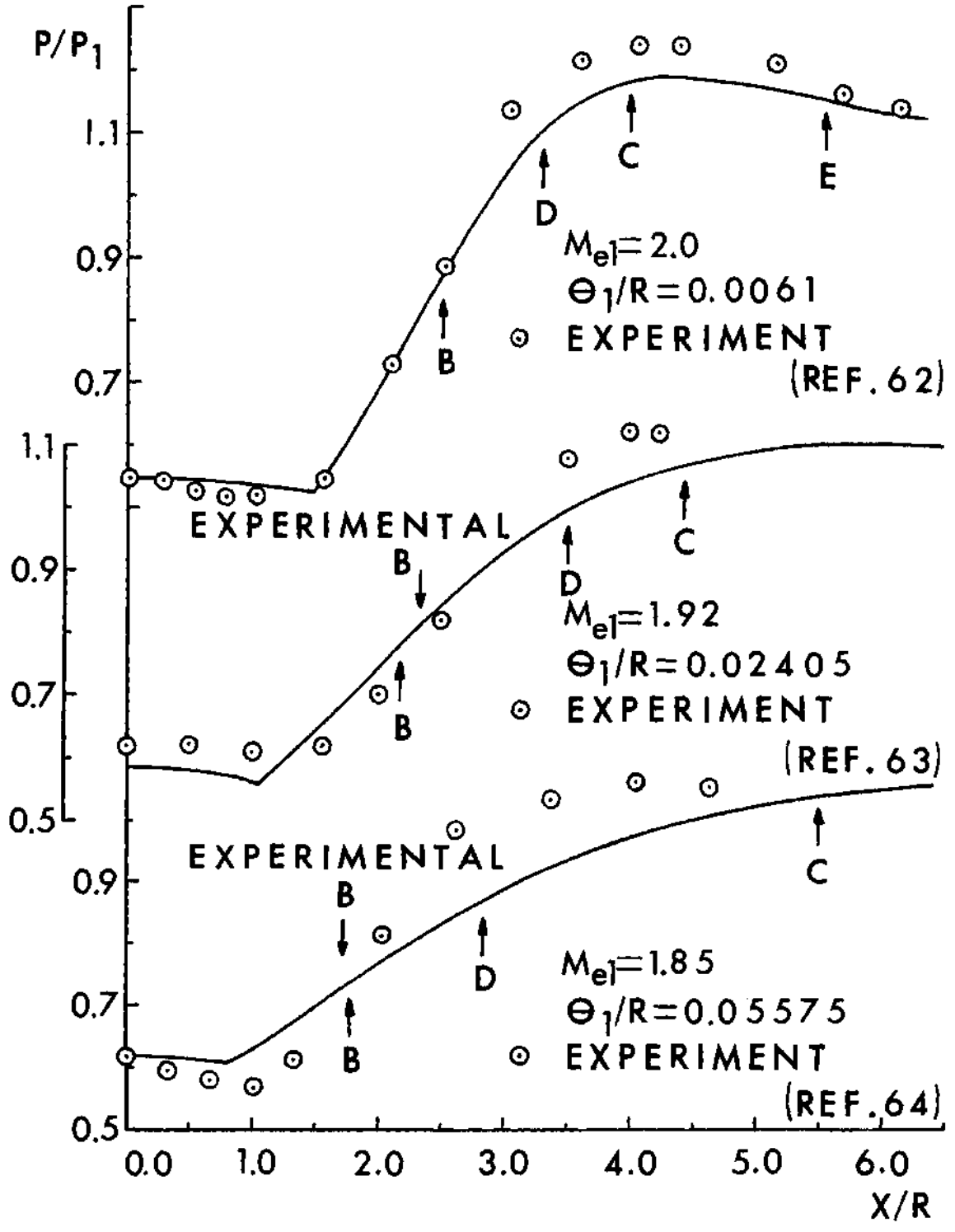

Figure 17. Comparison of Theoretical Centerline Pressure Variation with Axial Distance with Experiments Near Mach 2.

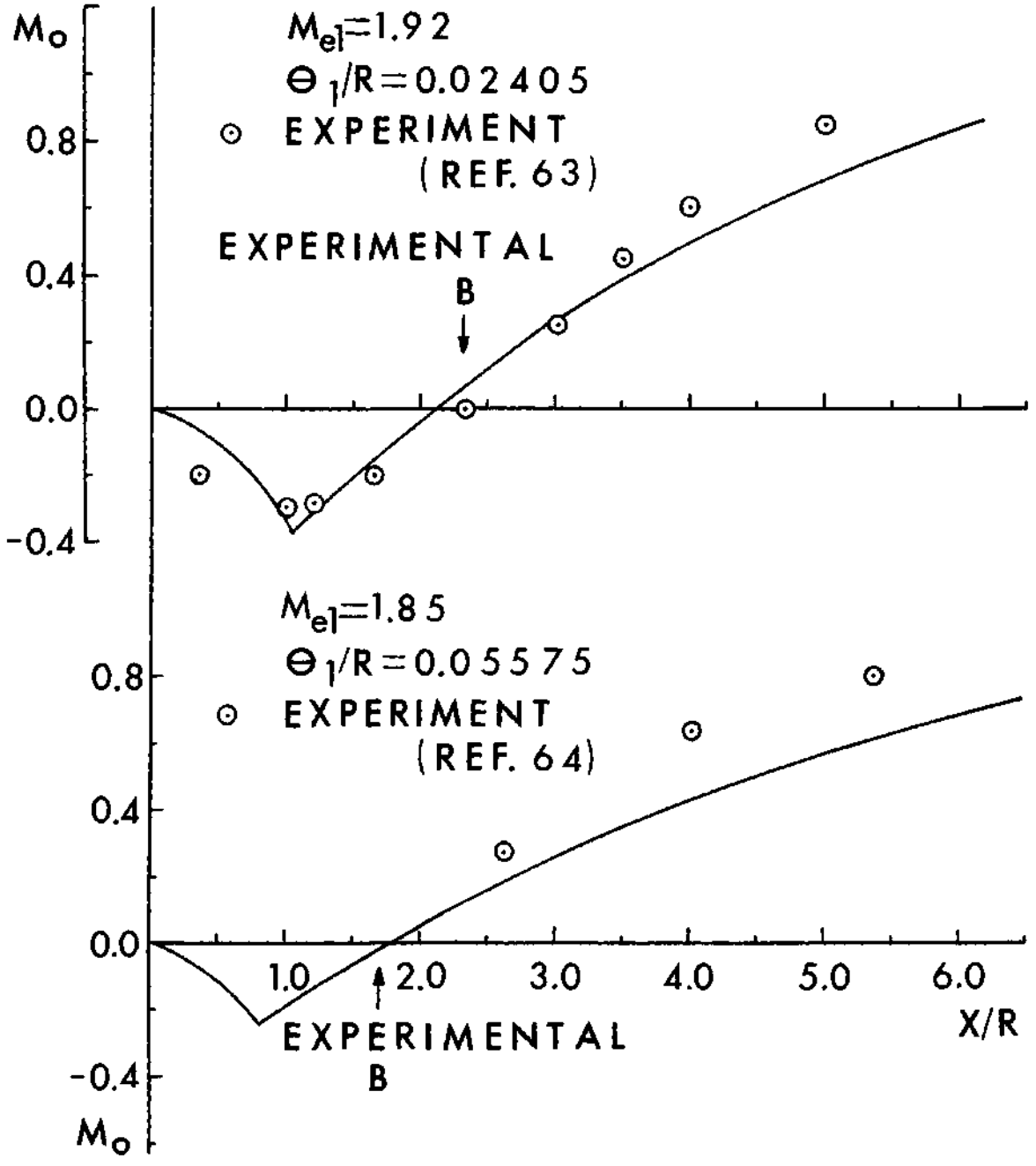

Figure 18. Comparison of Theoretical Centerline Mach Number with Axial Distance with Experiments near Mach 2.

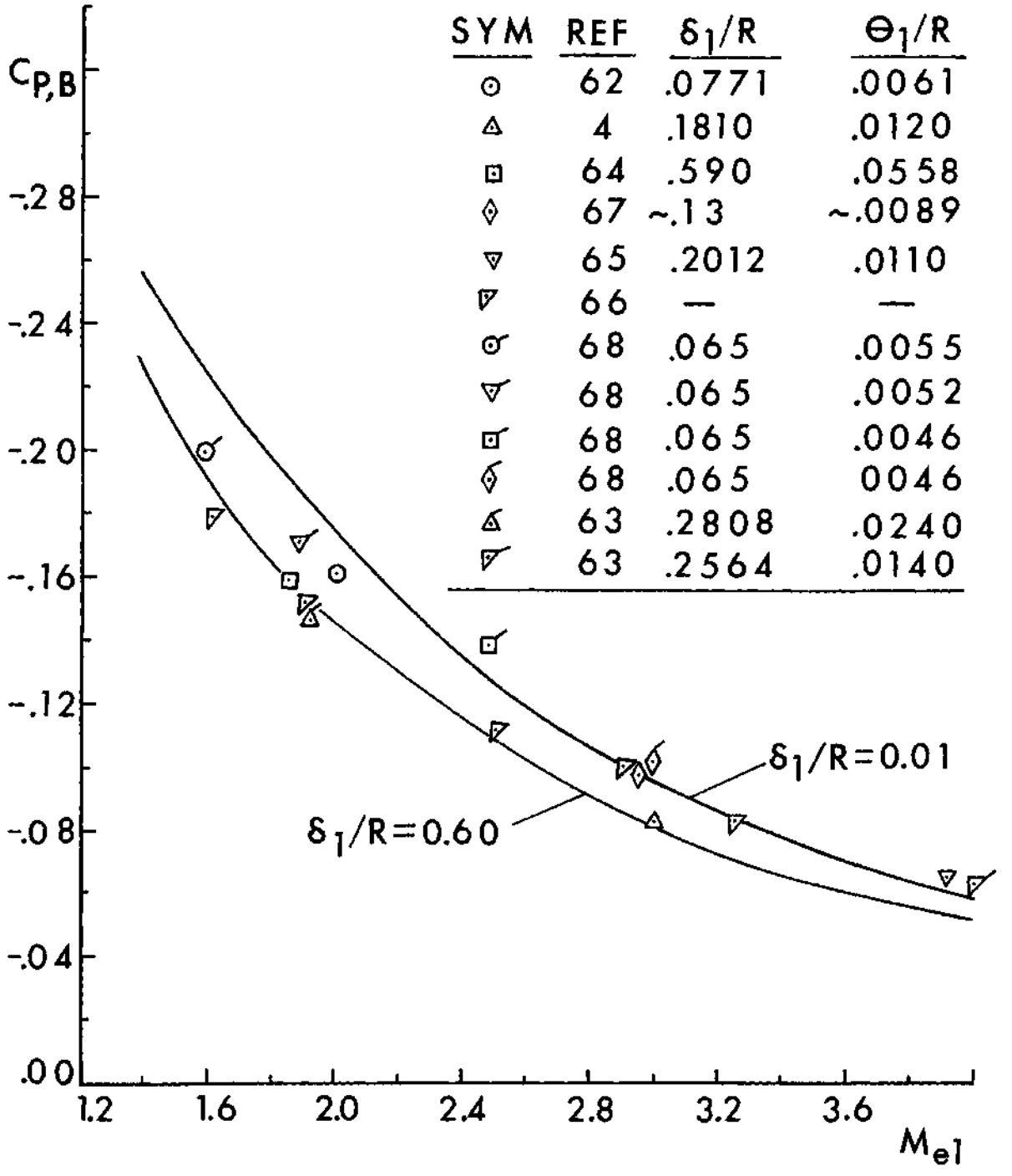

Figure 19. Effect of Upstream Mach Number on Base Pressure.

multiplies the right hand side by a factor $\sqrt{M_{e1}/2}$,* a much better correlation with the experimental results can be obtained for a wider range of Mach number, and hence, is recommended for further work. This new form for $\tilde{\epsilon}_T$ has been used for some of the computation at high Mach numbers and will be referred to as modified viscosity form (MVF).

Figures 20 and 21 show the effect of Mach number on the near wake flow field for a given initial boundary layer thickness. The pressure overshoot downstream of the RSP increases with Mach number. It is also observed that for lower Mach numbers, the critical point occurs before the maximum pressure point, while for higher Mach numbers, the critical point occurs before the minimum thickness point and in the large pressure gradient region. Another interesting feature to note is that there is not as strong an effect of Mach number on detailed quantities like location of rear stagnation point as on base pressure.

Figures 22 and 23 give the results at Mach 3 for which detailed experimental information[4,69] is available to the author. The experimental results show a slightly higher base pressure than the usual because of a slight compression caused by the boundary layer on the tunnel wall. The usually accepted value of the base pressure at this Mach number is about 0.4 (Refs. 67-68). This is also approximately the value obtained by using MVF as shown in Figure 22. A slightly disturbing trend that the slope of the experimental curve is higher than the analytical one near

---

*This is completely an empirical factor, purely based on the comparison between the present theory and the experimental results. However, to obtain the proper form of incompressible eddy viscosity ($M_{e1} \ll 1$) one can fit a polynomial, $1+aM+bM^2+..$, or a rational function, $\frac{1+a_1M+..}{1+b_1M+..}$ to obtain a behavior of $\sqrt{M_{e1}/2}$ in the range of $1.4 < M < 4.0$.

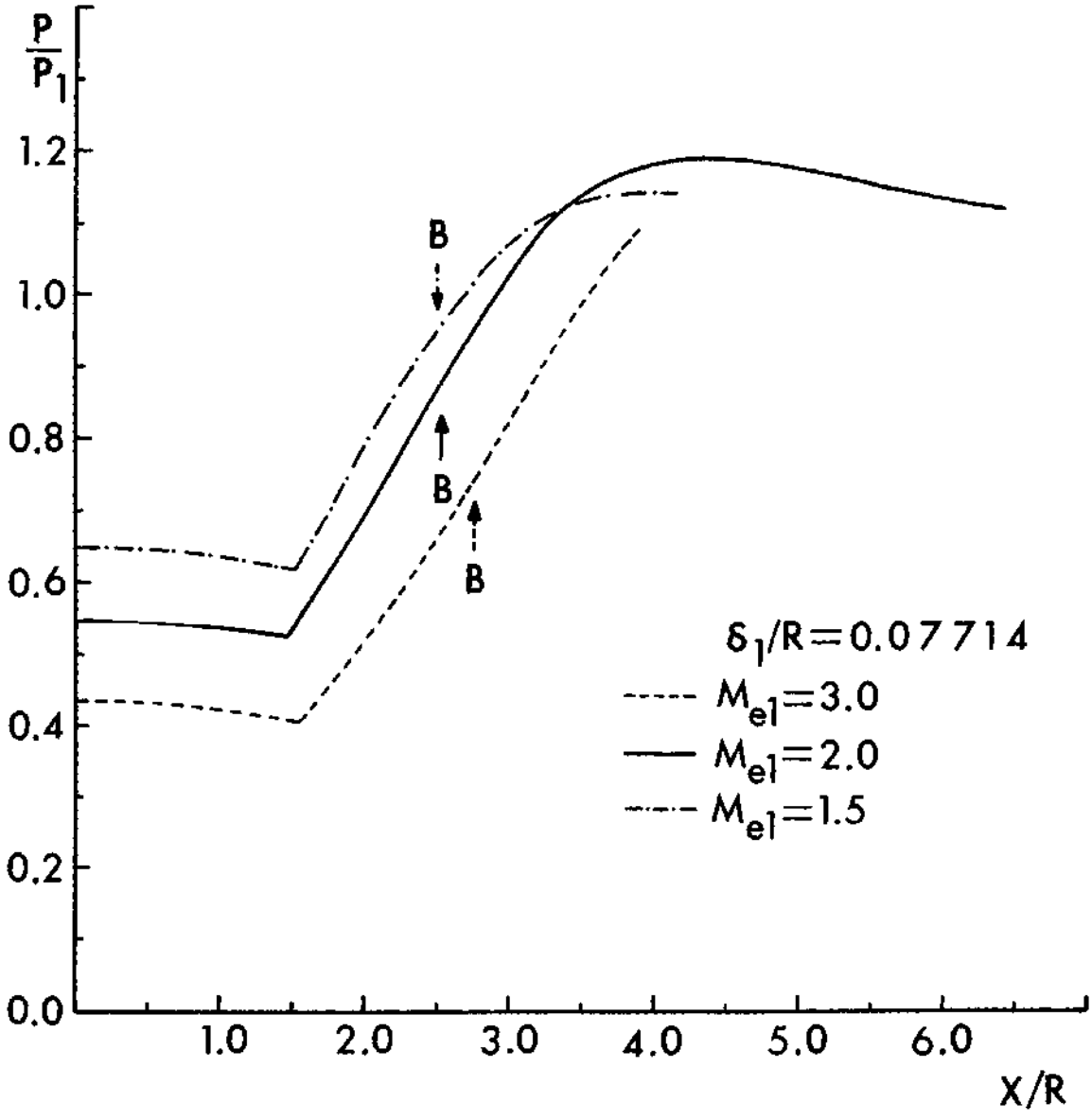

Figure 20. Effect of Upstream Mach Number on Centerline Pressure Distribution.

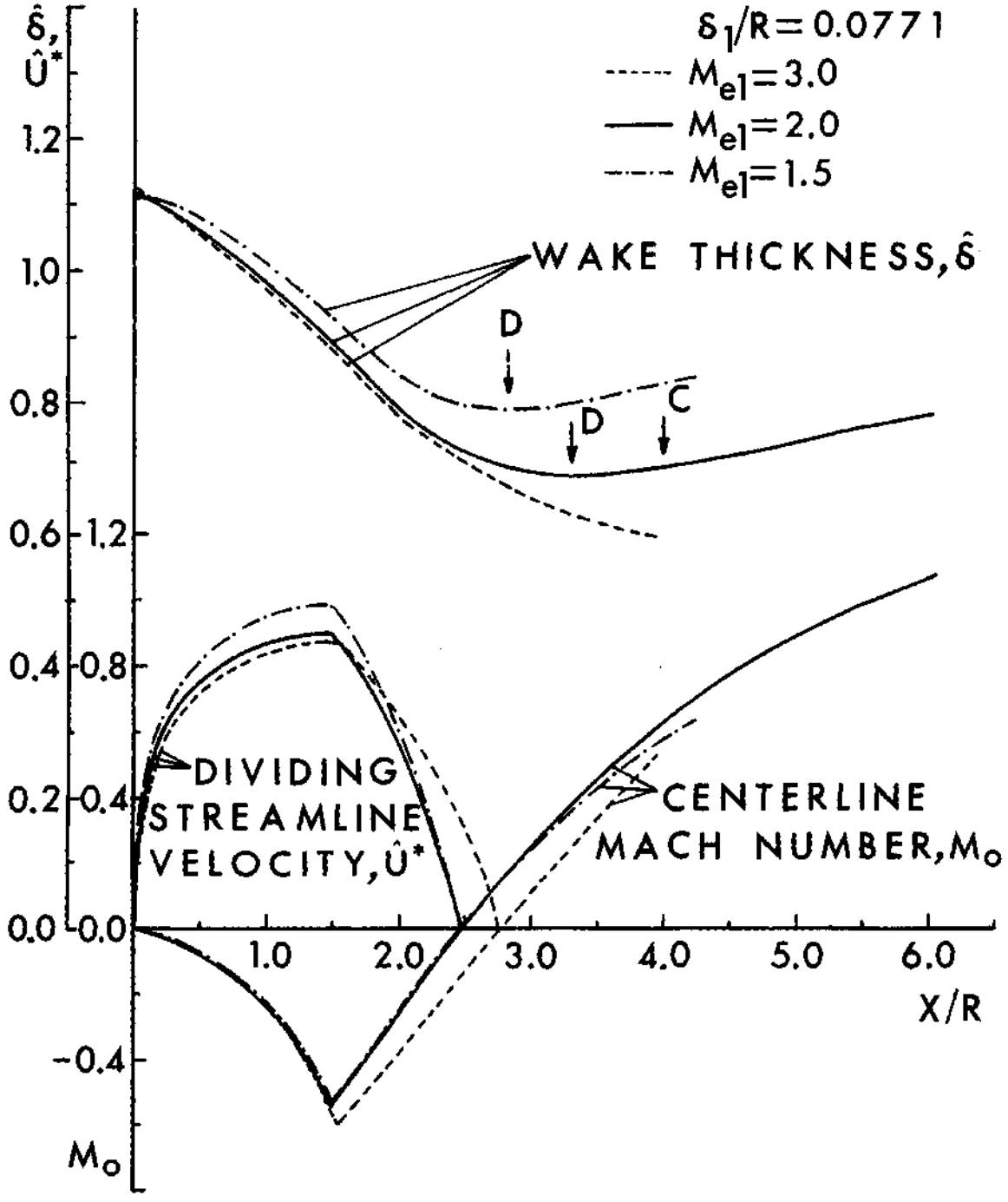

Figure 21. Effect of Upstream Mach Number on Wake Thickness, Velocity on Dividing Streamline and Centerline Mach Number Variation with Axial Distance.

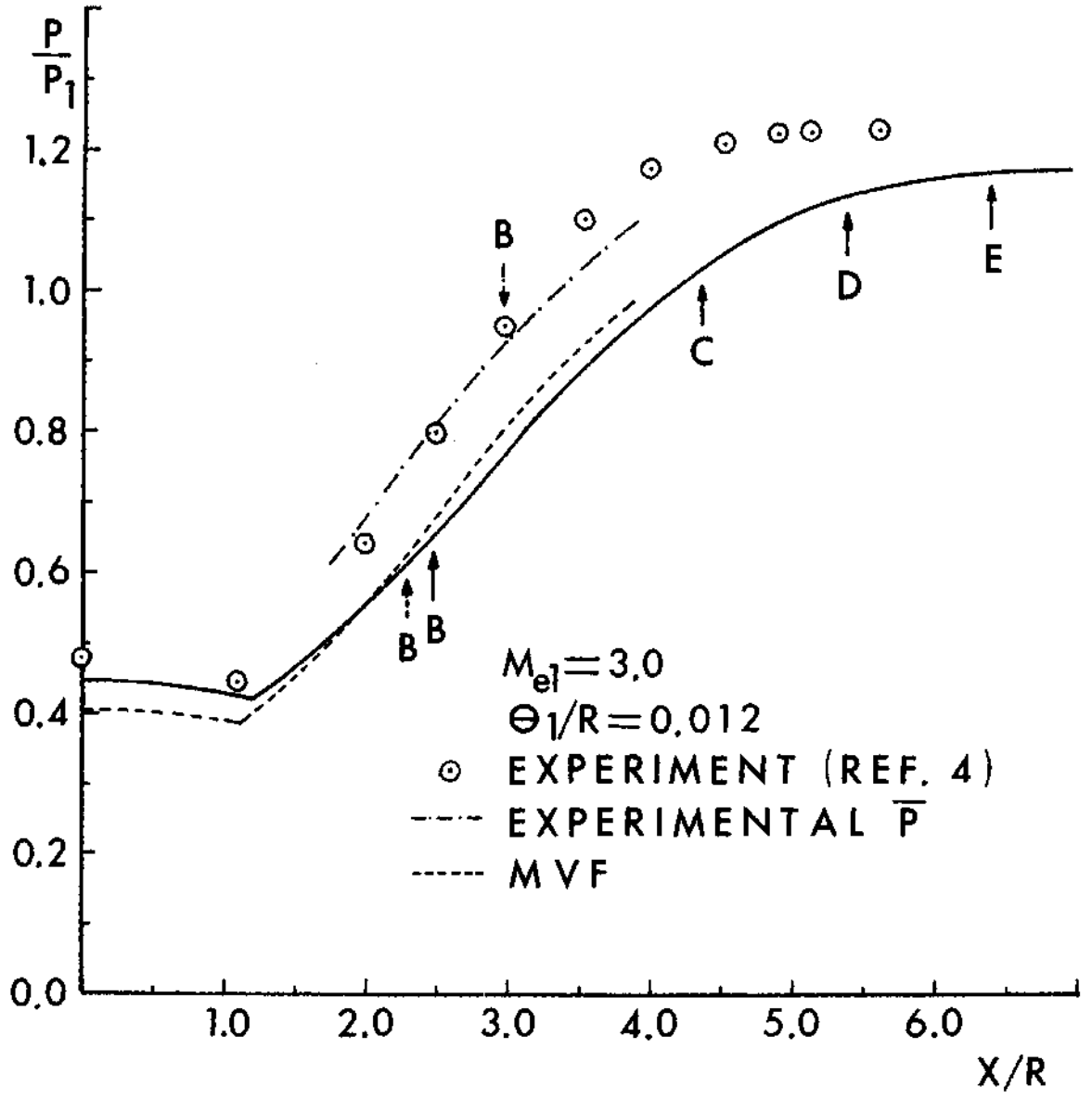

Figure 22. Comparison of Theoretical Centerline Pressure Distribution with Experiment at Mach 3. Also shown are the Area Mean of the Experimental Radial Pressure ($\bar{p}$) and the Solution using the MVF.

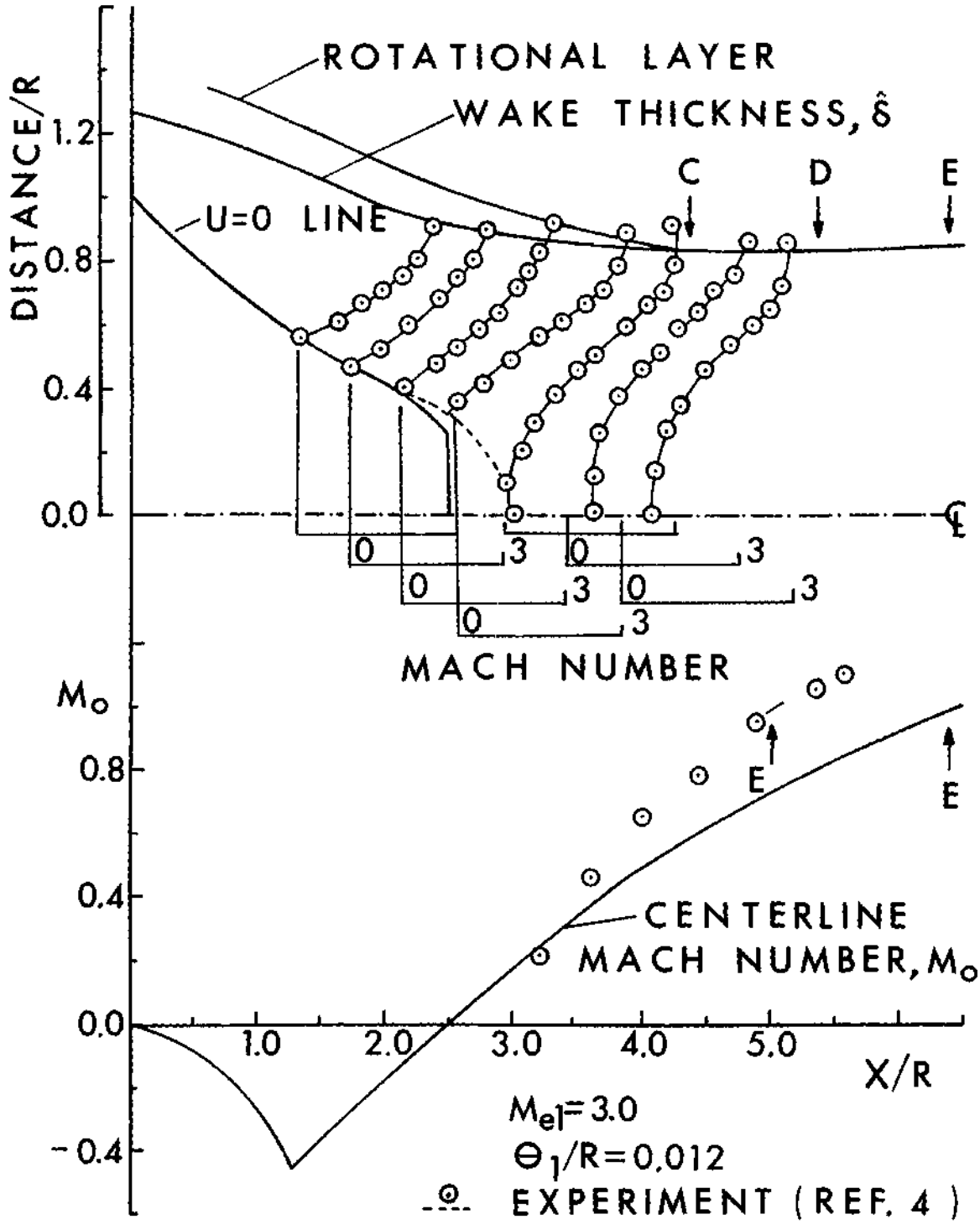

Figure 23. Comparison of Theoretical Centerline Mach Number, Wake Thickness and U = 0 Distance Distribution with Experiment at Mach 3.

the rear stagnation point is observed. This is probably due to the larger radial variation of pressure at higher Mach numbers. The area mean of the experimental radial pressure shows a better comparison with the theoretical curve in this respect. Also, Figure 23 shows a very good matching with the experimental U = 0 curve and the outer edge of the shear layer. There are quite large differences in the locations of the rear stagnation point and M = 1 points. The reason again can be the inadequacy of the cosine profile to represent the far wake satisfactorily. Also, it is difficult to find the exact location of the rear stagnation point experimentally, as the reversed flow velocities are very small.

Figure 24 shows the centerline pressure variation at about Mach 4 using MVF and the experimental result.[65] Base pressure prediction is very good, but again the slope of the experimental centerline pressure curve is higher than the theoretical one near the rear stagnation point, probably due to the reasons mentioned before. However at this and higher Mach numbers, one should start considering the lip shock, the wake shock and their interactions.

Figure 25 shows the effect of the upstream boundary layer thickness on the base pressure. The analysis shows an increase in base pressure or base pressure coefficient with the boundary layer thickness. Apart from the region of thin boundary layers the effect is small. The experimental evidence available regarding this parameter is somewhat contradictory. Reid and Hastings data[62] shows a comparatively strong dependence of base pressure on boundary layer thickness at Mach 2.03, while Chapman's[14] data shows almost no variation at Mach 2.0. This is because the boundary

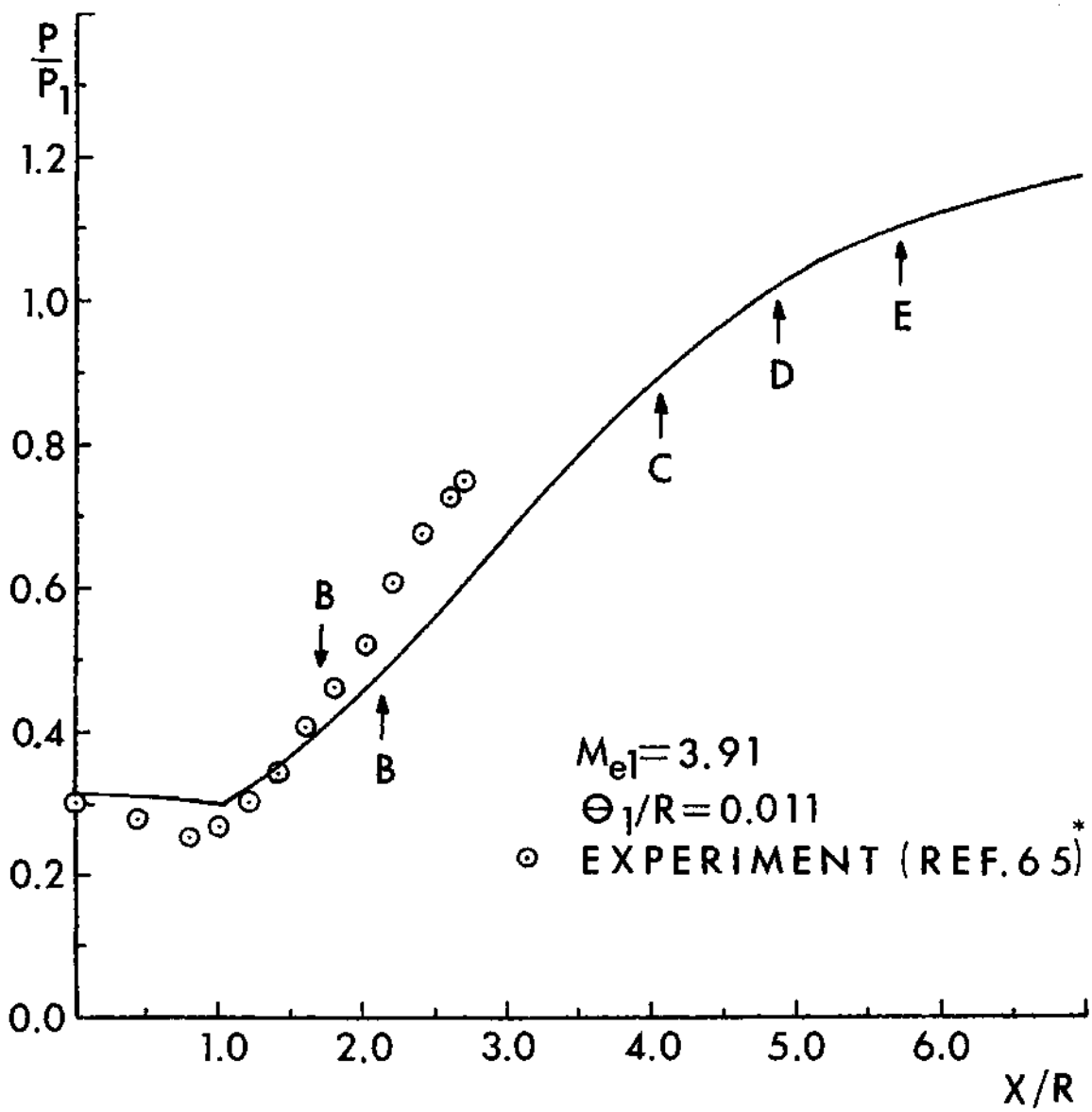

Figure 24. Comparison of Near Wake Solution with Experiment Near Mach 4 (*Data taken from Ref. 40).

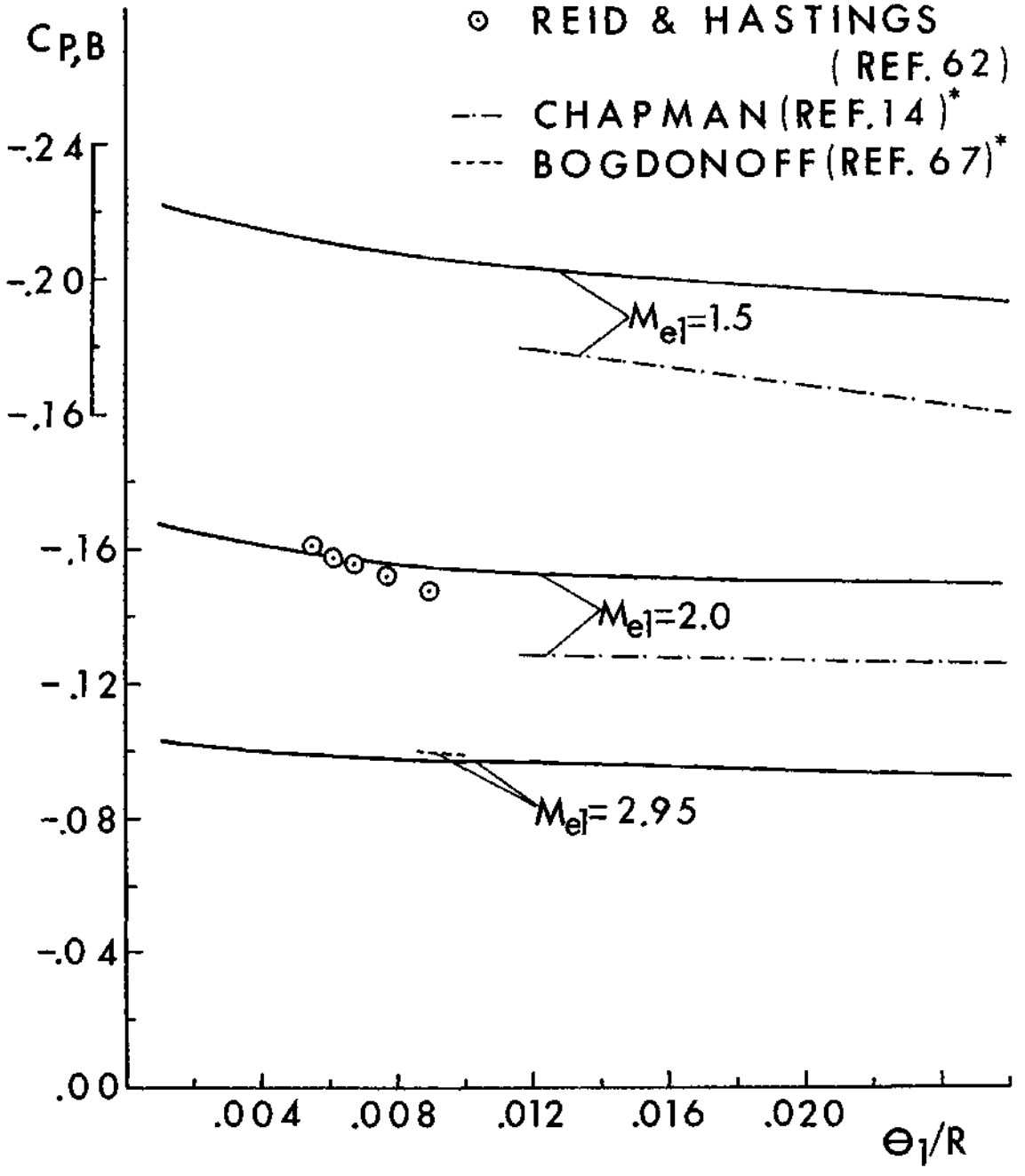

Figure 25. Upstream Momentum Thickness Influence on Base Pressure (*Data reduced from Reynolds Number Effect using Incompressible Turbulent Flat Plate Formula).

layer thickness effect is of secondary importance and probably is of the same order of magnitude as a) the effect of variation of pressure distribution on the model due to change in dimensions or shape, and b) the errors in experimental measurements. However, it is very encouraging that the base pressure predicted by this model near Mach number of two for boundary layer thicknesses varying from 0.07 to 0.6 base radii match well with the experimental data (Figures 17 and 18). This shows the adequacy of the present corner model, at least for moderate boundary layer thicknesses.

Figures 26 and 27 show the variation of various quantities in the near wake with variation of initial boundary layer thickness for fixed Mach number. Unlike the Mach number parametric study, the base pressure is seen to be a weak function of boundary layer thickness; all other quantities, such as centerline Mach number, velocity on the dividing streamline, centerline pressure, pressure overshoot are strong functions of the initial boundary layer thicknesses. Hence, measurement of the latter quantities can shed more light on the effect of boundary layer thickness rather than the measurement of base pressure and can help in improving the corner expansion model.

Figure 28 shows the effect of base bleed on the base pressure. The analytical results show a slower base pressure rise compared to experimental data[63,68] at lower values of the mass injection parameter, I, but attain the same slope as the experimental curve for large base bleed. This inability to match the low bleed effect may be due to the inaccuracy of the boundary layer approximation near the base, where both radial and axial pressure gradients are of the same order. Figures 29(a), 29(b) and

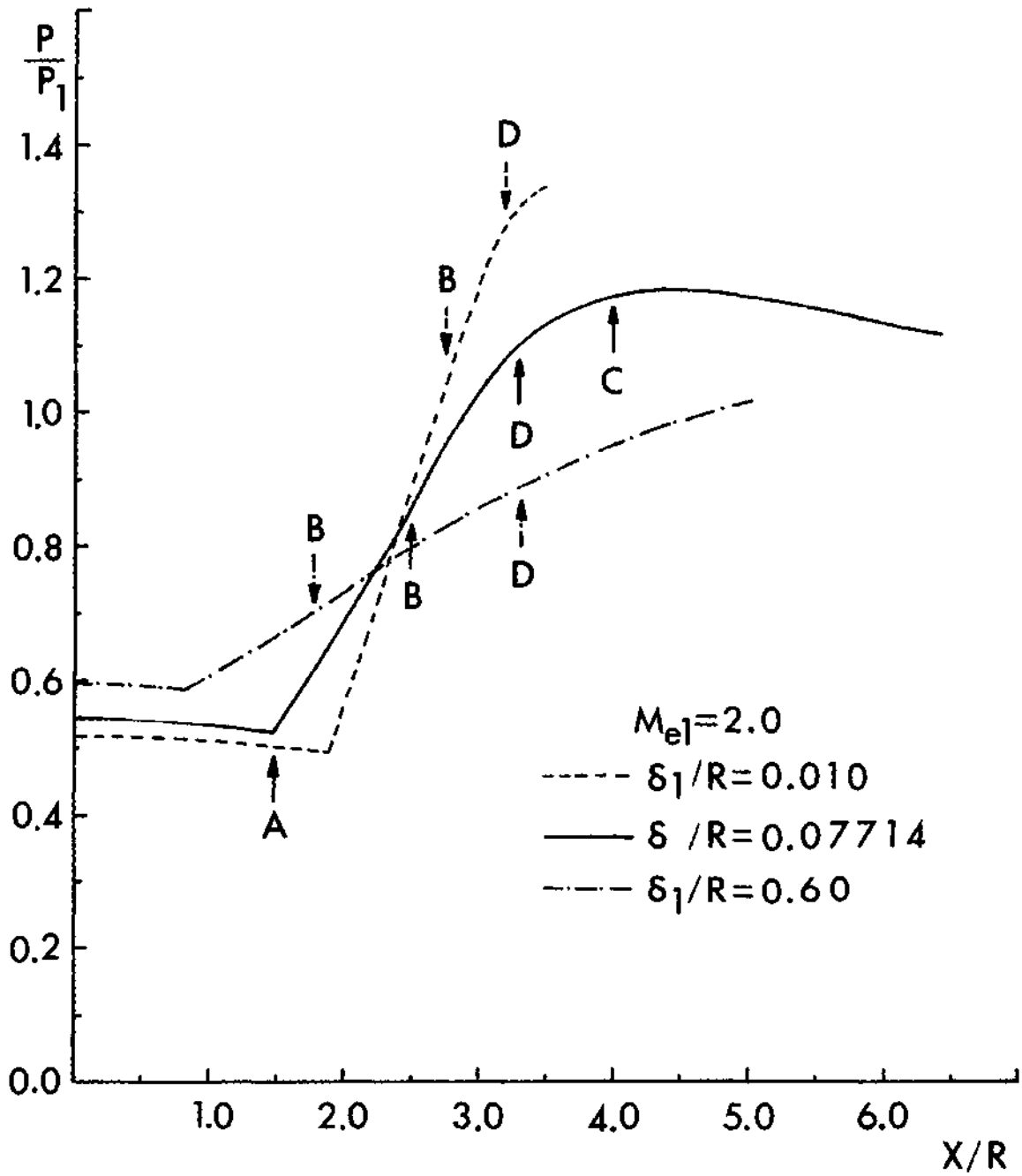

Figure 26. Effect of Upstream Boundary Layer Thickness on Centerline Pressure Distribution.

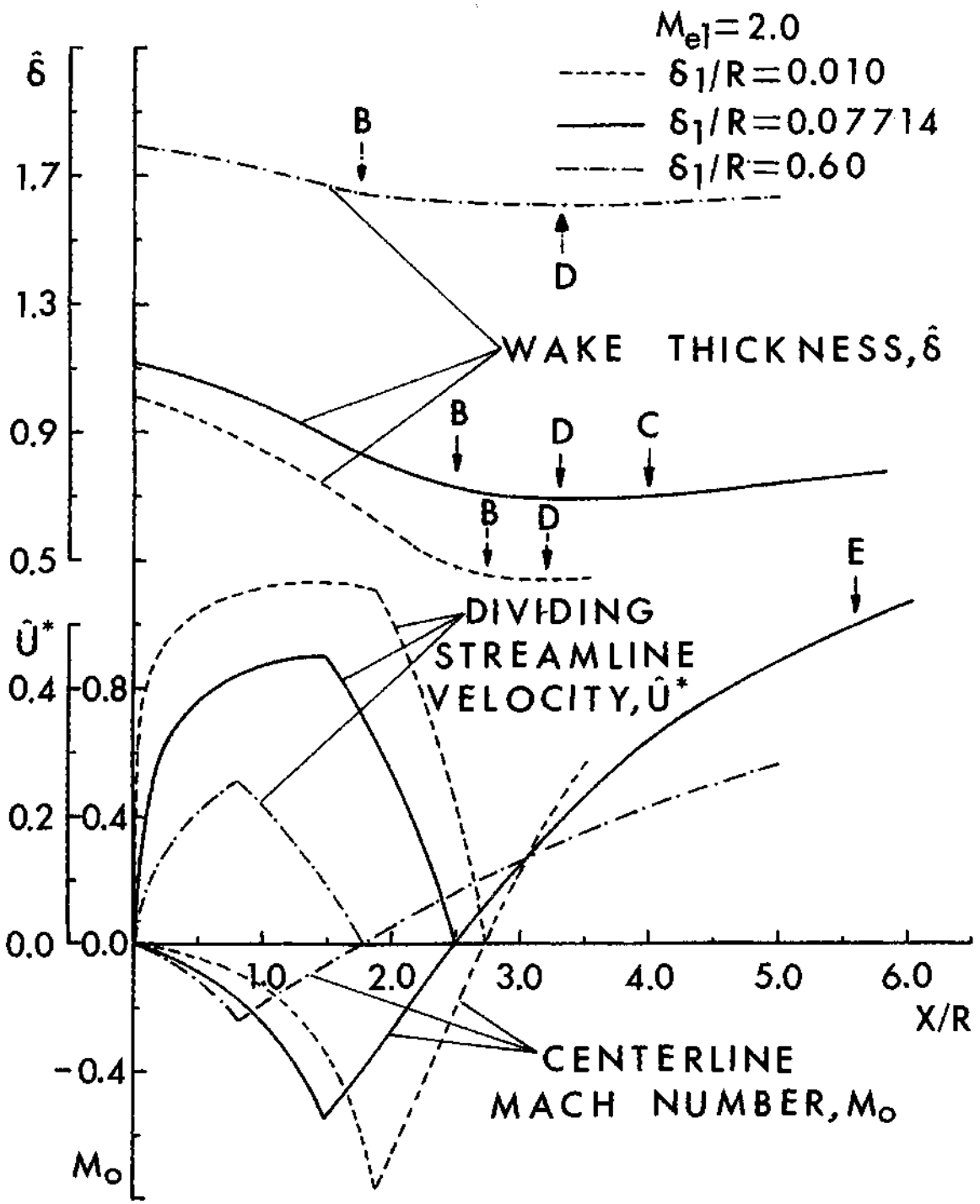

Figure 27. Effect of Upstream Boundary Layer Thickness on Wake Thickness, Velocity on Dividing Streamline and Centerline Mach Number Distributions.

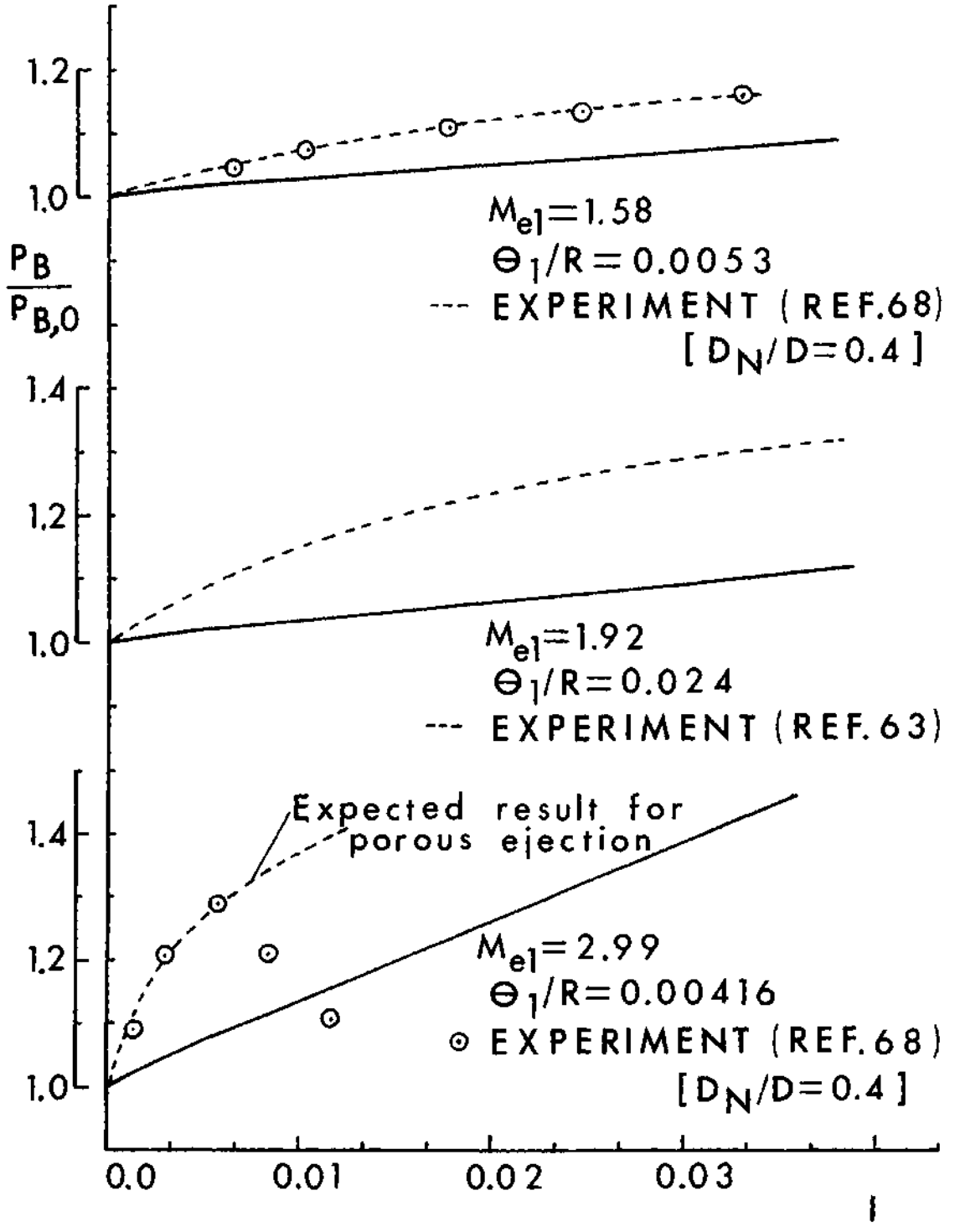

Figure 28. Variation of Base Pressure with Base Bleed and Comparison with Experiments (D_n/D is Ratio of the Injection Nozzle Diameter to the Base Diameter).

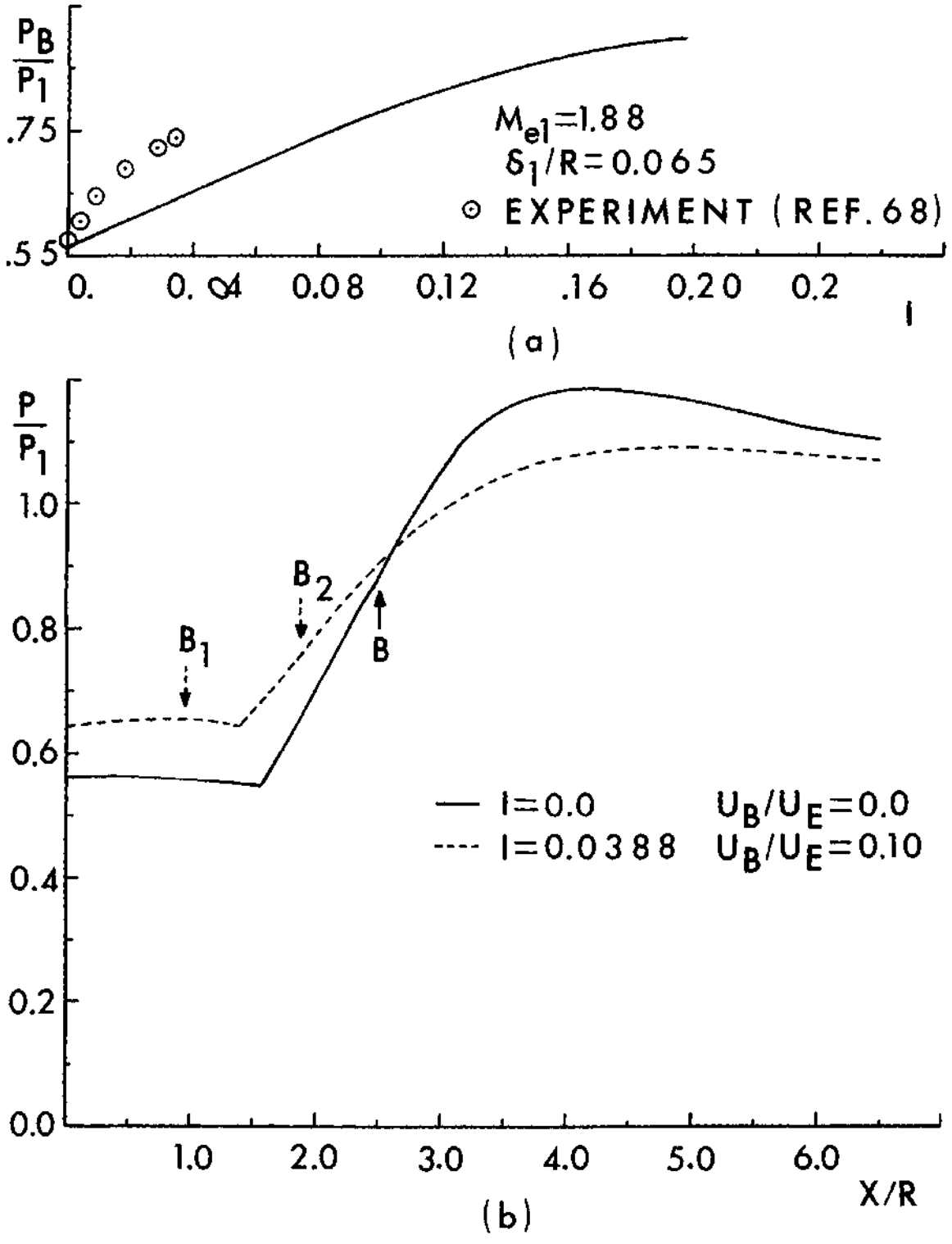

Figure 29. Effect of Base Bleed at Mach 1.88 on (a) Base Pressure and (b) Centerline Pressure Distribution.

30 show the base pressure variation with base bleed and the change of near wake flow field quantities that can be expected with base bleed, for constant upstream boundary layer thickness and Mach number. There are two stagnation points with small base bleed, and the recirculation region shrinks with base bleed. Also, the wake thickness increases with base bleed, resulting in smaller convergence of streamlines in the outer flow field, and the overshoot feature in the centerline pressure curve of the axisymmetric bodies reduces.

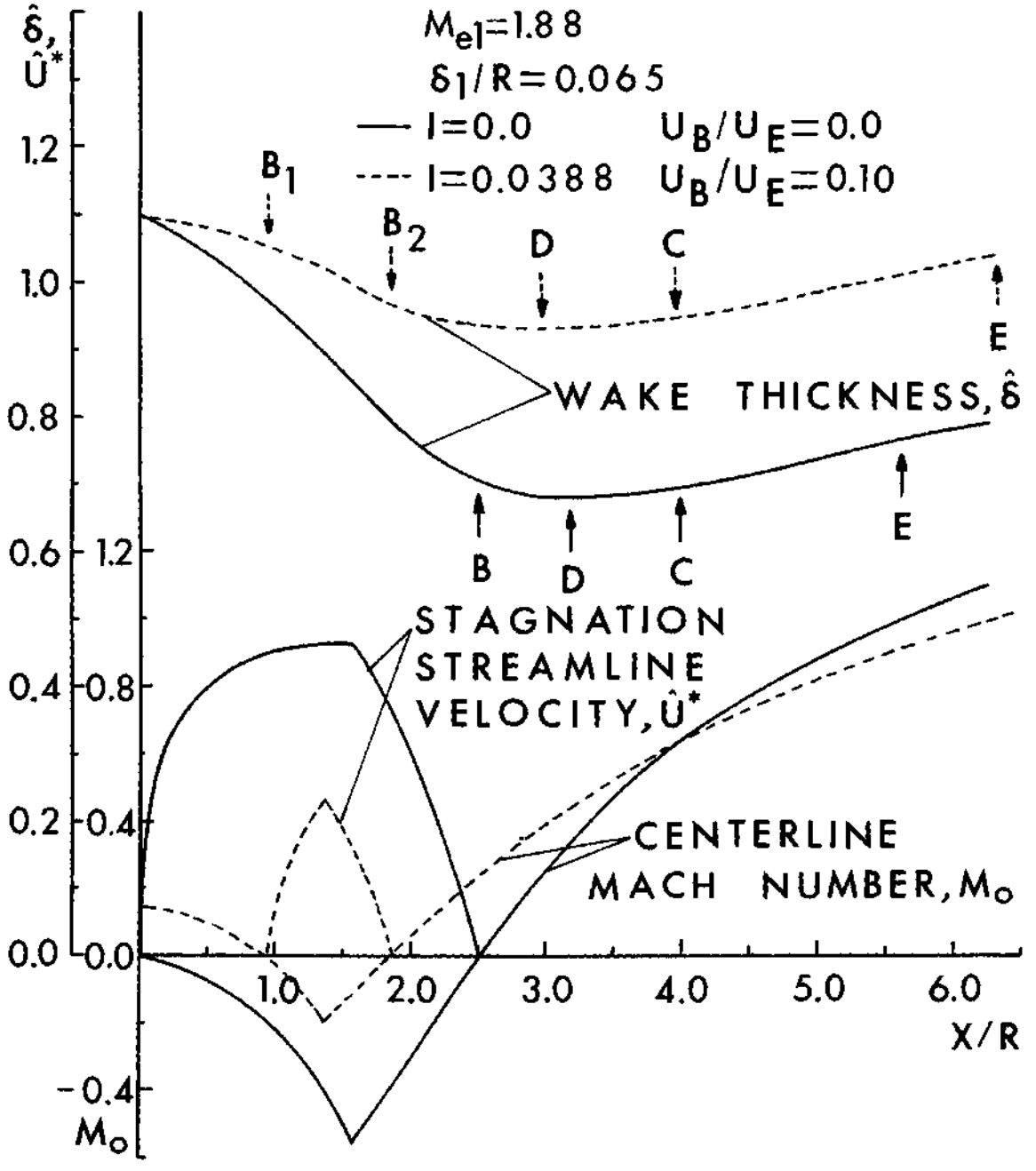

Figure 30. Effect of Base Bleed at Mach 1.88 on Wake Thickness, Centerline Mach Number and Velocity on Dividing Streamline Distributions. B_1 = Forward Stagnation Point, B_2 = Rear Stagnation Point.

CHAPTER VII

DISCUSSION, CONCLUSIONS AND RECOMMENDATIONS

As mentioned in the Introduction, a recent report[40] has appeared which contains a theory very similar to the present one. Because of the apparent similarity, it is thought necessary to point out the major differences between them. First, the present program takes significantly less computer run time compared to the work of Ref. 40. Although it is difficult to make an exact comparison between the two run times, as the programs were run on two different computers, they are believed to differ by a factor of 10 or so. This is primarily due to the approximate method of characteristics employed in this work. Second, the employment of a centerline momentum equation, instead of the constant pressure assumption of Ref. 40, in the initial development of wake, results in better prediction of the length of the approximately constant pressure region. Third, the mechanical energy equation has been employed in the present analysis instead of the half-radius momentum equation used in Ref. (40). Further, there is a difference in the treatment of the corner expansion region and the eddy viscosity model. Ref. (40) divides the upcoming boundary layer into inner and outer portions at the sonic line. The turbulent Reynolds number in the eddy viscosity model is treated as a function of geometry, Mach number, boundary layer thickness and pressure gradient. The exact form is obtained by comparison with the experimental base pressure data. In the present analysis, the eddy viscosity model has been derived from

the behavior of well known asymptotic simple flows. Using the corner model proposed, it was possible to predict the base pressure, and its dependence on Mach number and initial boundary layer thickness satisfactorily. However, as pointed out in the previous chapter, the eddy viscosity form should be slightly modified in order to have better agreement with experiment at large and small Mach numbers.

The major conclusions arrived at are as follows:

1) Mach number is the primary variable affecting the base pressure. Base pressure decreases with the increase of Mach number. There is good agreement between theory and experiment.

2) The upstream boundary layer thickness is a secondary parameter; the base pressure increases with the increase of boundary layer thickness. Again good agreement with a number of experimental data is obtained. This indicates that the present modelling of corner region and shear stress is reasonable for this approximate analysis.

3) The detailed results, such as centerline pressure variation, centerline Mach number variation and shear layer thickness variation, agree well with the experiments. At high Mach numbers, however, the theory gives smaller pressure gradients in the compression region than do the experiments. This is found due to the radial variation of pressure in the shear layer in the experiments.

4) At low base bleeds, the theory shows much smaller base pressure rise compare to experiments. The inaccuracy of the boundary layer equation, in representing the region close to the base, may be the major cause for this result.

In summary, the method developed here provides adequate details of the field structure, when compared with experiment, to provide the analytical framework for external burning studies. Apart from the inclusion of radial pressure gradient, which would require a major modifications to the present theory, necessary improvement in the theory should certainly include the removal of the adiabatic assumption. The theory should further be generalized, by including species conservation equations, in order to take care of various species generated during combustion. More experimental information about the boundary layer thickness influence is required to judge and improve the corner flow model. Here its effect on the centerline Mach number, rather than on the base pressure, should be measured, as the present analysis indicates that the centerline Mach number distribution is very sensitive to upstream boundary layer thickness. Also, experiments are necessary to verify the present handling of the eddy viscosity, particularly concerning the effect of compressibility.

The theory presented here is currently being used for external burning studies in situations where the near wake remains in an adiabatic condition.

APPENDIX

CURVE FITTING UTILIZING RATIONAL FUNCTION TECHNIQUE

In this dissertation, curve fitting is found advantageous at two places, viz., for obtaining intermediate values (interpolation) and derivatives, and secondly, for solving an implicit equation.

The first problem occurs when the Kubota et al. solutions are employed for representing the velocity profile of the inner region. Here the values of various properties (Figure 10) of these profiles at discrete points are known in terms of the parameter, n. It is necessary in the solution of the problem to obtain the value of these properties for any arbitrary n (requiring an interpolation scheme) and the derivatives with respect to n. Also, when the solution with the Green profiles is matched with the solution using the Kubota et al. profiles, it is necessary to obtain n for given A_2' (so easy inversion is preferable). The method of least squares using exponential functions and polynomials is found unsatisfactory for these curves as high degree polynomials, required to obtain reasonable accuracy, give peaks and troughs in the range of interest, and this results in odd behavior of derivatives. Also computation time increases with the increase in degree of the polynomial. On the other hand, phenomenal success is obtained using rational functions.

A rational function is a quotient of two polynomials, and in general can be written as

$$R(x) = \frac{1 + a_1 x + a_2 x^2 + a_3 x^3 + ..}{b_o + b_1 x + b_2 x^2 + b_3 x^3 + ..} \qquad \text{(A-1)}$$

Again the complexity and the possibility of extrema occurring in the range of interest increases with the use of higher degree polynomials. But it is obvious that (i) even with a finite degree of polynomial of the denominator, it has the characteristics of infinite series, (ii) one can satisfy the function at more points using lower degree polynomials, for example, at seven points using third degree polynomials for both numerator and denominator, and hence more accuracy but easy inversion. In the present case, it is found necessary to split the range of n into two parts, 0.5025 to 0.675, and 0.65 to 0.75. A third degree polynomial for both numerator and denominator is used, and the coefficients are found by solving seven algebraic equations simultaneously, viz.,

$$\begin{aligned} & x_1 a_1 + x_1^2 a_2 + x_1^3 a_3 - R_1 b_o - R_1 x_1 b_1 - R_1 x_1^2 b_2 - R_1 x_1^3 b_3 = -1 \\ & \vdots \\ & x_7 a_1 + x_7^2 a_2 + x_7^3 a_3 - R_7 b_o - R_7 x_7 b_1 - R_7 x_7^2 b_2 - R_7 x_7^3 b_3 = -1 \end{aligned} \qquad \text{(A-2)}$$

Sometimes, a little trial and error is found necessary to avoid the denominator going through zero in the range of interest. This is done by perturbing the values of properties slightly. The range of the two parts is allowed to overlap slightly and continuity of the first derivative is maintained at n = 0.65.

The second problem occurs in the solution of the external flow -- to get the Mach number from Prandtl-Meyer angle. This requires the

solution of Eq. (4-13) which contains hyperbolic functions. A direct solution method will involve an iteration scheme. And if a simple curve can be fitted in the range of interest with sufficient accuracy, it will save computational time. Again, a third degree polynomial is chosen for both numerator and denominator of Eq. (A-1), viz.

$$M = \frac{1 + a_1\nu + a_2\nu^2 + a_3\nu^3}{b_o + b_1\nu + b_2\nu^2 + b_3\nu^3} \qquad \text{(A-3)}$$

It is found necessary to split the Mach number range in two parts for better accuracy. The maximum error, in the range $1.2 < M < 1.72$, is in the fifth significant figure of M, and in the range $1.72 < M < 4.2$ is in the seventh significant figure of M.

REFERENCES

1. Hama, F. R., "Estimation of Strength of Lip Shock," AIAA Journal, Vol. 4, 1966, pp. 166-167.

2. Gilreath, H. E. and Shetz, J. A., "Transition and Mixing in the Shear Layer Produced by Tangential Injection in Supersonic Flow," Journal of Basic Engineering, Dec. 1971, pp. 610-618.

3. Strahle, W. C., "Theoretical Considerations of Combustion Effects on Base Pressure in Supersonic Flight," Twelfth Symposium (International) on Combustion, The Combustion Institute, 1969, pp. 1163-1173.

4. Strahle, W. C., Hubbartt, J. E., Neale, D. H., Mehta, G. K. and Wilson, W. W., "Turbulent Axisymmetric Base Flow Studies for External Burning Propulsion," to be published by the Chemical Propulsion Information Agency in the Proceedings of the 13th JANNAF Combustion Meeting.

5. Crocco, L. and Lees, L., "A Mixing Theory for the Interaction Between Dissipative Flows and Nearby Isentropic Streams," Journal of the Aeronautical Sciences, Vol. 19, Oct. 1952, pp. 649-676.

6. Gabeaud, A., "Sur la resistance de 1'air aux vitesses balistque," Comptes-rendus de 1'Academie des Sciences, Vol. 192, 1931, pp. 1630.

7. Gabeaud, A., "Recherches sur la resistance de 1'air," Memorial de 1'Aritllerie Francais, TOME XV, 4^{eme} faciule de 1936, 1936, pp. 1290-1300.

8. Gabeaud, A., "Base Pressures at Supersonic Velocities," Journal of the Aeronautical Sciences, Vol. 17, No. 8, Aug. 1950.

9. von-Karman, T. and Moore, N. B., "Resistance of Slender Bodies Moving with Supersonic Velocities, with Special Reference to Projectiles," Trans. ASME, Vol. 54, 1932, pp. 303.

10. Hill, F. K., "Base Pressures at Supersonic Velocities," Journal of the Aeronautical Sciences, Vol. 17, No. 3, Mar. 1950, pp. 185.

11. Cope, W. F., "The Effect of Reynolds Number on the Base Pressure of Projectiles," Engg. Div. 63/44, NPL, British A.R.C., Jan. 1945.

12. Cope, W. F., "Calculations of Reynolds Number Effect on Projectiles at Supersonic Speeds," 6th Int. Cong. of Appl. Mechs., Paris, 1946.

13. Hankins, G. A., "Experiments of Reynolds Number Effect on Projectiles at Supersonic Speeds," 6th Int. Cong. of Appl. Mechs., Paris, 1946.

14. Chapman, D. R., "An Analysis of Base Pressure at Supersonic Velocities and Comparison with Experiment," NACA TN 2137, July 1950.

15. Chapman, D. R., Kuhen, D. M. and Larson, H. K., "Investigation of Separated Flows in Supersonic and Subsonic Streams with Emphasis on Effects of Transition," NACA TN 3869, Mar. 1957.

16. Korst, H. H., "A Theory for Base Pressure in Transonic and Supersonic Flow," J. Appl. Mechs., Vol. 23, 1956, pp. 593-600.

17. Kirk, F. A., "An Approximate Theory of Base Pressure in Two Dimensional Flow at Supersonic Speed," RAE Tech. Note, Aero. 2377, Mar. 1954.

18. Nash, J. F., "An Analysis of Two Dimensional Turbulent Base Flow, indicating the Effect of the Approaching Boundary Layer," ARC R & M 3344, July 1962.

19. McDonald, H., "Turbulent Shear Layer Reattachment with Special Emphasis on the Base Pressure Problems," B.A.C. Report, Ae. 175, Issue 2, Aug. 1963.

20. McDonald, H., "An Analysis of Turbulent Base Pressure Problem in Supersonic Configuration Flow," Aeronautical Quarterly, Vol. 16, May 1965.

21. McDonald, H., "The Turbulent Supersonic Base Pressure Problem: A Comparison Between a Theory and Some Experimental Evidence," Aeronautical Quarterly, Vol. 17, May 1966.

22. Hill, W. G., Jr., "Initial Development of Compressible Turbulent Free Shear Layer," Ph.D. Thesis, Rutgers - The State University, May 1966.

23. Przirembel, C. E. G. and Page, R. H., "Analysis of Axisymmetric Supersonic Turbulent Base Flow," Proceedings of the 1968 Heat Transfer and Fluid Mechanics Institute, Stanford University Press, 1968, pp. 258-272.

24. Mueller, T. J., "Determination of the Turbulent Base Pressure in Supersonic Axisymmetric Flow," Journal of Spacecraft and Rockets, Vol. 5, Jan. 1968, pp. 101-107.

25. Roache, P. J., "Base Drag Calculation in Supersonic Turbulent Axisymmetric Flow," Journal of Spacecraft and Rockets, Vol. 10, Apr. 1973, pp. 285-287.

26. Korst, H. H., "Component Analysis and Synthesis for Fully Separated Flows with Special Consideration of Base Drag Reduction by Combustion," Progress in Astronautics and Aeronautics, Vol. 40, 1976, pp. 211-254.

27. Davis, D. D., "Extension of Simplified Mixing Theory to Axially Symmetric Supersonic Wake Flows and Application to the Base Pressure Problem for a Body of Revolution," Master's Thesis, Princeton University, 1952.

28. de Krasinski, J. E., "A Study of Axially Symmetric Base Flow Behind Bodies of Revolution at Supersonic Speed," AGARD C.P. No. 4, 1966, pp. 747-771.

29. Reeves, B. L. and Lees, L., "Theory of Laminar Near-Wake of Blunt Bodies in Hypersonic Flow," AIAA Journal, Vol. 3, Nov. 1965, pp. 2061-2074.

30. Stewartson, K., "Further Solutions of the Falkner-Skan Equation," Proc. Cambridge Phil. Soc., Vol. 50, 1954, pp. 454-465.

31. Cohen, C. B. and Reshotko, E., "Similar Solutions for the Compressible Laminar Boundary Layer with Heat Transfer and Pressure Gradient," NACA Rept. 1293, 1956.

32. Golik, R. J., Webb, W. H. and Lees, L., "Further Results of Viscous Interaction Theory for the Laminar Supersonic Near Wake," AIAA Paper 67-61, presented at the AIAA 5th Aerospace Sciences Meeting, New York, N. Y., Jan. 1967.

33. Alber, I. E. and Lees, L., "Integral Theory for Supersonic Turbulent Base Flows," AIAA Journal, Vol. 6, July 1968, pp. 1343-1351.

34. Murthy, S. N. B. and Osborn, J. R., "Base Flow Phenomena with and without Injection: Experiment Results, Theories and Bibliography," Progress in Astronautics and Aeronautics, Vol. 40, 1976, pp. 7-210.

35. Ohrenberger, J. T. and Baum, E., "A Theoretical Model of the Near Wake of a Slender Body in Supersonic Flow," AIAA Journal, Vol. 10, Sept. 1972, pp. 1165-1172.

36. Weiss, R. F., "A New Theoretical Solution of the Laminar Hypersonic Near Wake," AIAA Journal, Vol. 5, 1967, pp. 2142.

37. Amsden, A. A. and Harlow, F. H., "Numerical Calculations of Supersonic Wake Flow," AIAA Journal, Vol. 3, 1965, pp. 2081-2086.

38. Allen, J. S. and Cheng, S. I., "Numerical Solutions of the Compressible Navier-Stokes Equations for the Laminar Near Wake," Phys. of Fluids, Vol. 13, 1970, pp. 37-52.

39. Roache, P. J. and Mueller, T. J., "Numerical Solutions of Laminar, Separated Flows," AIAA Journal, Vol. 8, 1970, pp. 530.

40. Peters, C. E. and Phares, W. J., "Analytical Model of Supersonic, Turbulent Near-Wake Flows," AEDC-TR-76-127, Sept. 1976.

41. Hama, F. R., "Experimental Studies on the Lip Shock," AIAA Journal, Vol. 6, 1968, pp. 212-219.

42. Hastings, R. C., "Turbulent Flow Past Two-Dimensional Bases in Supersonic Streams," RAE Tech. Note, Aero 9931, 1963.

43. Adamson, T. C., "Effect of Transport Properties on Supersonic Expansion around a Corner," Phys. Fluids, Vol. 10, 1967, pp. 953-962.

44. Adamson, T. C., "Solutions for Supersonic Rotational Flow around a Corner using a New Coordinate System," J. Fluid Mechanics, Vol. 34, 1968, pp. 735-748.

45. Weinbaum, S., "Rapid Expansion of a Supersonic Boundary Layer and Its Application to the Near Wake," AIAA Journal, Vol. 4, 1966, pp. 217-226.

46. Donaldson, I. S., "On the Separation of a Supersonic Flow at a Sharp Corner," AIAA Journal, Vol. 5, 1967, pp. 1086-1088.

47. Shetz, J. A., Billig, F. S. and Favin, S., "Simplified Analysis of Supersonic Base Flows Including Injection and Combustion," VPI-Aero-039, Sept. 1975, Virginia Polytechnic Institute and State University, Blaksburg, Virginia.

48. Mellor, G. L. and Gibson, D. M., "Equilibrium Turbulent Boundary Layer," J. Fluid Mechanics, Vol. 24, Part 2, 1966.

49. Webb, W. H., "An Approximate Pressure-Angle Relation for the Axisymmetric Supersonic Near Wake," AIAA Journal, Vol. 6, July 1968, pp. 1427-1428.

50. Liepmann, H. W. and Roshko, A., Elements of Gasdynamics, Galcit Aeronautical Series, John Wiley and Sons, Inc., New York, 1957.

51. Boussinesq, J., "Theorie de l'ecoulement tourbillant," Mem. Pre. par. div. Sav. 23, Paris, 1877.

52. Townsend, A. A., The Structure of Turbulent Shear Flow," Cambridge Monographs on Mechanics and Applied Mathematics, The Cambridge University Press, 1956, pp. 62-63; pp. 170-171.

53. Tennekes, H. and Lumley, J. L., A First Course in Turbulence, The MIT Press, Massachusetts, pp. 179.

54. Abramovich, G. A., The Theory of Turbulent Jets, The MIT Press, pp. 28-30.

55. Schlichting, H., Boundary Layer Theory, 6th ed., McGraw Hill, New York, 1968, pp. 690.

56. Kubota, T., Reeves, B. L. and Buss, H., "A Family of Similar Solutions for Axisymmetric Incompressible Wakes," AIAA Journal, Vol. 2, Aug. 1964, pp. 1493-1495.

57. Green, J. E., "Two-Dimensional Turbulent Reattachment as a Boundary Value Problem," AGARD Conference Proceedings No. 4, Part I, May 1966, pp. 393-428.

58. Carnahan, B., Luther, H. A. and Wilkes, J. O., Applied Numerical Methods, John Wiley & Sons Inc., New York, 1969, pp. 179; pp. 290-291.

59. Pipes, L. A., Applied Mathematics for Engineers and Physicists, 2nd ed., McGraw-Hill, Kogakusha, pp. 693-698.

60. Golik, R. J., Webb, W. H. and Lees, L., "Further Results of Viscous Interaction Theory for the Laminar Supersonic Near Wake," AIAA Paper 67-61, presented at the AIAA 5th Aerospace Sciences Meeting, New York, Jan. 1967.

61. Ai, D. K., "On the Hypersonic Laminar Near Wake Critical Point of the Crocco-Lees Mixing Theory," AIAA 5th Aerospace Sciences Meeting, New York, Jan. 1967.

62. Reid, J. and Hastings, R. C., "Experiments on the Axisymmetric Flow over Afterbodies and Bases at M = 2.0," RAE Report No. Aero. 2628, Oct. 1959.

63. Siriex, M., Delery, J. and Monnerie, B., "Etude Experimentale du Proche Sillage de Corps de Revolution on Ecoulement Supersonique," ONERA TP-608, 1968.

64. Badrinaryan, M. A., "An Experimental Investigation of Base Flows at Supersonic Speeds," Journal of the Royal Aeronautical Society, Vol. 65, July 1961, pp. 475-482.

65. Seiling, W. R., Przirembel, C. E. G. and Page, R. H., "Axisymmetric Turbulent Near-Wake Studies at Mach Four: Blunt and Hemispherical Bases," AFOSR Report No. 68-2465, Nov. 1968.

66. Kurzwerg, H. H., "Interrelationship Between Boundary Layer and Base Pressure," Journal of the Aeronautical Sciences, Nov. 1951, pp. 743-748.

67. Bogdonoff, S. M., "A Preliminary Study of Reynolds Number Effects on Base Pressure at M = 2.95," Journal of the Aeronautical Sciences, Mar. 1952, pp. 201-206.

68. Bowman, J. E. and Clayden, W. A., "Cylindrical Afterbodies in Supersonic Flow with Gas Ejection," AIAA Journal, Vol. 5, Aug. 1967, pp. 1524-1525.

69. Hubbartt, J. E., Personal Communication, Georgia, Tech., Atlanta, Ga.

VITA

Gopal Krishna Mehta was born in Jammu Tawi, Kashmir, India on August 30, 1944. He graduated from the Ramjas Higher Secondary School, No. 2, Anand Parbat, New Delhi in 1960. He received Trade Certificate in Refrigeration from the Industrial Training Institute in 1962 and worked as a Refrigeration and Air-conditioning mechanic till 1963. He attended the Regional Engineering College, Warangal, Andhra Pradesh, affiliated to the Osmania University, from 1963-68 and received his Bachelor of Engineering degree in Mechanical Engineering in 1968. He was awarded the Gold Medal for standing first in the University. He received his Master of Engineering with Distinction in Aeronautical Engineering from the Indian Institute of Science, Bangalore, Mysore in 1968. During 1970-72, he worked as a Lecturer at the Indian Institute of Science, Bangalore. He entered the Georgia Institute of Technology in 1972 as a graduate student.